NASA/CR-2003-212401

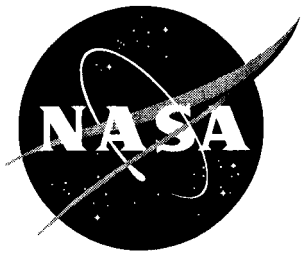

Development of a High Accuracy Angular Measurement System for Langley Research Center Hypersonic Wind Tunnel Facilities

Brett Newman and Si-bok Yu
Department of Aerospace Engineering
Old Dominion University, Norfolk, Virginia

August 2003

The NASA STI Program Office . . . in Profile

Since its founding, NASA has been dedicated to the advancement of aeronautics and space science. The NASA Scientific and Technical Information (STI) Program Office plays a key part in helping NASA maintain this important role.

The NASA STI Program Office is operated by Langley Research Center, the lead center for NASA's scientific and technical information. The NASA STI Program Office provides access to the NASA STI Database, the largest collection of aeronautical and space science STI in the world. The Program Office is also NASA's institutional mechanism for disseminating the results of its research and development activities. These results are published by NASA in the NASA STI Report Series, which includes the following report types:

- TECHNICAL PUBLICATION. Reports of completed research or a major significant phase of research that present the results of NASA programs and include extensive data or theoretical analysis. Includes compilations of significant scientific and technical data and information deemed to be of continuing reference value. NASA counterpart of peer-reviewed formal professional papers, but having less stringent limitations on manuscript length and extent of graphic presentations.

- TECHNICAL MEMORANDUM. Scientific and technical findings that are preliminary or of specialized interest, e.g., quick release reports, working papers, and bibliographies that contain minimal annotation. Does not contain extensive analysis.

- CONTRACTOR REPORT. Scientific and technical findings by NASA-sponsored contractors and grantees.

- CONFERENCE PUBLICATION. Collected papers from scientific and technical conferences, symposia, seminars, or other meetings sponsored or co-sponsored by NASA.

- SPECIAL PUBLICATION. Scientific, technical, or historical information from NASA programs, projects, and missions, often concerned with subjects having substantial public interest.

- TECHNICAL TRANSLATION. English-language translations of foreign scientific and technical material pertinent to NASA's mission.

Specialized services that complement the STI Program Office's diverse offerings include creating custom thesauri, building customized databases, organizing and publishing research results ... even providing videos.

For more information about the NASA STI Program Office, see the following:

- Access the NASA STI Program Home Page at ***http://www.sti.nasa.gov***

- E-mail your question via the Internet to help@sti.nasa.gov

- Fax your question to the NASA STI Help Desk at (301) 621-0134

- Phone the NASA STI Help Desk at (301) 621-0390

- Write to:
  NASA STI Help Desk
  NASA Center for AeroSpace Information
  7121 Standard Drive
  Hanover, MD 21076-1320

NASA/CR-2003-212401

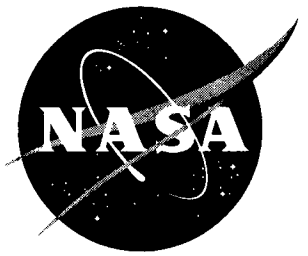

Development of a High Accuracy Angular Measurement System for Langley Research Center Hypersonic Wind Tunnel Facilities

Brett Newman and Si-bok Yu
Department of Aerospace Engineering
Old Dominion University, Norfolk, Virginia

National Aeronautics and
Space Administration

Langley Research Center
Hampton, Virginia 23681-2199

Prepared for Langley Research Center
under Purchase Order L-14635

August 2003

Available from:

NASA Center for AeroSpace Information (CASI)
7121 Standard Drive
Hanover, MD 21076-1320
(301) 621-0390

National Technical Information Service (NTIS)
5285 Port Royal Road
Springfield, VA 22161-2171
(703) 605-6000

Table of Contents

List of Figures

List of Tables

Section I
Introduction

This report describes the activities and accomplishments conducted under contract PO-L-14635 with NASA Langley Research Center. Subject matter is the development of a high accuracy angular measurement capability for hypersonic wind tunnel facilities located at NASA Langley Research Center (LaRC). Specifically, utilization of micro-electro-mechanical sensors (MEMS) including accelerometers and gyros, coupled with software driven data acquisition hardware, integrated within a prototype measurement system, is addressed. Development methodology must address basic design requirements formulated from wind tunnel facility constraints and current operating procedures, as well as engineering and scientific test objectives.[1,2] An important component of the development methodology should include a description of the analytical framework governing any relationships between time dependent multi-axis acceleration and angular rate sensor data and the desired three dimensional Eulerian angular state of the test model.[3,4] A calibration procedure for identifying and estimating critical parameters in the sensor hardware is also a key component of the development methodology.[5-7]

Modern experimental and test activities at LaRC demand innovative and adaptable procedures to maximize data content and quality while working within a severely constrained budgetary and facility resource environment. References 8-9 describe some of these modern test procedure philosophies. Unfortunately, many of the LaRC experimental facilities utilize dated methodologies and technologies during test activities. Current angular measurement capability in LaRC high-speed wind tunnel facilities is a prime example. These current systems are based on primitive electro-mechanical measurements of the model drive system and mathematical descriptions of flexural characteristics of the model sting. Resulting implications are low quality information on the test article pitch, yaw and roll states. In many cases, gross uncertainties enter the angular measurement process, which in turn, requires repeated testing and data averaging techniques to accomplish test objectives.

To overcome these deficiencies, this project focuses on developing a modern and adaptable sensor package capable of measuring pitch, yaw and roll while also meeting the size and accuracy requirements stipulated by LaRC high-speed short duration wind tunnels. In a general setting, pitch, yaw and roll orientation can be indirectly measured from two accelerometer packages that sense gravitational acceleration components in various reference frames combined with knowledge of the gravity vector orientation relative to the wind tunnel reference system. In applications with orthogonality existing between the wind tunnel base and gravity, and with yaw rotation about the vertical direction, yaw orientation is unobservable. However, if this yaw rotation is about a nonvertical axis, then yaw can be fully recovered. Further, angular orientation in all axes can be directly measured by a single gyro based sensor package. Mechanization of angular measurements in this project are based on a combination of both approaches. Commercially available MEMS sensor technology is utilized to maximize the overall sensor package applicability and adaptability to a wide spectrum of wind tunnel facilities. For example, use of small MEMS will facilitate sensor placement within the test article itself, rather than at the base of the sting support system. In a high-speed facility with significant sting loading, this arrangement has an advantage of directly measuring the model motion. Further, as the low cost MEMS age or fail, they can be easily replaced with upgraded, functioning units.

This work is heavily dependent upon NASA LaRC resources, and in particular resources allocated to the Models and Systems Branch. These resources include an array of MEMS accelerometers and gyros, data acquisition microprocessor cards, dedicated personal computer platform, commercial software tools, instrumentation, cables and connectors, high fidelity angular calibration tables, and laboratory space to conduct research activities. The project work is a research and development effort since the focus is to create a new kind of wind tunnel angular measurement system for a unique high-speed tunnel application. The work is also a mixed experimental-analytical effort. The experimental activities involve sensor utilization, electronic microprocessor data acquisition, software development and coding, and system integration. The analytical activities include derivation of required mathematical relationships for

multi-axis rotational motion, data processing and extraction, parameterized sensor models, and numerical algorithms. Access to NASA LaRC facilities proved challenging for the graduate student research assistant, who required escort restrictions at all times. Post September 11, 2001 security issues further slowed access to NASA LaRC.

The contract Statement of Work (see Appendix A) consisted of fifteen sequential, detailed tasks contributing to the overall objective. For purposes of final reporting, these tasks are translated into the following areas.

1. Survey tunnel angular measurement requirements and available MEMS performance.
2. Derive analytical relationships for angular motion and sensor characteristics.
3. Develop accelerometer and gyro sensor calibration and attitude construction procedures.
4. Design data acquisition hardware-software and conduct system integration and test.

These areas are briefly outlined here before moving on to the dedicated sections with detailed reporting of the activities. Emphasis during the first two thirds of the project was given to achieving delivery of a working prototype system at contract closure. After discussions with NASA LaRC, the final third of the project was focused on gyro calibration procedures. All key aspects of the angular measurement system prototype have been investigated. Due to limited commercially available or LaRC owned MEMS sensor performance, a fully working system that meets all design performance objectives was not achieved. However, the prototype system was sufficiently explored such that, if given appropriate MEMS performance, the prototype system would in fact satisfy the objectives. At contract closure, the prototype system consists of loosely integrated hardware and software components, many of which are NASA LaRC property and are thus not part of the deliverables. The main deliverables of the contract are the data acquisition software, sensor calibration software, attitude construction software, and final report describing how these components are integrated into an overall working system.

Section II describes the first area dealing with design requirements and sensor performance. High-speed wind tunnel operational constraints and environmental factors were collected for

purposes of bounding the measurement system design space and characterizing the current angular measurement fidelity. Wind tunnel data is based on a single but representative LaRC high-speed facility, the 31-Inch Continuous Flow Hypersonic Mach 10 Tunnel. This data was collected from a detailed facility tour coupled with in-depth discussions with technician staff. Constraint information covered operational, temporal, thermal, pressure, dimensional, electronic, range, and accuracy aspects. Baseline angular measurement accuracy is stated to be ±0.1 deg in pitch and ±0.5 deg in yaw. However, these estimates are most likely optimistic, with more realistic values being near ±1.0 deg in pitch and yaw. Desired resolution levels for high-speed aerodynamic flow phenomenon were also collected and estimated to be near ±0.1 deg. Based on vendor specification sheets, a survey of commercially available MEMS accelerometer and gyro units was also conducted. Some of these units are within the NASA LaRC hardware inventory. Based on manufacturer's stated performance, a first order estimate indicates the prototype MEMS based measurement system using accelerometers should attain an approximate accuracy of ±0.1 deg in pitch, yaw and roll. Similarly, a prototype system using gyros (assuming stable sensor characteristics, high fidelity calibration, and efficient pretest activities) is predicted to achieve approximately ±0.1 deg accuracy in pitch, yaw and roll. Unfortunately, as discussed latter, performance of the available MEMS gyro units fell significantly short of the manufacturer's claims.

Section III describes the second area dealing with the underlying analytical framework. In this section, appropriate reference frames for important components of the wind tunnel and angular measurement system are introduced. An Eulerian description of the test article attitude state, consistent with the tunnel hardware, is defined. Because of the limited hardware range of rotation, mathematical singularity conditions lie outside the tunnel operational limits. Thus, an Eulerian description for the angular state is appropriate in this application. A general rotation sequence, which is consistent with the 31-Inch Hypersonic Tunnel, is selected to facilitate multi-axis pitch, yaw and roll attitude estimation. Accelerometer based measurements will be used in an indirect and sequential procedure for extracting attitude information by sensing the

gravitational acceleration components first in the sting axes and second in the model axes and comparing with the known gravity vector orientation. Therefore, governing relationships between accelerometer sensed gravity components and the model angular state are developed and documented. In contrast, gyro based measurements will provide a direct procedure for extracting attitude information by sensing attitude rates and conducting integration. Fundamental equations describing gyro sensed multi-axis angular rates and their relationship to the model angular state are generated. Accelerometer and gyro sensor characteristics are also mathematically parameterized in this section. Accelerometer and gyro parameter models considered in the project include mechanical-electrical hardware aspects such as bias, sensitivity, and azimuth and coning misalignment angles. These parameters are considered in all axes. The analytical relationships derived in this section provide the basis for pre-measurement sensor calibration activities, as well as post-measurement attitude construction efforts.

Section IV describes the third area dealing with development of sensor calibration and attitude construction procedures and techniques. Development of calibration and construction algorithms was a major effort within the overall project. Gravity sensing accelerometer calibration, as well as angular rate sensing gyro calibration, can be mathematically described by a nonlinear algebraic relationship. Recommended sensor calibration procedures are based on an existing technique thoroughly described in Reference 5. This technique uses an iterative Gauss-Newton numeric solution strategy and was implemented by the contractors using MathWorks MATLAB.[10] These calibration procedures were tested with simulated data and found to be reliable and accurate. Gravity sensing accelerometer based attitude construction is also described mathematically with a nonlinear algebraic relationship. Here, an analytic closed-form solution for the attitude construction is possible, as well as a Gauss-Newton iterative solution. Both solutions were implemented by the contractors using MATLAB. Rate gyro based attitude construction is governed by a set of nonlinear differential relationships, thus making the attitude construction process here fundamentally distinct from the accelerometer based construction task. A direct Runge-Kutta numerical integration strategy was found to be effective in solving the

attitude construction equations. This technique was also implemented by the contractors in MATLAB. These attitude construction procedures were again tested with simulated data and found to be reliable and accurate. Note these full-blown calibration and construction procedures were not tested in the laboratory with real data and within the data acquisition control software environment. However, simplified single-axis versions of these concepts were tested in the laboratory with real data.

Section V documents the final area dealing with design of data acquisition hardware-software and system integration and test. For the prototype system, no freedom existed in hardware design or selection. Utilization of NASA LaRC supplied hardware was mandated. Major hardware components consisted of a Pentium II class personal computer with video monitor, National Instruments 4 channel 200 kHz NI-4452 data acquisition card, Analog Devices ADXL105 MEMS micromachined polysilicon vibrating structure accelerometer, and muRata ENC-03J piezoelectric vibrating gyroscope or rate gyro. A wide range of design freedom and selection existed with data acquisition controlling software. National Instruments LabVIEW[11,12] was selected for this function based on its powerful capabilities, ease of use, compatibility with the NI-4452 data card, and acceptance at NASA LaRC. LabVIEW's graphical user interface was used to create multi-functional control instrumentation that reads input signals from the data card, processes and filters the input signals, calibrates several key sensor parameters, transforms the acceleration and angular rate data to angular position states, records data to storage devices, and outputs real-time information to a video display in numeric and graphical formats. Real-time output can be monitored by the wind tunnel technicians and experimental aerodynamicists to evaluate ongoing test conditions. Software design and testing was a major effort within the overall project. A significant problem that was encountered related to critical LabVIEW functions interfacing with the NI-4452 card. To circumvent this problem, several core functions from Wyle Laboratories were utilized in the control software. Integration of the hardware and software components to a working end-to-end simplified angular measurement system prototype was successfully accomplished. This end-to-end operational capability was tested and

demonstrated in the laboratory. Note only simplified single-axis calibration-construction capability was demonstrated here. Angular measurement accuracy objectives using available MEMS accelerometers was achieved. Unfortunately, these objectives were not achieved with available MEMS gyros. Large performance discrepancies between manufacturer published data and observed data were discovered. A major conclusion of the work is that better performing gyros are required.

Section II
Design Requirements and Sensor Performance

A. Wind Tunnel Constraints

Design of a prototype wind tunnel Angular Measurement System (AMS) depends strongly upon the characteristics and constraints imposed by the wind tunnel facility itself. Further, such information will benchmark the current AMS accuracy for the purpose of latter comparison with the new AMS system. In this project, the 31-Inch Continuous Flow Hypersonic Mach 10 Tunnel is selected as a basis for the AMS design because this facility is frequently used and is representative of several other LaRC high-speed wind tunnel facilities. Wind tunnel constraints and characteristics were collected from a detailed facility tour coupled with in-depth discussions with technician staff, as well as internet information on the tunnel. Detailed information was collected and recorded in several areas including operational, accuracy, dimensional, temporal, dynamic, range, thermal, and pressure aspects.

Figure 1 illustrates the sequence of events during a test in the 31-Inch Hypersonic Tunnel. The aerodynamic model is prepared for testing while the injection housing is in the exposed position. The test article is mounted on the pitch-yaw sting drive system and the system is rotated to the desired initial angles. Fixed roll orientation is achieved by direct sting mounting. Figure 2 shows the sting drive system arrangement. Instrumentation attached to the model is verified for correct and stable readings. Electro-mechanical measurements are taken of the model orientation. The injection housing is then rotated to the closed position while the wind tunnel flow conditions are adjusted to the desired values. When the flow conditions are met, the model is injected rapidly into the high-speed flow. As the model is injected into the test chamber, high-speed airflow loads the drive system and flexes the sting. Consequently, the model orientation during test is different from the measured pre-injection condition. Correction factors based on models of the drive system hysteresis and sting flexural characteristics are commonly used in an attempt to improve knowledge of the model attitude test conditions. However, significant uncertainties

remain in the baseline measurement process. Baseline angular measurement accuracy was stated to be ±0.1 deg in pitch and ±0.5 deg in yaw. Further discussion revealed these estimates are most likely optimistic, with more realistic values being near ±1.0 deg in pitch and yaw. More important than the exact value for angular accuracy is the knowledge that sizeable unknowns exist in the current AMS. The new AMS should provide an accuracy level significantly better than existing system performance described here. Thus, a requirement for reliable angular measurement accuracy of ±0.1 deg in all axes will be considered for the AMS design.

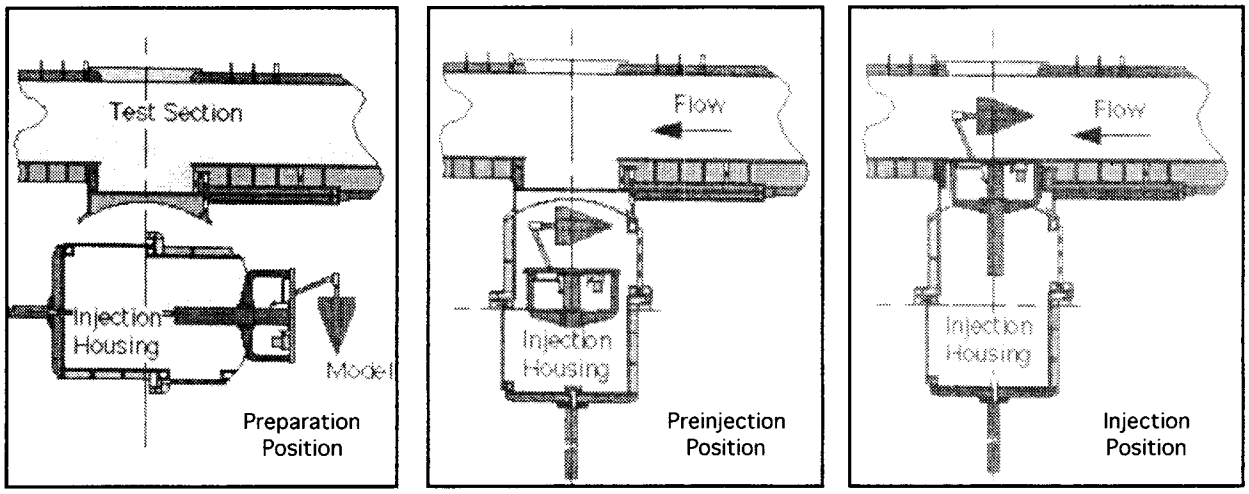

Figure 1 Test Sequence

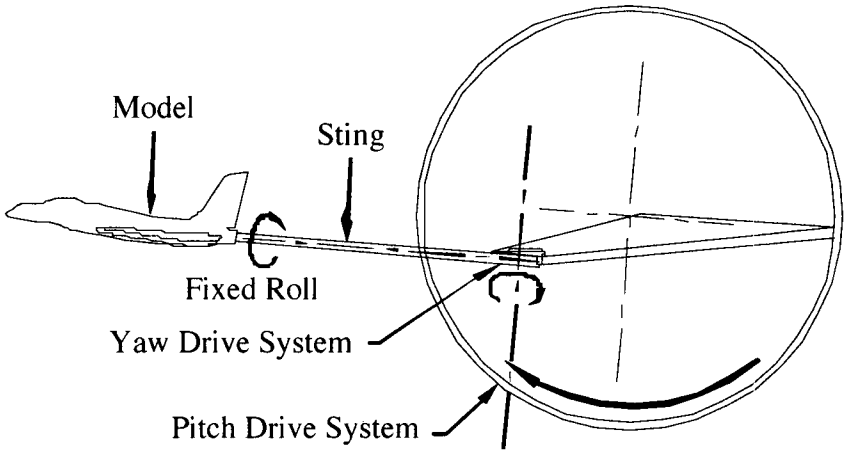

Figure 2 Model and Sting Drive System

Now consider dimensional constraints placed on the AMS design. Typical model size in the 31-Inch Hypersonic Tunnel is 12-15 in. Models are constructed to meet center of gravity and moment of inertia requirements precisely. Sting mounting is accomplished with rear attachment geometry as shown in Figure 2 using several standardized interface dimensions. To circumvent any necessary altering of the model and its associated inertial characteristics, and to avoid variability with each model, mounting of the sensor package internally within the sting tip is recommended. Such mounting will minimize modification to the existing facility and test procedures, and in particular interfacing with the test article. Stings for the 31-Inch Hypersonic Tunnel are typically slender, hollow cylindrical 1-1.5 ft long tubes constructed from various metallic alloys. Internal sting diameters range between 0.5 and 0.75 in. Volume and dimension constraints placed on the sensor package are thus quite small, and the weight is also suggested to be as light as possible. An ability to reliably secure and unsecure the package within the sting tip is also desired. Electrical wiring to and from the sensors can also be accomplished through the hollow sting shaft.

Next, consider constraints from test duration and drive system angular range. Typical test times for the 31-Inch Hypersonic Tunnel will be less than 2 min. This duration does not pose any significant constraint on the AMS design. However, the model preparation time during which the injection housing is in the exposed position can be significantly longer than the actual test time. Preparation time could be an order of magnitude longer. Since final alignment of the AMS will be performed somewhere in this window, further constraints are placed on the AMS design. The drift characteristics of the MEMS accelerometer and gyro units, in combination with drift estimation accuracy, must accommodate durations on the order of 10-15 min in meeting the angular measurement requirements. The pitch-yaw drive system has an operational rotation range of ±60 deg in pitch and ±15 deg in yaw. Common testing angles, however, fall within ±15 deg pitch and ±5 deg yaw. Roll capability is unlimited (±180 deg), but again is commonly held within ±15 deg. It is important to note that pitch and yaw orientation can be varied during the test while roll is fixed. The model is usually held for 2-3 s at each test point with transition time

between test points requiring approximately the same duration. This dynamic motion places a mild constraint on the required dynamic response of the MEMS units and data acquisition sample time. Modern sensors and data input cards will have no problem in satisfying these constraints. Because of the small hardware range of rotation, there are no constraints for using a singularity free, non-minimal angular state description. Thus, a simpler Eulerian description for the angular state will be acceptable.

Finally, the harsh environment of the hypersonic test chamber requires the sensor package to be functional in a high temperature, vacuum environment. Temperature within the 31-Inch Hypersonic Tunnel test chamber commonly rises to 1,350 °F. This temperature is well beyond the operational range of any MEMS gyroscope or accelerometer. However, the expected temperature within the sting tip, which itself is inside the test article is significantly lower than test chamber temperatures. The actual temperature within the sting tip is not provided but is estimated to be 100-300 °F. This temperature is on the fringe of most commercially available MEMS temperature range capabilities. Further, MEMS units are typically temperature sensitive. Thus, another constraint imposed from the tunnel facility is for thermal compensation of some type, and detailed thermal calibration. The test chamber also experiences a vacuum condition on the order of 1-2 psi during operation. Constraints for acceptable operational performance in a vacuum will also be placed on any AMS design. Due to limited project resources, thermal and pressure characteristics in the design of the prototype AMS are not considered, and will have to be addressed in follow on efforts.

B. Aerodynamic Test Objectives

Design of the prototype wind tunnel AMS also depends strongly on the engineering and scientific test objectives. NASA LaRC high–speed wind tunnel facilities are typically used to explore and quantify the aerodynamic characteristics of advanced hypersonic concepts, air-to-air missiles, orbital launch systems, and re-entry vehicles over a wide range of speeds and aerodynamic attitudes. For example, hypersonic wave rider concepts in the cruise configuration

would be tested at very low (near zero) angles of attack and side slip angles, while maneuvering re-entry vehicles would be tested at large (possibly approaching 45 to 60 deg) angles of attack and side slip angles. Associated flow physics are complex and may exhibit attached oblique shocks, detached bow shocks, large regions of separated chaotic flow, body generated vortices, and thick turbulent boundary layers. These characteristics may be highly sensitive to and dependent on the aerodynamic angles, thus requiring a high fidelity model orientation measurement capability. Reference 2 implies current industry-government experimental program goals are to achieve an angular wind tunnel measurement resolution of ±0.1 deg or better. Therefore, an engineering and scientific test imposed requirement for reliable angular measurement accuracy of ±0.1 deg in all axes will be considered for the AMS design. This requirement is consistent with previous accuracy requirements driven by current wind tunnel facility capabilities and the need to improve upon this capabilities.

C. MEMS Survey

Several MEMS accelerometers under consideration for the prototype AMS are listed in Table 1. Many other MEMS accelerometers are commercially available, but this report will focus only on those units listed in Table 1. These units include Analog Devices' ADXL105, and MEMSIC's MX201A, MXA2500A and MXD2020A units. NASA LaRC has a large supply of the ADXL105 units but currently does not have any units from MEMSIC. Detail sensor specifications can be found in References 13-14. The ADXL105 MEMS accelerometer uses an open-loop architecture consisting of a micromachined polysilicon vibrating structure outfitted with a central capacitance plate and positioned between two other fixed capacitor plates. The fixed plates are used to nominally vibrate the central plate, as well as to sense unsymmetric motion resulting from accelerations. The MX201A, MXA2500A and MXD2020A MEMS accelerometers measure internal heat transfer changes within a gaseous proof mass through natural convection caused by acceleration. A gaseous cavity is thermally loaded by a heater bar and instrumented with several thermocouples. Acceleration results in an unsymmetrical thermal

Table 1 MEMS Accelerometer Specifications

Vendor	Analog Devices	MEMSIC	MEMSIC	MEMSIC
Model	ADXL105	MX201A	MXA2500A	MXD2020A
Linear Resolution (mg)	2	1	< 2	< 2
Angular Resolution (deg)	0.1146	0.0573	< 0.1146	< 0.1146
Sensitivity (mv/g)	250	500	500	-
Max Acceleration (g)	±5	±1	±1	±1
Bandwidth (Hz)	10k	40	30	30
Noise ($\mu g/Hz^{1/2}$)	225	750	750	40
Dimension (h/w/d mm)	10.64/12.07/5.08	5/5/2	5/5/2	5/5/2
Mass (g)	< 2	< 1	< 1	< 1
No. of Axes	1	2	2	2
Temperature Range (°C)	0/+70	-40/+125	-40/+105	-40/+105
Temperature Sensor	Included	Included	Included	Included

gradient in the cavity leading to a thermocouple voltage signal that is proportional to acceleration. These sensors are also open-loop devices.

All four accelerometer models are sufficiently small to satisfy the dimensional constraints from the internal sting diameter. Even though thermal effects are not considered in the AMS design at this time, the MEMSIC units are noted to provide a somewhat larger but still marginal window for temperature range. No information is available on acceptable pressure ranges. Linear resolution of all four accelerometers range between 1 to 2 mg, and sensitivity ranges between 250 and 500 mv/g. For the gravity sensing wind tunnel application, this resolution can be converted to an angular resolution. Linear resolution is converted to angular resolution through an inverse sine operation. In the case of the ADXL105 accelerometer, 2 mg linear resolution corresponds to an angular resolution of 0.1146 deg ($\Delta\Theta = \sin^{-1}(R + \sin(\Theta)) - \Theta$ with $R = 0.002$ and $\Theta = 0$ deg). Note the angular resolution is a function of geometry and is best when the sensing axis of the accelerometer is orthogonal to the gravity vector. When the accelerometer is

rotated, the angular resolution degrades as the transformation from linear to angular occurs on a flatter region of the sine function curve. For ADXL105, the resolution becomes 0.1187 deg when the accelerometer is rotated by 15 deg. With multi-axis sensing, resolution of any of the four candidate accelerometer units is very close to meeting the angular measurement requirement of ±0.1 deg. Dynamic response performance noted in Table 1 should easily satisfy any constraints from the drive system duty cycle motion. Also, test duration related constraints are not critical here since the accelerometer signals do not require integration for angle construction.

Next, a set of MEMS gyroscopes listed in Table 2 are considered. Many other MEMS gyros are commercially available, but this report will focus only on those units listed in Table 2. These units include muRata's ENC-03J and ENV-05F-03, and Samsung's MGL80301ZT0 and MG-L106C units. NASA LaRC has a large supply of the ENC-03J units but currently does not have any units from Samsung. Detail sensor specifications can be found in References 15-16. The gyroscopes under consideration are rate gyros which give output signals proportional to sensor angular rate. The ENC-03J and ENV-05F-03 MEMS gyros use an open-loop architecture consisting of a ceramic bimorph vibrating structure excited electrically. When this oscillating unit experiences an angular rate, an electrical signal is generated proportional to the resulting Coriolis force. The MGL80301ZT0 and MG-L106C MEMS gyros function in a similar way but incorporate proprietary material and manufacturing techniques. These sensors are also open-loop devices.

Table 2 shows the ENC-03J, MGL80301ZT0 and MG-L106C gyros satisfy the dimensional constraints. Note the ENV-05F-03 gyro width dimension exceeds the sting internal diameter constraint (0.772 in width vs. 0.75 in diameter). Even though thermal effects are not considered in the AMS design at this time, both the muRata and Samsung units provide only a marginal window for operation within an elevated thermal environment. No information is available on acceptable pressure ranges. Although not directly supplied by the manufacturer, an angular rate resolution value can be estimated by dividing sensitivity into noise. Only the muRata ENV-05F-03 gyro gives a reasonable resolution when compared with expected model

Table 2 MEMS Gyro Specifications

Vendor	muRata	muRata	Samsung	Samsung
Model	ENC-03J	ENV-05F-03	MGL80301ZT0	MG-L106C
DC Drift (deg/s)	< 5	< 9	0.2	0.2
Sensitivity (mv/deg/s)	0.67	25	0.6	0.6
Max Angular Rate (deg/s)	±300	±60	±500	±500
Bandwidth (Hz)	50	7	15	50
Noise (mv)	-	5	18	18
Dimension (h/w/d mm)	8/15.44/6.55	27.2/19.6/11.5	8/15/6.55	8/15/6.55
Mass (g)	1	20	-	-
No. of Axes	1	1	1	1
Temperature Range (°C)	-5/+75	-30/+80	-5/+55	-5/+75

drive rate schedules. The gyros under consideration show significant output signal drift. The Samsung gyros exhibit better drift performance than muRata units, but the maximum drift value indicates accumulation of 0.2 deg/s drift over a 2 min test results in 24 deg offset. Recall model preparation time could lead to significantly larger test durations which only exacerbate the problem. If 1) gyro drift characteristics of 0.2 deg/s were highly repeatable and stable, 2) drift calibration performance is on the order of 1% (±0.002 deg/s knowledge of actual drift), and 3) operational duration could be limited to 120 s with efficient test procedures, then and only then does the angular measurement accuracy being to approach the ±0.1 deg requirement. Under these drift assumptions, only the ENV-05F-03 gyro is theoretically feasible for satisfying angular resolution objectives. Unfortunately, as discussed in Section V-C, the actual drift value observed in test for the available gyros was much higher than stated by the manufacturer, and more importantly, the drift characteristics were highly variable. Therefore, drift performance for any gyro based prototype AMS will be a critical parameter. Finally, dynamic response performance noted in Table 2 should easily satisfy any constraints from the drive system duty cycle motion.

D. Prototype Angular Measurement System

A rough schematic of the prototype AMS is described in Figure 3. The architecture in Figure 3 shows the hardware and software components, their relationship to one another, and the major functions occurring within the AMS prototype. The AMS operates in one of two modes: sensor calibration or attitude construction. AMS hardware includes an accelerometer-gyro sensor package, data acquisition board, personal computer with video monitor, and electrical connections between these devices. Major functions performed by these components include motion detection and motion measurement, data sampling and analog-to-digital signal conversion, engine for real-time and post-measurement processing, and data storage and data display. AMS software resides entirely within the computer and incorporates multiple languages with command line and graphical interface modes. Although the prototype AMS can not function properly without the presence of high performance hardware components such as motion sensors and acquisition devices, as can be observed in Figure 3, software is the most critical component in AMS operation. In the sensor calibration and attitude construction modes, software functions include data processing and filtering, data transfer, storage and display, estimation of sensor characteristics (calibration), and Euler angle reconstruction from raw data. Note the attitude construction mode requires information from the sensor calibration mode. Further note the attitude construction mode can operate in a lower functionality real-time submode or a higher functionality post-test submode.

Utilization of the AMS is envisioned as follows. Sensor calibration activities will be conducted in the Instrumentation Laboratory of the Models and Systems Branch at NASA LaRC. This activity will make use of the Dual Axis or Single Axis High Precision Angle Indexing Tables in the lab. Once the calibration parameters are identified, the AMS will be transported to the appropriate hypersonic wind tunnel facility. The AMS will then be integrated with the test article and tunnel data acquisition system to perform attitude construction functions during and after the actual test. Independently obtained angles from the accelerometer sensors and gyro sensors can be used in a redundancy role to monitor for corrupted data in either channel, or they

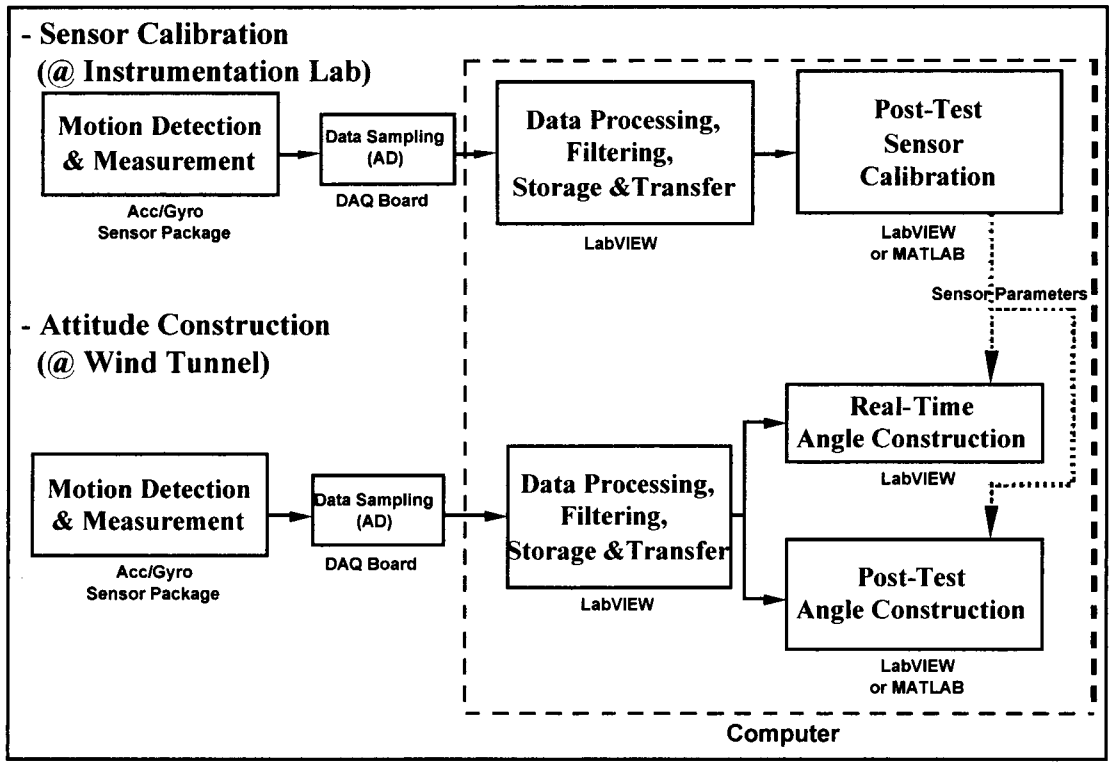

Figure 3 Angular Measurement System

can be fused in such a fashion to supplement either source's weaknesses, although such functions were not considered in this project. At this preliminary development stage, the prototype system consists of loosely integrated hardware and software components, many of which are NASA LaRC property that are currently being utilized in other projects. At one time during the later stages of the contract, these components were in place and formed a working prototype demonstration. Only simplified single-axis laboratory calibration and construction capability was demonstrated. Currently, the AMS prototype components are disassembled and therefore not able to perform working system demonstrations. However, this report describes the working system details and performance, and how it could be easily re-assembled. AMS prototype characteristics of this sort are consistent with the main project objective of exploring and demonstrating the feasibility of an AMS capability, as opposed to constructing a professionally packaged and fully completed system.

Section III
Analytical Framework

A. Angular State Description

An Eulerian description for the model angular state will be utilized by the AMS. This formulation provides advantages by working with insightful physical variables and a minimum state description. Singularity conditions are automatically avoided by the limited pitch-yaw drive system operational range. Right-handed coordinate systems used in this report are described in Figure 4. The tunnel fixed coordinate system ($x_t y_t z_t$) is regarded as an inertial frame, while the model (body) fixed coordinate system ($x_m y_m z_m$) and sting fixed coordinate system ($x_{st} y_{st} z_{st}$) are rotated relative to the tunnel fixed coordinate system. These systems are oriented conventionally: x_t along tunnel axis (flow direction), y_t orthogonal to tunnel axis (horizontal), z_t orthogonal to tunnel axis (vertical), x_m along model longitudinal axis (nose), y_m along model lateral axis (right wing), z_m along model normal axis (down), x_{st} along sting axis (forward), y_{st} along pitch drive axis (horizontal), and z_{st} along yaw drive axis (tilted vertical). For simplification purposes, the wind tunnel and associated reference frame are assumed to be oriented relative to the earth fixed coordinate system (also assumed inertial) such that the gravitational acceleration vector points along the $-z_t$ direction. If a more general geometric condition is required, the mathematical framework could be easily modified.

Initial orientation of the sting fixed and model fixed axes is such that $x_{st} = x_m = -x_t$, $y_{st} = y_m = y_t$, and $z_{st} = z_m = -z_t$. Note at the initial orientation, axes are aligned but $x_{st} = x_m$ and $z_{st} = z_m$ have opposite directions from x_t and z_t. This initial sting fixed and model fixed orientation is obtained from the tunnel fixed axes by a +180 deg rotation about y_t. A non-standard three angle Euler rotation sequence is used to describe the transformation relationship between the initial and final orientations of the sting fixed and model fixed reference frames. To transform from initial orientation to the sting and model axes, the Euler rotation sequence is specified as pitch-yaw-roll (Θ-Ψ-Φ). First, the initial orientation is rotated an angle Θ about y_t. Second, the resulting

intermediate axes are rotated an angle Ψ about the corresponding z axis. This rotation sequence leads to the sting fixed axes. Third, sting fixed axes are rotated an angle Φ about the x_{st} axis. The indicated Euler rotation sequence leads to the model fixed axes. This rotation sequence is consistent with the 31-Inch Hypersonic Tunnel model sting drive system and test procedure. In this facility the azimuth (yaw) drive system rides on the elevation (pitch) drive system. Further, the test model is attached to the sting with a fixed rotation (roll), which can be interpreted as a roll drive system riding on the yaw drive system in an advanced state of the art tunnel facility. Roll angle can always be set to a known fixed value to represent specific characteristics of the 31-Inch Hypersonic Tunnel. Figure 4 describes the pitch-yaw-roll angle sequence.

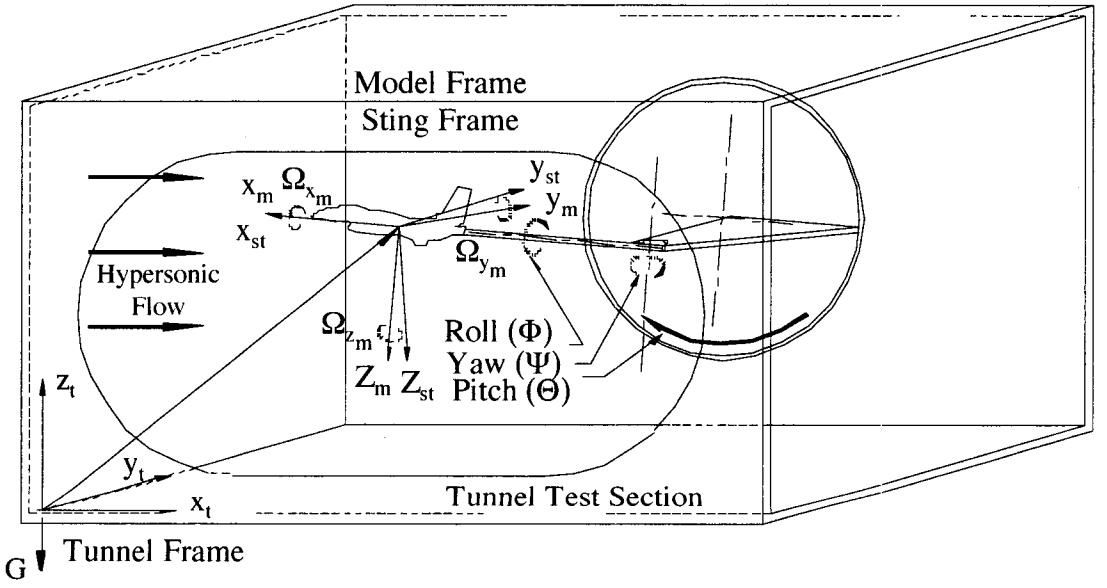

Figure 4 Tunnel-Sting-Model Axes and Euler Sequence Description

Misalignment between the sting and/or model fixed axes and the sensor fixed axes can exist due to attachment and mounting inaccuracies associated with sting-model-sensor interfacing, as well as internal sensor manufacturing inaccuracies. Here, sensor fixed axes refer to the true internal excitation axes within the sensor. Such misalignment will be described by the coning angle (C) and azimuth angle (A). Figure 5 illustrates the definition of these two

misalignment angles for the case where x_{st} (sting x axis) is the desired measurement axis and x_{sn} (sensor x axis) is the true measurement axis. Coning angle is defined as the angle subtended by the desired and true measurement axes. A cone shape is created when the excitation axis is rotated about the desired axis. To define the azimuth angle, consider projecting the cone and excitation axis onto the y_{st}-z_{st} plane. The projected shape is a circle with a radial marking. Azimuth angle is defined as the angle subtended by the $-z_{st}$ axis and projected excitation axis. The internal sensor fixed excitation axes relative to the sting fixed axes can be defined by a rotational transformation associated with the coning and azimuth angles. This transformation is geometrically defined by 1) heading (A) around the circle relative to y_{st}, and 2) spin (C) about the heading radial. Other important parameters associated with the sensor behavior are bias (B) and sensitivity (S). A systematic deviation exhibited by a measurement value from a reference value is defined as bias. Further, sensitivity is defined as the ratio of observed output signal produced with respect to a specified unit of sensor input change.

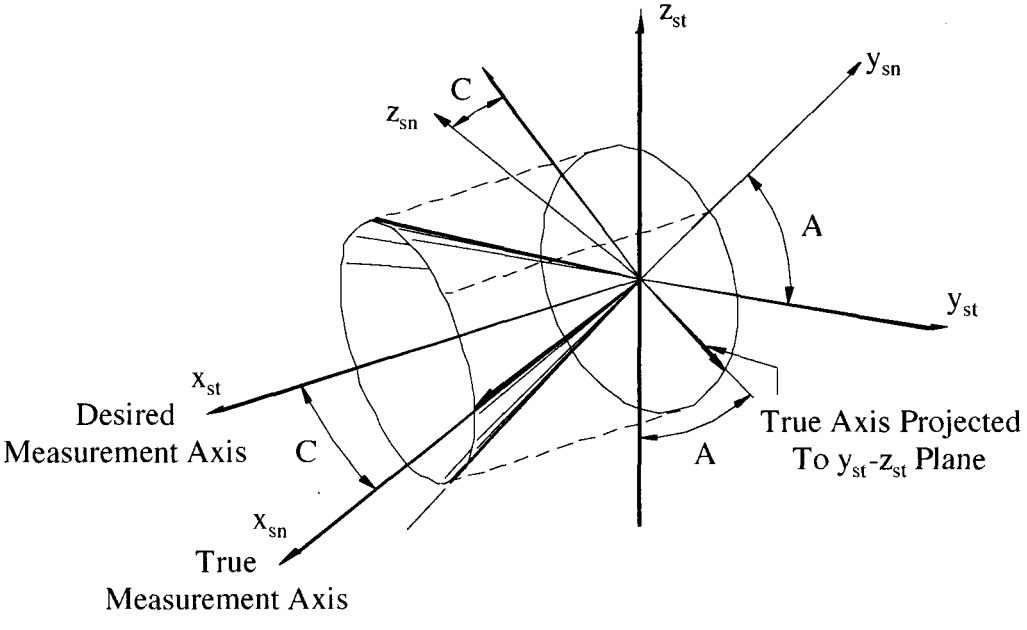

Figure 5 Azimuth and Coning Angle Description

B. Accelerometer Equations

Derivation of the underlying analytical framework between multi-axis gravitational acceleration data measured by two accelerometer sensor packages and the desired three dimensional Eulerian angular state of the test model is considered in this subsection. This analytical framework provides the basis for accelerometer sensor calibration and attitude construction logic presented in Section IV. With the geometry described in Figure 4, the gravitational acceleration vector (algebraic form) expressed in the tunnel fixed reference frame is

$$\mathbf{G_t} = \begin{bmatrix} 0 & 0 & -G \end{bmatrix}^T \qquad \text{(III-B.1)}$$

where G denotes the local value of gravity. $\mathbf{G_t}$ is considered to be the known reference vector.

General orientation of a three axis set with respect to an orthogonal reference frame is defined by a minimum of three angles. However, the general orientation of a vector with respect to this same reference is defined with a minimum of two angles. Therefore, extraction of the complete pitch-yaw-roll orientation state from a gravity vector measurement scheme employing a single accelerometer sensor package is not feasible. For example, as the generally oriented model fixed frame is rotated about the gravity vector, an infinite set of pitch-yaw-roll solutions is generated corresponding to a single set of model fixed gravity components. Therefore, in a general framework, gravitational acceleration will be measured in both the sting fixed and model fixed axes using two accelerometer sensor packages. By relating these measured acceleration components with known components in Equation (III-B.1) in a two-step process, the full angular state can be determined. This approach is applied to development of the general angular measurement system. A simplified case, with known roll angle and only pitch-yaw construction based on a single sensor package mounted in the sting fixed axes (i.e., the 31-Inch Hypersonic Tunnel application), can always be extracted from the general framework.

Consider the following sequential transformations of the gravity vector in tunnel fixed axes through the model fixed axes. In Equations (III-B.2)-(III-B.5), $\mathbf{G_i}$ denotes the gravity vector expressed in frame i, G_{x_i}-G_{y_i}-G_{z_i} denote components of $\mathbf{G_i}$, $\mathbf{T_{i/j}}$ denotes the transformation

matrix from frame j to frame i, and i, j = t, i, i1, st, m representing tunnel fixed, initial orientation, first intermediate, sting fixed, and model fixed axes, respectively.

$$\mathbf{G_i} = \mathbf{T_{i/t}}\mathbf{G_t} \qquad \mathbf{G_i} = \left[G_{x_i}\ G_{y_i}\ G_{z_i}\right]^T \qquad \mathbf{T_{i/t}} = \begin{bmatrix} -1 & 0 & 0 \\ 0 & 1 & 0 \\ 0 & 0 & -1 \end{bmatrix} \tag{III-B.2}$$

$$\mathbf{G_{i1}} = \mathbf{T_{i1/i}}\mathbf{G_i} \qquad \mathbf{G_{i1}} = \left[G_{x_{i1}}\ G_{y_{i1}}\ G_{z_{i1}}\right]^T \qquad \mathbf{T_{i1/i}} = \begin{bmatrix} \cos(\Theta) & 0 & -\sin(\Theta) \\ 0 & 1 & 0 \\ \sin(\Theta) & 0 & \cos(\Theta) \end{bmatrix} \tag{III-B.3}$$

$$\mathbf{G_{st}} = \mathbf{T_{st/i1}}\mathbf{G_{i1}} \qquad \mathbf{G_{st}} = \left[G_{x_{st}}\ G_{y_{st}}\ G_{z_{st}}\right]^T \qquad \mathbf{T_{st/i1}} = \begin{bmatrix} \cos(\Psi) & \sin(\Psi) & 0 \\ -\sin(\Psi) & \cos(\Psi) & 0 \\ 0 & 0 & 1 \end{bmatrix} \tag{III-B.4}$$

$$\mathbf{G_m} = \mathbf{T_{m/st}}\mathbf{G_{st}} \qquad \mathbf{G_m} = \left[G_{x_m}\ G_{y_m}\ G_{z_m}\right]^T \qquad \mathbf{T_{m/st}} = \begin{bmatrix} 1 & 0 & 0 \\ 0 & \cos(\Phi) & \sin(\Phi) \\ 0 & -\sin(\Phi) & \cos(\Phi) \end{bmatrix} \tag{III-B.5}$$

The gravitational acceleration vector expressed in the sting fixed reference frame in terms of the known gravity vector is obtained by combining Equations (III-B.2)-(III-B.4), or

$$\mathbf{G_{st}} = \underbrace{\mathbf{T_{st/i1}}\mathbf{T_{i1/i}}\mathbf{T_{i/t}}}_{\mathbf{T_{st/t}}}\mathbf{G_t} \tag{III-B.6}$$

The overall transformation matrix $\mathbf{T_{st/t}}$ from tunnel fixed to sting fixed axes in Equation (III-B.6) is obtained from a product of the component transformation matrices. Note the gravitational acceleration vector expressed in the model fixed reference frame as a function of the gravity vector expressed in the sting fixed axes is given by Equation (III-B.5).

Now consider effects from misalignment errors due to the azimuth and coning angles in the sting mounted accelerometer sensor package. The following analysis must be conducted individually for each desired measurement axis. First consider the sting x_{st} axis as the desired measurement axis (Figure 5). A sequential transformation consisting first of azimuth rotation ($A_{x_{st}}$) about x_{st} leading to a second intermediate frame, and next of coning rotation ($C_{x_{st}}$) about

the intermediate y axis which leads to the true measurement or sensor fixed reference frame ($x_{sn_{x_{st}}} y_{sn_{x_{st}}} z_{sn_{x_{st}}}$) associated with x_{st}, is implemented. For the y_{st} axis, azimuth rotation ($A_{y_{st}}$) is about y_{st} and coning rotation ($C_{y_{st}}$) is about the intermediate z axis leading to the y_{st} specific sensor fixed axes ($x_{sn_{y_{st}}} y_{sn_{y_{st}}} z_{sn_{y_{st}}}$). Finally, for the z_{st} axis, azimuth rotation ($A_{z_{st}}$) is about z_{st} and coning rotation ($C_{z_{st}}$) is about the intermediate x axis leading to the z_{st} specific sensor fixed axes ($x_{sn_{z_{st}}} y_{sn_{z_{st}}} z_{sn_{z_{st}}}$). These transformation relationships are summarized in Equations (III-B.7)-(III-B.12) where $\mathbf{G_i}$, G_{x_i}-G_{y_i}-G_{z_i}, and $\mathbf{T_{i/j}}$ have the same meaning as before, but with i, j = st, $i2_k$, sn_k representing sting fixed, second intermediate, and sensor fixed axes, respectively, and k = x_{st}, y_{st}, and z_{st}.

$$\mathbf{G_{i2_{x_{st}}}} = \mathbf{T_{i2_{x_{st}}/st}} \mathbf{G_{st}} \tag{III-B.7}$$

$$\mathbf{G_{i2_{x_{st}}}} = \begin{bmatrix} G_{x_{i2_{x_{st}}}} & G_{y_{i2_{x_{st}}}} & G_{z_{i2_{x_{st}}}} \end{bmatrix}^T \qquad \mathbf{T_{i2_{x_{st}}/st}} = \begin{bmatrix} 1 & 0 & 0 \\ 0 & \cos(A_{x_{st}}) & \sin(A_{x_{st}}) \\ 0 & -\sin(A_{x_{st}}) & \cos(A_{x_{st}}) \end{bmatrix}$$

$$\mathbf{G_{sn_{x_{st}}}} = \mathbf{T_{sn_{x_{st}}/i2_{x_{st}}}} \mathbf{G_{i2_{x_{st}}}} \tag{III-B.8}$$

$$\mathbf{G_{sn_{x_{st}}}} = \begin{bmatrix} G_{x_{sn_{x_{st}}}} & G_{y_{sn_{x_{st}}}} & G_{z_{sn_{x_{st}}}} \end{bmatrix}^T \qquad \mathbf{T_{sn_{x_{st}}/i2_{x_{st}}}} = \begin{bmatrix} \cos(C_{x_{st}}) & 0 & -\sin(C_{x_{st}}) \\ 0 & 1 & 0 \\ \sin(C_{x_{st}}) & 0 & \cos(C_{x_{st}}) \end{bmatrix}$$

$$\mathbf{G_{i2_{y_{st}}}} = \mathbf{T_{i2_{y_{st}}/st}} \mathbf{G_{st}} \tag{III-B.9}$$

$$\mathbf{G_{i2_{y_{st}}}} = \begin{bmatrix} G_{x_{i2_{y_{st}}}} & G_{y_{i2_{y_{st}}}} & G_{z_{i2_{y_{st}}}} \end{bmatrix}^T \qquad \mathbf{T_{i2_{y_{st}}/st}} = \begin{bmatrix} \cos(A_{y_{st}}) & 0 & -\sin(A_{y_{st}}) \\ 0 & 1 & 0 \\ \sin(A_{y_{st}}) & 0 & \cos(A_{y_{st}}) \end{bmatrix}$$

$$\mathbf{G_{sn_{y_{st}}}} = \mathbf{T_{sn_{y_{st}}/i2_{y_{st}}}} \mathbf{G_{i2_{y_{st}}}} \tag{III-B.10}$$

$$\mathbf{G_{sn_{y_{st}}}} = \begin{bmatrix} G_{x_{sn_{y_{st}}}} & G_{y_{sn_{y_{st}}}} & G_{z_{sn_{y_{st}}}} \end{bmatrix}^T \qquad \mathbf{T_{sn_{y_{st}}/i2_{y_{st}}}} = \begin{bmatrix} \cos(C_{y_{st}}) & \sin(C_{y_{st}}) & 0 \\ -\sin(C_{y_{st}}) & \cos(C_{y_{st}}) & 0 \\ 0 & 0 & 1 \end{bmatrix}$$

$$\mathbf{G_{i2_{z_{st}}}} = \mathbf{T_{i2_{z_{st}}/st}} \mathbf{G_{st}} \tag{III-B.11}$$

$$\mathbf{G}_{\mathbf{i2}_{\mathbf{z_{st}}}} = \begin{bmatrix} G_{x_{i2_{z_{st}}}} & G_{y_{i2_{z_{st}}}} & G_{z_{i2_{z_{st}}}} \end{bmatrix}^T \qquad \mathbf{T}_{\mathbf{i2}_{\mathbf{z_{st}}}/\mathbf{st}} = \begin{bmatrix} \cos(A_{z_{st}}) & \sin(A_{z_{st}}) & 0 \\ -\sin(A_{z_{st}}) & \cos(A_{z_{st}}) & 0 \\ 0 & 0 & 1 \end{bmatrix}$$

$$\mathbf{G}_{\mathbf{sn}_{\mathbf{z_{st}}}} = \mathbf{T}_{\mathbf{sn}_{\mathbf{z_{st}}}/\mathbf{i2}_{\mathbf{z_{st}}}} \mathbf{G}_{\mathbf{i2}_{\mathbf{z_{st}}}} \tag{III-B.12}$$

$$\mathbf{G}_{\mathbf{sn}_{\mathbf{z_{st}}}} = \begin{bmatrix} G_{x_{sn_{z_{st}}}} & G_{y_{sn_{z_{st}}}} & G_{z_{sn_{z_{st}}}} \end{bmatrix}^T \qquad \mathbf{T}_{\mathbf{sn}_{\mathbf{z_{st}}}/\mathbf{i2}_{\mathbf{z_{st}}}} = \begin{bmatrix} 1 & 0 & 0 \\ 0 & \cos(C_{z_{st}}) & \sin(C_{z_{st}}) \\ 0 & -\sin(C_{z_{st}}) & \cos(C_{z_{st}}) \end{bmatrix}$$

The gravitational acceleration vector expressed in the three sensor fixed reference frames in terms of the sting fixed gravity vector is obtained by combining Equations (III-B.7)-(III-B.12), or

$$\mathbf{G}_{\mathbf{sn}_{\mathbf{x_{st}}}} = \underbrace{\mathbf{T}_{\mathbf{sn}_{\mathbf{x_{st}}}/\mathbf{i2}_{\mathbf{x_{st}}}} \mathbf{T}_{\mathbf{i2}_{\mathbf{x_{st}}}/\mathbf{st}}}_{\mathbf{T}_{\mathbf{sn}_{\mathbf{x_{st}}}/\mathbf{st}}} \mathbf{G}_{\mathbf{st}} \qquad \mathbf{G}_{\mathbf{sn}_{\mathbf{y_{st}}}} = \underbrace{\mathbf{T}_{\mathbf{sn}_{\mathbf{y_{st}}}/\mathbf{i2}_{\mathbf{y_{st}}}} \mathbf{T}_{\mathbf{i2}_{\mathbf{y_{st}}}/\mathbf{st}}}_{\mathbf{T}_{\mathbf{sn}_{\mathbf{y_{st}}}/\mathbf{st}}} \mathbf{G}_{\mathbf{st}}$$

$$\mathbf{G}_{\mathbf{sn}_{\mathbf{z_{st}}}} = \underbrace{\mathbf{T}_{\mathbf{sn}_{\mathbf{z_{st}}}/\mathbf{i2}_{\mathbf{z_{st}}}} \mathbf{T}_{\mathbf{i2}_{\mathbf{z_{st}}}/\mathbf{st}}}_{\mathbf{T}_{\mathbf{sn}_{\mathbf{z_{st}}}/\mathbf{st}}} \mathbf{G}_{\mathbf{st}} \tag{III-B.13}$$

The overall transformation matrices $\mathbf{T}_{\mathbf{sn}_{\mathbf{x_{st}}}/\mathbf{st}}$, $\mathbf{T}_{\mathbf{sn}_{\mathbf{y_{st}}}/\mathbf{st}}$, and $\mathbf{T}_{\mathbf{sn}_{\mathbf{z_{st}}}/\mathbf{st}}$ from sting fixed to sensor fixed axes in Equation (III-B.13) are obtained from a product of the component transformation matrices. Note only the x, y, and z components, respectively, in these three vector expressions are of interest. Extracting these three components and constructing a new vector relationship yields Equation (III-B.14).

$$\mathbf{G}_{\mathbf{sn}_{\mathbf{st}}} = \mathbf{T}_{\mathbf{sn}_{\mathbf{st}}/\mathbf{st}} \mathbf{G}_{\mathbf{st}}$$

$$\mathbf{G}_{\mathbf{sn}_{\mathbf{st}}} = \begin{bmatrix} G_{x_{sn_{st}}} & G_{y_{sn_{st}}} & G_{z_{sn_{st}}} \end{bmatrix}^T \qquad \mathbf{T}_{\mathbf{sn}_{\mathbf{st}}/\mathbf{st}} = \begin{bmatrix} \mathbf{T}_{\mathbf{sn}_{\mathbf{x_{st}}}/\mathbf{st}_1} \\ \mathbf{T}_{\mathbf{sn}_{\mathbf{y_{st}}}/\mathbf{st}_2} \\ \mathbf{T}_{\mathbf{sn}_{\mathbf{z_{st}}}/\mathbf{st}_3} \end{bmatrix} \tag{III-B.14}$$

In Equation (III-B.14), $\mathbf{T}_{\mathbf{sn}_{\mathbf{x_{st}}}/\mathbf{st}_1}$, $\mathbf{T}_{\mathbf{sn}_{\mathbf{y_{st}}}/\mathbf{st}_2}$, and $\mathbf{T}_{\mathbf{sn}_{\mathbf{z_{st}}}/\mathbf{st}_3}$ denote the first, second, and third rows of $\mathbf{T}_{\mathbf{sn}_{\mathbf{x_{st}}}/\mathbf{st}}$, $\mathbf{T}_{\mathbf{sn}_{\mathbf{y_{st}}}/\mathbf{st}}$, and $\mathbf{T}_{\mathbf{sn}_{\mathbf{z_{st}}}/\mathbf{st}}$, respectively. Consequently, $\mathbf{T}_{\mathbf{sn}_{\mathbf{st}}/\mathbf{st}}$, is not a true coordinate transformation matrix in the rigorous sense.

Azimuth and coning angle misalignment effects must also be applied to the accelerometer sensor package associated with the model fixed reference frame. The development is highly similar to Equations (III-B.7)-(III-B.14) in that each axis must be treated individually, and a sequential transformation of first azimuth rotation and second coning rotation is considered. Details of this process will not be discussed but are expressed in Equations (III-B.15)-(III-B.22).

$$\mathbf{G}_{\mathbf{i2}_{\mathbf{x_m}}} = \mathbf{T}_{\mathbf{i2}_{\mathbf{x_m}}/\mathbf{m}} \mathbf{G}_{\mathbf{m}} \tag{III-B.15}$$

$$\mathbf{G}_{\mathbf{i2}_{\mathbf{x_m}}} = \begin{bmatrix} G_{x_{i2_{x_m}}} & G_{y_{i2_{x_m}}} & G_{z_{i2_{x_m}}} \end{bmatrix}^T \quad \mathbf{T}_{\mathbf{i2}_{\mathbf{x_m}}/\mathbf{m}} = \begin{bmatrix} 1 & 0 & 0 \\ 0 & \cos(A_{x_m}) & \sin(A_{x_m}) \\ 0 & -\sin(A_{x_m}) & \cos(A_{x_m}) \end{bmatrix}$$

$$\mathbf{G}_{\mathbf{sn}_{\mathbf{x_m}}} = \mathbf{T}_{\mathbf{sn}_{\mathbf{x_m}}/\mathbf{i2}_{\mathbf{x_m}}} \mathbf{G}_{\mathbf{i2}_{\mathbf{x_m}}} \tag{III-B.16}$$

$$\mathbf{G}_{\mathbf{sn}_{\mathbf{x_m}}} = \begin{bmatrix} G_{x_{sn_{x_m}}} & G_{y_{sn_{x_m}}} & G_{z_{sn_{x_m}}} \end{bmatrix}^T \quad \mathbf{T}_{\mathbf{sn}_{\mathbf{x_m}}/\mathbf{i2}_{\mathbf{x_m}}} = \begin{bmatrix} \cos(C_{x_m}) & 0 & -\sin(C_{x_m}) \\ 0 & 1 & 0 \\ \sin(C_{x_m}) & 0 & \cos(C_{x_m}) \end{bmatrix}$$

$$\mathbf{G}_{\mathbf{i2}_{\mathbf{y_m}}} = \mathbf{T}_{\mathbf{i2}_{\mathbf{y_m}}/\mathbf{m}} \mathbf{G}_{\mathbf{m}} \tag{III-B.17}$$

$$\mathbf{G}_{\mathbf{i2}_{\mathbf{y_m}}} = \begin{bmatrix} G_{x_{i2_{y_m}}} & G_{y_{i2_{y_m}}} & G_{z_{i2_{y_m}}} \end{bmatrix}^T \quad \mathbf{T}_{\mathbf{i2}_{\mathbf{y_m}}/\mathbf{m}} = \begin{bmatrix} \cos(A_{y_m}) & 0 & -\sin(A_{y_m}) \\ 0 & 1 & 0 \\ \sin(A_{y_m}) & 0 & \cos(A_{y_m}) \end{bmatrix}$$

$$\mathbf{G}_{\mathbf{sn}_{\mathbf{y_m}}} = \mathbf{T}_{\mathbf{sn}_{\mathbf{y_m}}/\mathbf{i2}_{\mathbf{y_m}}} \mathbf{G}_{\mathbf{i2}_{\mathbf{y_m}}} \tag{III-B.18}$$

$$\mathbf{G}_{\mathbf{sn}_{\mathbf{y_m}}} = \begin{bmatrix} G_{x_{sn_{y_m}}} & G_{y_{sn_{y_m}}} & G_{z_{sn_{y_m}}} \end{bmatrix}^T \quad \mathbf{T}_{\mathbf{sn}_{\mathbf{y_m}}/\mathbf{i2}_{\mathbf{y_m}}} = \begin{bmatrix} \cos(C_{y_m}) & \sin(C_{y_m}) & 0 \\ -\sin(C_{y_m}) & \cos(C_{y_m}) & 0 \\ 0 & 0 & 1 \end{bmatrix}$$

$$\mathbf{G}_{\mathbf{i2}_{\mathbf{z_m}}} = \mathbf{T}_{\mathbf{i2}_{\mathbf{z_m}}/\mathbf{m}} \mathbf{G}_{\mathbf{m}} \tag{III-B.19}$$

$$\mathbf{G}_{\mathbf{i2}_{\mathbf{z_m}}} = \begin{bmatrix} G_{x_{i2_{z_m}}} & G_{y_{i2_{z_m}}} & G_{z_{i2_{z_m}}} \end{bmatrix}^T \quad \mathbf{T}_{\mathbf{i2}_{\mathbf{z_m}}/\mathbf{m}} = \begin{bmatrix} \cos(A_{z_m}) & \sin(A_{z_m}) & 0 \\ -\sin(A_{z_m}) & \cos(A_{z_m}) & 0 \\ 0 & 0 & 1 \end{bmatrix}$$

$$\mathbf{G}_{\mathbf{sn}_{\mathbf{z_m}}} = \mathbf{T}_{\mathbf{sn}_{\mathbf{z_m}}/\mathbf{i2}_{\mathbf{z_m}}} \mathbf{G}_{\mathbf{i2}_{\mathbf{z_m}}} \tag{III-B.20}$$

$$\mathbf{G}_{\mathbf{sn}_{\mathbf{z_m}}} = \begin{bmatrix} G_{x_{sn_{z_m}}} & G_{y_{sn_{z_m}}} & G_{z_{sn_{z_m}}} \end{bmatrix}^T \qquad \mathbf{T}_{\mathbf{sn}_{\mathbf{z_m}}/\mathbf{i2}_{\mathbf{z_m}}} = \begin{bmatrix} 1 & 0 & 0 \\ 0 & \cos(C_{z_m}) & \sin(C_{z_m}) \\ 0 & -\sin(C_{z_m}) & \cos(C_{z_m}) \end{bmatrix}$$

$$\mathbf{G}_{\mathbf{sn}_{\mathbf{x_m}}} = \underbrace{\mathbf{T}_{\mathbf{sn}_{\mathbf{x_m}}/\mathbf{i2}_{\mathbf{x_m}}} \mathbf{T}_{\mathbf{i2}_{\mathbf{x_m}}/\mathbf{m}}}_{\mathbf{T}_{\mathbf{sn}_{\mathbf{x_m}}/\mathbf{m}}} \mathbf{G}_{\mathbf{m}} \qquad \mathbf{G}_{\mathbf{sn}_{\mathbf{y_m}}} = \underbrace{\mathbf{T}_{\mathbf{sn}_{\mathbf{y_m}}/\mathbf{i2}_{\mathbf{y_m}}} \mathbf{T}_{\mathbf{i2}_{\mathbf{y_m}}/\mathbf{m}}}_{\mathbf{T}_{\mathbf{sn}_{\mathbf{y_m}}/\mathbf{m}}} \mathbf{G}_{\mathbf{m}}$$

$$\mathbf{G}_{\mathbf{sn}_{\mathbf{z_m}}} = \underbrace{\mathbf{T}_{\mathbf{sn}_{\mathbf{z_m}}/\mathbf{i2}_{\mathbf{z_m}}} \mathbf{T}_{\mathbf{i2}_{\mathbf{z_m}}/\mathbf{m}}}_{\mathbf{T}_{\mathbf{sn}_{\mathbf{z_m}}/\mathbf{m}}} \mathbf{G}_{\mathbf{m}} \qquad \text{(III-B.21)}$$

$$\mathbf{G}_{\mathbf{sn_m}} = \mathbf{T}_{\mathbf{sn_m/m}} \mathbf{G}_{\mathbf{m}} \qquad \mathbf{T}_{\mathbf{sn_m/m}} = \begin{bmatrix} \mathbf{T}_{\mathbf{sn}_{\mathbf{x_m}}/\mathbf{m_1}} \\ \mathbf{T}_{\mathbf{sn}_{\mathbf{y_m}}/\mathbf{m_2}} \\ \mathbf{T}_{\mathbf{sn}_{\mathbf{z_m}}/\mathbf{m_3}} \end{bmatrix}$$

$$\mathbf{G}_{\mathbf{sn_m}} = \begin{bmatrix} G_{x_{sn_m}} & G_{y_{sn_m}} & G_{z_{sn_m}} \end{bmatrix}^T \qquad \text{(III-B.22)}$$

Finally consider bias and sensitivity characteristics of the sensor packages. The sting fixed and model fixed accelerometer sensor package bias and sensitivity characteristics are modeled by the following relationships.

$$\mathbf{V}_{\mathbf{sn_{st}}} = \mathbf{B}_{\mathbf{sn_{st}}} + \mathbf{S}_{\mathbf{sn_{st}}} \mathbf{G}_{\mathbf{sn_{st}}}$$

$$\mathbf{V}_{\mathbf{sn_{st}}} = \begin{bmatrix} V_{x_{sn_{st}}} & V_{y_{sn_{st}}} & V_{z_{sn_{st}}} \end{bmatrix}^T \qquad \mathbf{S}_{\mathbf{sn_{st}}} = \begin{bmatrix} S_{x_{sn_{st}}} & 0 & 0 \\ 0 & S_{y_{sn_{st}}} & 0 \\ 0 & 0 & S_{z_{sn_{st}}} \end{bmatrix} \qquad \text{(III-B.23)}$$

$$\mathbf{B}_{\mathbf{sn_{st}}} = \begin{bmatrix} B_{x_{sn_{st}}} & B_{y_{sn_{st}}} & B_{z_{sn_{st}}} \end{bmatrix}^T$$

$$\mathbf{V}_{\mathbf{sn_m}} = \mathbf{B}_{\mathbf{sn_m}} + \mathbf{S}_{\mathbf{sn_m}} \mathbf{G}_{\mathbf{sn_m}}$$

$$\mathbf{V}_{\mathbf{sn_m}} = \begin{bmatrix} V_{x_{sn_m}} & V_{y_{sn_m}} & V_{z_{sn_m}} \end{bmatrix}^T \qquad \mathbf{S}_{\mathbf{sn_m}} = \begin{bmatrix} S_{x_{sn_m}} & 0 & 0 \\ 0 & S_{y_{sn_m}} & 0 \\ 0 & 0 & S_{z_{sn_m}} \end{bmatrix} \qquad \text{(III-B.24)}$$

$$\mathbf{B}_{\mathbf{sn_m}} = \begin{bmatrix} B_{x_{sn_m}} & B_{y_{sn_m}} & B_{z_{sn_m}} \end{bmatrix}^T$$

In Equations (III-B.23)-(III-B.24), $\mathbf{V_{sn_i}}$ denotes the sensor package output voltage vector, $V_{x_{sn_i}}$-$V_{y_{sn_i}}$-$V_{z_{sn_i}}$ denote components of $\mathbf{V_{sn_i}}$, $\mathbf{B_{sn_i}}$ denotes the sensor package bias vector, $B_{x_{sn_i}}$-$B_{y_{sn_i}}$-$B_{z_{sn_i}}$ denote components of $\mathbf{B_{sn_i}}$, $\mathbf{S_{sn_i}}$ denotes the sensor package diagonal sensitivity matrix, $S_{x_{sn_i}}$-$S_{y_{sn_i}}$-$S_{z_{sn_i}}$ denote components of $\mathbf{S_{sn_i}}$, and i = st, m for the sting fixed and model fixed sensor packages. $\mathbf{V_{sn_{st}}}$ and $\mathbf{V_{sn_m}}$ are considered to be known vectors outputed by the sensors.

Overall vector expressions for the accelerometer sensor packages are obtained by combining Equations (III-B.6), (III-B.14), and (III-B.23) and (III-B.5), (III-B.22), and (III-B.24). These expressions are

$$\mathbf{V_{sn_{st}}} = \mathbf{B_{sn_{st}}} + \mathbf{S_{sn_{st}}}\mathbf{T_{sn_{st}/st}}\mathbf{T_{st/t}}\mathbf{G_t} \tag{III-B.25}$$

$$\mathbf{V_{sn_m}} = \mathbf{B_{sn_m}} + \mathbf{S_{sn_m}}\mathbf{T_{sn_m/m}}\mathbf{T_{m/st}}\mathbf{G_{st}} \tag{III-B.26}$$

In scalar form, Equations (III-B.25)-(III-B.26) become

$$V_{x_{sn_{st}}} = B_{x_{sn_{st}}} + S_{x_{sn_{st}}}\{-C_{C_{x_{st}}}S_\Theta C_\Psi + S_{A_{x_{st}}}S_{C_{x_{st}}}S_\Theta S_\Psi - C_{A_{x_{st}}}S_{C_{x_{st}}}C_\Theta\}G \tag{III-B.27}$$

$$V_{y_{sn_{st}}} = B_{y_{sn_{st}}} + S_{y_{sn_{st}}}\{C_{A_{y_{st}}}S_{C_{y_{st}}}S_\Theta C_\Psi + C_{C_{y_{st}}}S_\Theta S_\Psi + S_{A_{y_{st}}}S_{C_{y_{st}}}C_\Theta\}G \tag{III-B.28}$$

$$V_{z_{sn_{st}}} = B_{z_{sn_{st}}} + S_{z_{sn_{st}}}\{-S_{A_{z_{st}}}S_{C_{z_{st}}}S_\Theta C_\Psi - C_{A_{z_{st}}}S_{C_{z_{st}}}S_\Theta S_\Psi + C_{C_{z_{st}}}C_\Theta\}G \tag{III-B.29}$$

$$\begin{aligned} V_{x_{sn_m}} = {} & B_{x_{sn_m}} + S_{x_{sn_m}}\{(C_{C_{x_m}})G_{x_{st}} + (S_{A_{x_m}}S_{C_{x_m}}C_\Phi + C_{A_{x_m}}S_{C_{x_m}}S_\Phi)G_{y_{st}} \\ & + (S_{A_{x_m}}S_{C_{x_m}}S_\Phi - C_{A_{x_m}}S_{C_{x_m}}C_\Phi)G_{z_{st}}\} \end{aligned} \tag{III-B.30}$$

$$\begin{aligned} V_{y_{sn_m}} = {} & B_{y_{sn_m}} + S_{y_{sn_m}}\{(-C_{A_{y_m}}S_{C_{y_m}})G_{x_{st}} + (C_{C_{y_m}}C_\Phi - S_{A_{y_m}}S_{C_{y_m}}S_\Phi)G_{y_{st}} \\ & + (C_{C_{y_m}}S_\Phi + S_{A_{y_m}}S_{C_{y_m}}C_\Phi)G_{z_{st}}\} \end{aligned} \tag{III-B.31}$$

$$\begin{aligned} V_{z_{sn_m}} = {} & B_{z_{sn_m}} + S_{z_{sn_m}}\{(S_{A_{z_m}}S_{C_{z_m}})G_{x_{st}} + (-C_{A_{z_m}}S_{C_{z_m}}C_\Phi - C_{C_{z_m}}S_\Phi)G_{y_{st}} \\ & + (-C_{A_{z_m}}S_{C_{z_m}}S_\Phi + C_{C_{z_m}}C_\Phi)G_{z_{st}}\} \end{aligned} \tag{III-B.32}$$

where the notation C_α and S_α denote $\cos(\alpha)$ and $\sin(\alpha)$. Equations (III-B.27)-(III-B.32) provide the underlying analytical framework between the multi-axis gravitational acceleration measurement data in voltage form and the desired three dimensional Eulerian angular state of the

test model. These expressions contain both calibration parameters and the rotation angles, and provide the basis for accelerometer sensor calibration and attitude construction logic presented in Section IV.

C. Gyro Equations

Derivation of the underlying analytical framework between multi-axis angular rate data measured by a single rate gyro sensor package and the desired three dimensional Eulerian angular state of the test model is considered in this subsection. This analytical framework provides the basis for gyro sensor calibration and attitude construction logic presented in Section IV. With the geometry described in Figure 4, the angular velocity vector (algebraic form) of the model expressed in the model fixed reference frame is

$$\boldsymbol{\Omega}_{\mathbf{m}} = \left[\Omega_{x_m}\ \Omega_{y_m}\ \Omega_{z_m}\right]^T \tag{III-C.1}$$

where Ω_{x_m}-Ω_{y_m}-Ω_{z_m} denote the model angular velocity components. $\boldsymbol{\Omega}_{\mathbf{m}}$ is considered to be a known vector outputed by the sensors (or determined from the sensor outputs). Extraction of the complete pitch-yaw-roll orientation state from an angular rate measurement and integration scheme employing a single gyro sensor package is feasible. Therefore, in the general framework of this research, angular velocity will only be measured in the model fixed axes using a single gyro sensor package. By relating these measured angular rate components with the temporal rates of change of the Euler rotation angles, the full angular state can be determined. This approach is applied to development of the general angular measurement system. A simplified case corresponding to the 31-Inch Hypersonic Tunnel Application (fixed known roll angle) can always be extracted from the general framework.

Based on the pitch-yaw-roll rotation sequence, the angular velocity vector can be built-up from the component rotation rates, or

$$\boldsymbol{\Omega}_{\mathbf{m}} = \mathbf{T}_{\mathbf{m/i1}}\dot{\boldsymbol{\Theta}}_{\mathbf{i1}} + \mathbf{T}_{\mathbf{m/st}}\dot{\boldsymbol{\Psi}}_{\mathbf{st}} + \mathbf{T}_{\mathbf{m/m}}\dot{\boldsymbol{\Phi}}_{\mathbf{m}} \tag{III-C.2}$$

$$\dot{\boldsymbol{\Theta}}_{i1} = \begin{bmatrix} 0 & \dot{\Theta} & 0 \end{bmatrix}^T \qquad \dot{\boldsymbol{\Psi}}_{st} = \begin{bmatrix} 0 & 0 & \dot{\Psi} \end{bmatrix}^T \qquad \dot{\boldsymbol{\Phi}}_{m} = \begin{bmatrix} \dot{\Phi} & 0 & 0 \end{bmatrix}^T \tag{III-C.3}$$

$$\mathbf{T}_{m/i1} = \mathbf{T}_{m/st}\mathbf{T}_{st/i1} \qquad \mathbf{T}_{m/m} = \mathbf{I} \tag{III-C.4}$$

$$\mathbf{T}_{st/i1} = \begin{bmatrix} \cos(\Psi) & \sin(\Psi) & 0 \\ -\sin(\Psi) & \cos(\Psi) & 0 \\ 0 & 0 & 1 \end{bmatrix} \qquad \mathbf{T}_{m/st} = \begin{bmatrix} 1 & 0 & 0 \\ 0 & \cos(\Phi) & \sin(\Phi) \\ 0 & -\sin(\Phi) & \cos(\Phi) \end{bmatrix} \tag{III-C.5}$$

Note Euler pitch rate $\dot{\Theta}$ is executed about the first intermediate y axis (y_{i1}), Euler yaw rate $\dot{\Psi}$ is executed about the sting z axis (z_{st}), and Euler roll rate $\dot{\Phi}$ is executed about the model x axis (x_m). In Equation (III-C.2), $\mathbf{T_{m/m}}$ is the identity matrix, and $\mathbf{T_{m/i1}}$ is computed from the component transformation matrices $\mathbf{T_{st/i1}}$ and $\mathbf{T_{m/st}}$.

Now consider effects from misalignment errors due to the azimuth and coning angles in the model mounted gyro sensor package. The following analysis must be conducted individually for each desired measurement axis. First consider the model x_m axis as the desired measurement axis. A sequential transformation consisting first of azimuth rotation (A_{x_m}) about x_m leading to a second intermediate frame, and next of coning rotation (C_{x_m}) about the intermediate y axis which leads to the true measurement or sensor fixed reference frame ($x_{sn_{x_m}} y_{sn_{x_m}} z_{sn_{x_m}}$) associated with x_m, is implemented. For the y_m axis, azimuth rotation (A_{y_m}) is about y_m and coning rotation (C_{y_m}) is about the intermediate z axis leading to the y_m specific sensor fixed axes ($x_{sn_{y_m}} y_{sn_{y_m}} z_{sn_{y_m}}$). Finally, for the z_m axis, azimuth rotation (A_{z_m}) is about z_m and coning rotation (C_{z_m}) is about the intermediate x axis leading to the z_m specific sensor fixed axes ($x_{sn_{z_m}} y_{sn_{z_m}} z_{sn_{z_m}}$). These transformation relationships are summarized in Equations (III-C.6)-(III-C.11) where $\boldsymbol{\Omega_i}$ is the model angular velocity expressed in frame i, Ω_{x_i}-Ω_{y_i}-Ω_{z_i} are the components of $\boldsymbol{\Omega_i}$, and $\mathbf{T_{i/j}}$ is the transformation matrix from frame j to frame i. Here i, j = m, $i2_k$, sn_k representing model fixed, second intermediate, and sensor fixed axes, respectively, and k = x_m, y_m, and z_m.

$$\boldsymbol{\Omega}_{i2_{x_m}} = \mathbf{T}_{i2_{x_m}/m}\boldsymbol{\Omega}_m \tag{III-C.6}$$

$$\boldsymbol{\Omega}_{i2_{x_m}} = \begin{bmatrix} \Omega_{x_{i2_{x_m}}} & \Omega_{y_{i2_{x_m}}} & \Omega_{z_{i2_{x_m}}} \end{bmatrix}^T \qquad \mathbf{T}_{i2_{x_m}/m} = \begin{bmatrix} 1 & 0 & 0 \\ 0 & \cos(A_{x_m}) & \sin(A_{x_m}) \\ 0 & -\sin(A_{x_m}) & \cos(A_{x_m}) \end{bmatrix}$$

$$\boldsymbol{\Omega}_{sn_{x_m}} = \mathbf{T}_{sn_{x_m}/i2_{x_m}} \boldsymbol{\Omega}_{i2_{x_m}} \tag{III-C.7}$$

$$\boldsymbol{\Omega}_{sn_{x_m}} = \begin{bmatrix} \Omega_{x_{sn_{x_m}}} & \Omega_{y_{sn_{x_m}}} & \Omega_{z_{sn_{x_m}}} \end{bmatrix}^T \qquad \mathbf{T}_{sn_{x_m}/i2_{x_m}} = \begin{bmatrix} \cos(C_{x_m}) & 0 & -\sin(C_{x_m}) \\ 0 & 1 & 0 \\ \sin(C_{x_m}) & 0 & \cos(C_{x_m}) \end{bmatrix}$$

$$\boldsymbol{\Omega}_{i2_{y_m}} = \mathbf{T}_{i2_{y_m}/m} \boldsymbol{\Omega}_m \tag{III-C.8}$$

$$\boldsymbol{\Omega}_{i2_{y_m}} = \begin{bmatrix} \Omega_{x_{i2_{y_m}}} & \Omega_{y_{i2_{y_m}}} & \Omega_{z_{i2_{y_m}}} \end{bmatrix}^T \qquad \mathbf{T}_{i2_{y_m}/m} = \begin{bmatrix} \cos(A_{y_m}) & 0 & -\sin(A_{y_m}) \\ 0 & 1 & 0 \\ \sin(A_{y_m}) & 0 & \cos(A_{y_m}) \end{bmatrix}$$

$$\boldsymbol{\Omega}_{sn_{y_m}} = \mathbf{T}_{sn_{y_m}/i2_{y_m}} \boldsymbol{\Omega}_{i2_{y_m}} \tag{III-C.9}$$

$$\boldsymbol{\Omega}_{sn_{y_m}} = \begin{bmatrix} \Omega_{x_{sn_{y_m}}} & \Omega_{y_{sn_{y_m}}} & \Omega_{z_{sn_{y_m}}} \end{bmatrix}^T \qquad \mathbf{T}_{sn_{y_m}/i2_{y_m}} = \begin{bmatrix} \cos(C_{y_m}) & \sin(C_{y_m}) & 0 \\ -\sin(C_{y_m}) & \cos(C_{y_m}) & 0 \\ 0 & 0 & 1 \end{bmatrix}$$

$$\boldsymbol{\Omega}_{i2_{z_m}} = \mathbf{T}_{i2_{z_m}/m} \boldsymbol{\Omega}_m \tag{III-C.10}$$

$$\boldsymbol{\Omega}_{i2_{z_m}} = \begin{bmatrix} \Omega_{x_{i2_{z_m}}} & \Omega_{y_{i2_{z_m}}} & \Omega_{z_{i2_{z_m}}} \end{bmatrix}^T \qquad \mathbf{T}_{i2_{z_m}/m} = \begin{bmatrix} \cos(A_{z_m}) & \sin(A_{z_m}) & 0 \\ -\sin(A_{z_m}) & \cos(A_{z_m}) & 0 \\ 0 & 0 & 1 \end{bmatrix}$$

$$\boldsymbol{\Omega}_{sn_{z_m}} = \mathbf{T}_{sn_{z_m}/i2_{z_m}} \boldsymbol{\Omega}_{i2_{z_m}} \tag{III-C.11}$$

$$\boldsymbol{\Omega}_{sn_{z_m}} = \begin{bmatrix} \Omega_{x_{sn_{z_m}}} & \Omega_{y_{sn_{z_m}}} & \Omega_{z_{sn_{z_m}}} \end{bmatrix}^T \qquad \mathbf{T}_{sn_{z_m}/i2_{z_m}} = \begin{bmatrix} 1 & 0 & 0 \\ 0 & \cos(C_{z_m}) & \sin(C_{z_m}) \\ 0 & -\sin(C_{z_m}) & \cos(C_{z_m}) \end{bmatrix}$$

The angular velocity vector expressed in the three sensor fixed reference frames in terms of the model fixed angular rate vector is obtained by combining Equations (III-C.6)-(III-C.11), or

$$\boldsymbol{\Omega}_{sn_{x_m}} = \underbrace{\mathbf{T}_{sn_{x_m}/i2_{x_m}} \mathbf{T}_{i2_{x_m}/m}}_{\mathbf{T}_{sn_{x_m}/m}} \boldsymbol{\Omega}_m \qquad \boldsymbol{\Omega}_{sn_{y_m}} = \underbrace{\mathbf{T}_{sn_{y_m}/i2_{y_m}} \mathbf{T}_{i2_{y_m}/m}}_{\mathbf{T}_{sn_{y_m}/m}} \boldsymbol{\Omega}_m$$

$$\boldsymbol{\Omega}_{sn_{z_m}} = \underbrace{\mathbf{T}_{sn_{z_m}/i2_{z_m}} \mathbf{T}_{i2_{z_m}/m}}_{\mathbf{T}_{sn_{z_m}/m}} \boldsymbol{\Omega}_m \tag{III-C.12}$$

The overall transformation matrices $\mathbf{T}_{sn_{x_m}/m}$, $\mathbf{T}_{sn_{y_m}/m}$, and $\mathbf{T}_{sn_{z_m}/m}$ from model fixed to sensor fixed axes in Equation (III-C.12) are obtained from a product of the component transformation matrices. Note only the x, y, and z components, respectively, in these three vector expressions are of interest. Extracting these three components and constructing a new vector relationship yields Equation (III-C.13).

$$\boldsymbol{\Omega}_{sn_m} = \mathbf{T}_{sn_m/m} \boldsymbol{\Omega}_m$$

$$\boldsymbol{\Omega}_{sn_m} = \begin{bmatrix} \Omega_{x_{sn_m}} & \Omega_{y_{sn_m}} & \Omega_{z_{sn_m}} \end{bmatrix}^T \qquad \mathbf{T}_{sn_m/m} = \begin{bmatrix} \mathbf{T}_{sn_{x_m}/m_1} \\ \mathbf{T}_{sn_{y_m}/m_2} \\ \mathbf{T}_{sn_{z_m}/m_3} \end{bmatrix} \tag{III-C.13}$$

In Equation (III-C.13), $\mathbf{T}_{sn_{x_m}/m_1}$, $\mathbf{T}_{sn_{y_m}/m_2}$, and $\mathbf{T}_{sn_{z_m}/m_3}$ denote the first, second, and third rows of $\mathbf{T}_{sn_{x_m}/m}$, $\mathbf{T}_{sn_{y_m}/m}$, and $\mathbf{T}_{sn_{z_m}/m}$, respectively. Consequently, $\mathbf{T}_{sn_m/m}$, is not a true coordinate transformation matrix in the rigorous sense.

Finally consider bias and sensitivity characteristics of the sensor package. The model fixed gyro sensor package bias and sensitivity characteristics are modeled by the following relationships.

$$\mathbf{V}_{sn_m} = \mathbf{B}_{sn_m} + \mathbf{S}_{sn_m} \boldsymbol{\Omega}_{sn_m}$$

$$\mathbf{V}_{sn_m} = \begin{bmatrix} V_{x_{sn_m}} & V_{y_{sn_m}} & V_{z_{sn_m}} \end{bmatrix}^T \qquad \mathbf{S}_{sn_m} = \begin{bmatrix} S_{x_{sn_m}} & 0 & 0 \\ 0 & S_{y_{sn_m}} & 0 \\ 0 & 0 & S_{z_{sn_m}} \end{bmatrix} \tag{III-C.14}$$

$$\mathbf{B}_{sn_m} = \begin{bmatrix} B_{x_{sn_m}} & B_{y_{sn_m}} & B_{z_{sn_m}} \end{bmatrix}^T$$

In Equation (III-C.14), $\mathbf{V}_{sn_m}$ denotes the sensor package output voltage vector, $V_{x_{sn_m}}$-$V_{y_{sn_m}}$-$V_{z_{sn_m}}$ denote components of $\mathbf{V}_{sn_m}$, $\mathbf{B}_{sn_m}$ denotes the sensor package bias vector, $B_{x_{sn_m}}$-$B_{y_{sn_m}}$-$B_{z_{sn_m}}$ denote components of $\mathbf{B}_{sn_m}$, $\mathbf{S}_{sn_m}$ denotes the sensor package diagonal sensitivity matrix,

and $S_{x_{sn_m}}$-$S_{y_{sn_m}}$-$S_{z_{sn_m}}$ denote components of $\mathbf{S_{sn_m}}$. $\mathbf{V_{sn_m}}$ is considered to be a known vector outputed by the sensor.

An overall vector expression for the gyro sensor package is obtained by combining Equations (III-C.2), (III-C.13), and (III-C.14). This expression is

$$\mathbf{V_{sn_m}} = \mathbf{B_{sn_m}} + \mathbf{S_{sn_m}}\mathbf{T_{sn_m/m}}\{\mathbf{T_{m/i1}}\dot{\boldsymbol{\Theta}}_{\mathbf{i1}} + \mathbf{T_{m/st}}\dot{\boldsymbol{\Psi}}_{\mathbf{st}} + \mathbf{T_{m/m}}\dot{\boldsymbol{\Phi}}_{\mathbf{m}}\} \qquad \text{(III-C.15)}$$

In scalar form, Equation (III-C.15) becomes

$$\begin{aligned} V_{x_{sn_m}} = {} & B_{x_{sn_m}} + S_{x_{sn_m}}\{(C_{C_{x_m}}S_{\Psi} + S_{A_{x_m}}S_{C_{x_m}}C_{\Psi}C_{\Phi} + C_{A_{x_m}}S_{C_{x_m}}C_{\Psi}S_{\Phi})\dot{\Theta} \\ & + (S_{A_{x_m}}S_{C_{x_m}}S_{\Phi} - C_{A_{x_m}}S_{C_{x_m}}C_{\Phi})\dot{\Psi} + (C_{C_{x_m}})\dot{\Phi}\} \end{aligned} \qquad \text{(III-C.16)}$$

$$\begin{aligned} V_{y_{sn_m}} = {} & B_{y_{sn_m}} + S_{y_{sn_m}}\{(-C_{A_{y_m}}S_{C_{y_m}}S_{\Psi} + C_{C_{y_m}}C_{\Psi}C_{\Phi} - S_{A_{y_m}}S_{C_{y_m}}C_{\Psi}S_{\Phi})\dot{\Theta} \\ & + (C_{C_{y_m}}S_{\Phi} + S_{A_{y_m}}S_{C_{y_m}}C_{\Phi})\dot{\Psi} + (-C_{A_{y_m}}S_{C_{y_m}})\dot{\Phi}\} \end{aligned} \qquad \text{(III-C.17)}$$

$$\begin{aligned} V_{z_{sn_m}} = {} & B_{z_{sn_m}} + S_{z_{sn_m}}\{(S_{A_{z_m}}S_{C_{z_m}}S_{\Psi} - C_{A_{z_m}}S_{C_{z_m}}C_{\Psi}C_{\Phi} - C_{C_{z_m}}C_{\Psi}S_{\Phi})\dot{\Theta} \\ & + (-C_{A_{z_m}}S_{C_{z_m}}S_{\Phi} + C_{C_{z_m}}C_{\Phi})\dot{\Psi} + (S_{A_{z_m}}S_{C_{z_m}})\dot{\Phi}\} \end{aligned} \qquad \text{(III-C.18)}$$

Equations (III-C.16)-(III-C.18) provide the underlying analytical framework between the multi-axis angular rate measurement data in voltage form and the temporal rate of change of the desired three dimensional Eulerian angular state of the test model. These expressions contain both calibration parameters and the rotation angles and their time derivatives, and provide the basis for gyro sensor calibration and attitude construction logic presented in Section IV.

Section IV
Sensor Calibration and Attitude Construction

A. Accelerometer Sensor Calibration

Before the AMS prototype can be used in the attitude construction mode, the accelerometer sensor packages must be calibrated. A consistent set of sensor output voltages and pitch-yaw-roll excitation angles, obtained from a controlled high-precision laboratory environment, can be used to determine unknown calibration parameters for each of the three accelerometers in both the sting fixed and model fixed packages. Synthetically generated data simulating the laboratory environment, however, will be used for calibration procedure development. Calibration parameters to be addressed include bias ($B_{x_{sn_{st}}}$, $B_{y_{sn_{st}}}$, $B_{z_{sn_{st}}}$, $B_{x_{sn_m}}$, $B_{y_{sn_m}}$, $B_{z_{sn_m}}$), sensitivity ($S_{x_{sn_{st}}}$, $S_{y_{sn_{st}}}$, $S_{z_{sn_{st}}}$, $S_{x_{sn_m}}$, $S_{y_{sn_m}}$, $S_{z_{sn_m}}$), azimuth angle ($A_{x_{st}}$, $A_{y_{st}}$, $A_{z_{st}}$, A_{x_m}, A_{y_m}, A_{z_m}), and coning angle ($C_{x_{st}}$, $C_{y_{st}}$, $C_{z_{st}}$, C_{x_m}, C_{y_m}, C_{z_m}). The calibration parameters for each accelerometer are determined independently but in a sequential fashion. Sting fixed accelerometer sensors are addressed first, and model fixed accelerometer sensors are considered second. If deemed to be important, other sensor imperfections could be incorporated into the calibration procedure. For example, temperature corrections, although judged to be an important factor for the 31-Inch Hypersonic Tunnel application, were not considered in the prototype development stage. However, calibration for thermal effects can be appended to the algorithm presented in this section at a more advanced AMS development stage.

A Gauss-Newton iterative nonlinear regression method outlined in Reference 5 will be used as a basis for accelerometer calibration. Further details of the Gauss-Newton algorithm can be found in Reference 17. Recall the governing sting fixed accelerometer sensor relationships in Equations (III-B.27)-(III-B.29). From a sensor calibration perspective, voltages, angular orientation states, and gravity are known parameters while bias, sensitivity, azimuth angle, and coning angle are unknown variables implying a set of nonlinear algebraic equations must be solved. Implications from sensor model assumptions are that each scalar equation involves only a

single unknown quadruple (bias, sensitivity, azimuth angle, coning angle), allowing an independent solution strategy. Represent any one of the three sting fixed accelerometer sensor relationships as

$$V = F(B, S, A, C, \Theta, \Psi, G) \tag{IV-A.1}$$

where function F denotes the nonlinear functional dependency of voltage V on bias B, sensitivity S, azimuth rotation A, coning rotation C, pitch-yaw angles Θ-Ψ, and gravity G. The right-hand side of this equality can also be expanded in a Taylor series about a reference solution.

$$V = V_r + \frac{\partial F(X,P)}{\partial X}_r (X - X_r) + \ldots \tag{IV-A.2}$$

$$X = \left[B\ S\ A\ C\right]^T \qquad \frac{\partial F(X,P)}{\partial X} = \left[\frac{\partial F}{\partial B}\ \frac{\partial F}{\partial S}\ \frac{\partial F}{\partial A}\ \frac{\partial F}{\partial C}\right] \qquad P = \left[\Theta\ \Psi\ G\right]^T \tag{IV-A.3}$$

In Equation (IV-A.2), X denotes a vector containing the unknown variables, P denotes a vector of known parameters, and subscript "r" denotes evaluation at the known reference condition.

Suppose initial estimates for the bias, sensitivity, azimuth, and coning variables are known and interpreted to be the reference solution X_r in Equation (IV-A.2). Further suppose that a consistent data set of n quadruples for voltage, pitch, yaw, and gravity is available. A single quadruple from this set can be interpreted as V and P appearing in Equation (IV-A.2). Using the reference solution and parameter data, voltage and it's partial derivatives can also be computed from Equation (IV-A.1) and interpreted as V_r and $\partial F(X,P)/\partial X_r$. Construct a vector equivalent to Equation (IV-A.2) using the n×(1+2+1) data set to yield

$$\mathbf{V} = \mathbf{V_r} + \frac{\partial \mathbf{F(X,P)}}{\partial \mathbf{X}}_{\mathbf{r}} (X - X_r) + \ldots \tag{IV-A.4}$$

$$\mathbf{V} = \begin{bmatrix} V_1 \\ V_2 \\ \\ V_n \end{bmatrix} \qquad \mathbf{V_r} = \begin{bmatrix} V_{1_r} \\ V_{2_r} \\ \\ V_{n_r} \end{bmatrix} \qquad \frac{\partial \mathbf{F(X,P)}}{\partial \mathbf{X}}_{\mathbf{r}} = \begin{bmatrix} \frac{\partial F}{\partial B_{1_r}} & \frac{\partial F}{\partial S_{1_r}} & \frac{\partial F}{\partial A_{1_r}} & \frac{\partial F}{\partial C_{1_r}} \\ \frac{\partial F}{\partial B_{2_r}} & \frac{\partial F}{\partial S_{2_r}} & \frac{\partial F}{\partial A_{2_r}} & \frac{\partial F}{\partial C_{2_r}} \\ & & & \\ \frac{\partial F}{\partial B_{n_r}} & \frac{\partial F}{\partial S_{n_r}} & \frac{\partial F}{\partial A_{n_r}} & \frac{\partial F}{\partial C_{n_r}} \end{bmatrix} \qquad \text{(IV-A.5)}$$

Multiply this expression by $\partial \mathbf{F(X,P)}/\partial \mathbf{X_r}^T$ on the left, perform matrix inversion, neglect higher order terms, and rearrange to yield

$$X = X_r + \left(\frac{\partial \mathbf{F(X,P)}}{\partial \mathbf{X}}_{\mathbf{r}}^T \frac{\partial \mathbf{F(X,P)}}{\partial \mathbf{X}}_{\mathbf{r}}\right)^{-1} \frac{\partial \mathbf{F(X,P)}}{\partial \mathbf{X}}_{\mathbf{r}}^T (\mathbf{V} - \mathbf{V_r}) \qquad \text{(IV-A.6)}$$

Equation (IV-A.6) represents the iterative Gauss-Newton regression algorithm. X is computed from Equation (IV-A.6) and reinterpreted as the reference solution for the next computational cycle. This process is repeated until a solution tolerance is met.

For completeness, partial derivatives of Equations (III-B.27)-(III-B.29) are given below. For the sting $x_{sn_{st}}$ axis accelerometer sensor, partial derivatives are

$$\frac{\partial V_{x_{sn_{st}}}}{\partial B_{x_{sn_{st}}}} = 1 \qquad \text{(IV-A.7)}$$

$$\frac{\partial V_{x_{sn_{st}}}}{\partial S_{x_{sn_{st}}}} = \{-C_{C_{x_{st}}} S_\Theta C_\Psi + S_{A_{x_{st}}} S_{C_{x_{st}}} S_\Theta S_\Psi - C_{A_{x_{st}}} S_{C_{x_{st}}} C_\Theta\} G \qquad \text{(IV-A.8)}$$

$$\frac{\partial V_{x_{sn_{st}}}}{\partial A_{x_{st}}} = S_{x_{sn_{st}}} \{C_{A_{x_{st}}} S_{C_{x_{st}}} S_\Theta S_\Psi + S_{A_{x_{st}}} S_{C_{x_{st}}} C_\Theta\} G \qquad \text{(IV-A.9)}$$

$$\frac{\partial V_{x_{sn_{st}}}}{\partial C_{x_{st}}} = S_{x_{sn_{st}}} \{S_{C_{x_{st}}} S_\Theta C_\Psi + S_{A_{x_{st}}} C_{C_{x_{st}}} S_\Theta S_\Psi - C_{A_{x_{st}}} C_{C_{x_{st}}} C_\Theta\} G \qquad \text{(IV-A.10)}$$

For the sting $y_{sn_{st}}$ axis accelerometer sensor, partial derivatives are

$$\frac{\partial V_{y_{sn_{st}}}}{\partial B_{y_{sn_{st}}}} = 1 \tag{IV-A.11}$$

$$\frac{\partial V_{y_{sn_{st}}}}{\partial S_{y_{sn_{st}}}} = \{C_{A_{y_{st}}} S_{C_{y_{st}}} S_\Theta C_\Psi + C_{C_{y_{st}}} S_\Theta S_\Psi + S_{A_{y_{st}}} S_{C_{y_{st}}} C_\Theta\} G \tag{IV-A.12}$$

$$\frac{\partial V_{y_{sn_{st}}}}{\partial A_{y_{st}}} = S_{y_{sn_{st}}} \{- S_{A_{y_{st}}} S_{C_{y_{st}}} S_\Theta C_\Psi + C_{A_{y_{st}}} S_{C_{y_{st}}} C_\Theta\} G \tag{IV-A.13}$$

$$\frac{\partial V_{y_{sn_{st}}}}{\partial C_{y_{st}}} = S_{y_{sn_{st}}} \{C_{A_{y_{st}}} C_{C_{y_{st}}} S_\Theta C_\Psi - S_{C_{y_{st}}} S_\Theta S_\Psi + S_{A_{y_{st}}} C_{C_{y_{st}}} C_\Theta\} G \tag{IV-A.14}$$

For the sting $z_{sn_{st}}$ axis accelerometer sensor, partial derivatives are

$$\frac{\partial V_{z_{sn_{st}}}}{\partial B_{z_{sn_{st}}}} = 1 \tag{IV-A.15}$$

$$\frac{\partial V_{z_{sn_{st}}}}{\partial S_{z_{sn_{st}}}} = \{- S_{A_{z_{st}}} S_{C_{z_{st}}} S_\Theta C_\Psi - C_{A_{z_{st}}} S_{C_{z_{st}}} S_\Theta S_\Psi + C_{C_{z_{st}}} C_\Theta\} G \tag{IV-A.16}$$

$$\frac{\partial V_{z_{sn_{st}}}}{\partial A_{z_{st}}} = S_{z_{sn_{st}}} \{- C_{A_{z_{st}}} S_{C_{z_{st}}} S_\Theta C_\Psi + S_{A_{z_{st}}} S_{C_{z_{st}}} S_\Theta S_\Psi\} G \tag{IV-A.17}$$

$$\frac{\partial V_{z_{sn_{st}}}}{\partial C_{z_{st}}} = S_{z_{sn_{st}}} \{- S_{A_{z_{st}}} C_{C_{z_{st}}} S_\Theta C_\Psi - C_{A_{z_{st}}} C_{C_{z_{st}}} S_\Theta S_\Psi - S_{C_{z_{st}}} C_\Theta\} G \tag{IV-A.18}$$

Now focus attention on calibration of the model fixed accelerometer sensors and their corresponding relationships in Equations (III-B.30)-(III-B.32). Development is highly similar to Equations (IV-A.1)-(IV-A.18) and is only briefly discussed here. Voltages, angular orientation states (Φ only), and now sting fixed gravity components are the known parameters while bias, sensitivity, azimuth angle, and coning angle remain the unknown variables leading to a set of nonlinear algebraic equations. Note the sting fixed gravity components can be computed from Equation (III-B.6). The iterative Gauss-Newton regression algorithm represented in Equations

(IV-A.1)-(IV-A.6) is again applicable with the only changes affecting the functional dependence on parameters. For the model fixed sensor package, expressions for V and P become

$$V = F(B, S, A, C, \Phi, G_{x_{st}}, G_{y_{st}}, G_{z_{st}}) \tag{IV-A.19}$$

$$P = \left[\Phi\ G_{x_{st}}\ G_{y_{st}}\ G_{z_{st}}\right]^T \tag{IV-A.20}$$

For completeness, partial derivatives of Equations (III-B.30)-(III-B.32) are given below. For the model x_{sn_m} axis accelerometer sensor, partial derivatives are

$$\frac{\partial V_{x_{sn_m}}}{\partial B_{x_{sn_m}}} = 1 \tag{IV-A.21}$$

$$\begin{aligned}\frac{\partial V_{x_{sn_m}}}{\partial S_{x_{sn_m}}} &= (C_{C_{x_m}})G_{x_{st}} + (S_{A_{x_m}} S_{C_{x_m}} C_\Phi + C_{A_{x_m}} S_{C_{x_m}} S_\Phi)G_{y_{st}} \\ &\quad + (S_{A_{x_m}} S_{C_{x_m}} S_\Phi - C_{A_{x_m}} S_{C_{x_m}} C_\Phi)G_{z_{st}}\end{aligned} \tag{IV-A.22}$$

$$\begin{aligned}\frac{\partial V_{x_{sn_m}}}{\partial A_{x_m}} &= S_{x_{sn_m}}\{(C_{A_{x_m}} S_{C_{x_m}} C_\Phi - S_{A_{x_m}} S_{C_{x_m}} S_\Phi)G_{y_{st}} \\ &\quad + (C_{A_{x_m}} S_{C_{x_m}} S_\Phi + S_{A_{x_m}} S_{C_{x_m}} C_\Phi)G_{z_{st}}\}\end{aligned} \tag{IV-A.23}$$

$$\begin{aligned}\frac{\partial V_{x_{sn_m}}}{\partial C_{x_m}} &= S_{x_{sn_m}}\{(-S_{C_{x_m}})G_{x_{st}} + (S_{A_{x_m}} C_{C_{x_m}} C_\Phi + C_{A_{x_m}} C_{C_{x_m}} S_\Phi)G_{y_{st}} \\ &\quad + (S_{A_{x_m}} C_{C_{x_m}} S_\Phi - C_{A_{x_m}} C_{C_{x_m}} C_\Phi)G_{z_{st}}\}\end{aligned} \tag{IV-A.24}$$

For the model y_{sn_m} axis accelerometer sensor, partial derivatives are

$$\frac{\partial V_{y_{sn_m}}}{\partial B_{y_{sn_m}}} = 1 \tag{IV-A.25}$$

$$\begin{aligned}\frac{\partial V_{y_{sn_m}}}{\partial S_{y_{sn_m}}} &= (-C_{A_{y_m}} S_{C_{y_m}})G_{x_{st}} + (C_{C_{y_m}} C_\Phi - S_{A_{y_m}} S_{C_{y_m}} S_\Phi)G_{y_{st}} \\ &\quad + (C_{C_{y_m}} S_\Phi + S_{A_{y_m}} S_{C_{y_m}} C_\Phi)G_{z_{st}}\end{aligned} \tag{IV-A.26}$$

$$\frac{\partial V_{y_{sn_m}}}{\partial A_{y_m}} = S_{y_{sn_m}}\{(S_{A_{y_m}} S_{C_{y_m}})G_{x_{st}} + (-C_{A_{y_m}} S_{C_{y_m}} S_{\Phi})G_{y_{st}} + (C_{A_{y_m}} S_{C_{y_m}} C_{\Phi})G_{z_{st}}\} \tag{IV-A.27}$$

$$\frac{\partial V_{y_{sn_m}}}{\partial C_{y_m}} = S_{y_{sn_m}}\{(-C_{A_{y_m}} C_{C_{y_m}})G_{x_{st}} + (-S_{C_{y_m}} C_{\Phi} - S_{A_{y_m}} C_{C_{y_m}} S_{\Phi})G_{y_{st}} + (-S_{C_{y_m}} S_{\Phi} + S_{A_{y_m}} C_{C_{y_m}} C_{\Phi})G_{z_{st}}\} \tag{IV-A.28}$$

For the model z_{sn_m} axis accelerometer sensor, partial derivatives are

$$\frac{\partial V_{z_{sn_m}}}{\partial B_{z_{sn_m}}} = 1 \tag{IV-A.29}$$

$$\frac{\partial V_{z_{sn_m}}}{\partial S_{z_{sn_m}}} = (S_{A_{z_m}} S_{C_{z_m}})G_{x_{st}} + (-C_{A_{z_m}} S_{C_{z_m}} C_{\Phi} - C_{C_{z_m}} S_{\Phi})G_{y_{st}} + (-C_{A_{z_m}} S_{C_{z_m}} S_{\Phi} + C_{C_{z_m}} C_{\Phi})G_{z_{st}} \tag{IV-A.30}$$

$$\frac{\partial V_{z_{sn_m}}}{\partial A_{z_m}} = S_{z_{sn_m}}\{(C_{A_{z_m}} S_{C_{z_m}})G_{x_{st}} + (S_{A_{z_m}} S_{C_{z_m}} C_{\Phi})G_{y_{st}} + (S_{A_{z_m}} S_{C_{z_m}} S_{\Phi})G_{z_{st}}\} \tag{IV-A.31}$$

$$\frac{\partial V_{z_{sn_m}}}{\partial C_{z_m}} = S_{z_{sn_m}}\{(S_{A_{z_m}} C_{C_{z_m}})G_{x_{st}} + (-C_{A_{z_m}} C_{C_{z_m}} C_{\Phi} + S_{C_{z_m}} S_{\Phi})G_{y_{st}} + (-C_{A_{z_m}} C_{C_{z_m}} S_{\Phi} - S_{C_{z_m}} C_{\Phi})G_{z_{st}}\} \tag{IV-A.32}$$

The Gauss-Newton regression algorithms for accelerometer sensor calibration are validated here within a simulated laboratory environment with synthetically generated data using MATLAB. It is important to note the general calibration algorithms presented here are not tested in the laboratory with real data within the data acquisition control software environment using LabVIEW. An angular motion profile was generated and the corresponding sensor voltages were computed for specified bias, sensitivity, azimuth angle, and coning angle parameters. This data is intended to represent actual data that would be collected from hardware using the angular

calibration table in the laboratory. The motion profile consisted of a linear progression from 0 deg to 10 deg for Θ-Ψ-Φ over 10 s with a time step of 0.01 s which yields n = 1,001. Table 3 lists the specified and computed calibration parameters for all accelerometer sensors. Specified values are based on the manufacture's published data. The computed values are all in excellent agreement with the specified values validating the accelerometer sensor calibration methodology. Appendix B lists the MATLAB software pertaining to accelerometer sensor calibration.

Table 3 Accelerometer Calibration Test Results

Axis	Parameter			
	Specified	Computed	Specified	Computed
	B (v)		S (v/g)	
$x_{sn_{st}}$	1.25	1.2500	0.51	0.5100
$y_{sn_{st}}$	1.27	1.2700	0.47	0.4700
$z_{sn_{st}}$	1.19	1.1900	0.54	0.5400
x_{sn_m}	1.26	1.2600	0.52	0.5200
y_{sn_m}	1.28	1.2800	0.49	0.4900
z_{sn_m}	1.20	1.2000	0.53	0.5300
	A (deg)		C (deg)	
$x_{sn_{st}}$	0.05	0.0500	0.06	0.0600
$y_{sn_{st}}$	0.12	0.1200	0.15	0.1500
$z_{sn_{st}}$	0.11	0.1100	0.11	0.1100
x_{sn_m}	0.08	0.0800	0.08	0.0800
y_{sn_m}	0.10	0.1000	0.09	0.0900
z_{sn_m}	0.09	0.0900	0.12	0.1200

B. Accelerometer Attitude Construction

Once the accelerometer sensor packages have been calibrated, the AMS prototype can be used for attitude construction. Given numeric knowledge of the calibration parameters, a set of sensor output voltages can be used to determine unknown pitch-yaw-roll angles associated with the two accelerometer packages mounted in the sting fixed and model fixed reference frames. To verify accurate attitude construction, utilization of a consistent set of sensor output voltages and pitch-yaw-roll excitation angles, obtained from a controlled high-precision laboratory environment, is highly desirable. Synthetically generated data simulating the laboratory environment, however, will be used for construction procedure development. The attitude states are constructed sequentially. Pitch-yaw angles (Θ-Ψ) are addressed first, and roll angle (Φ) is considered second. Two different construction methodologies are considered and include an analytic closed-form strategy and an iterative numeric strategy. The closed-form strategy facilitates a real-time attitude construction submode for the AMS, while the iterative strategy is incrementally more accurate.[5]

The analytic closed-form attitude construction strategy will be addressed first. Recall the governing sting fixed and model fixed accelerometer sensor relationships in Equations (III-B.25)-(III-B.26). After performing matrix operations on these relationships, one can find

$$\mathbf{T}^{-1}_{\mathbf{sn_{st}}/\mathbf{st}}\mathbf{S}^{-1}_{\mathbf{sn_{st}}}(\mathbf{V}_{\mathbf{sn_{st}}} - \mathbf{B}_{\mathbf{sn_{st}}}) = \mathbf{T}_{\mathbf{st/t}}\mathbf{G}_{\mathbf{t}} \tag{IV-B.1}$$

$$\mathbf{T}^{-1}_{\mathbf{sn_m}/\mathbf{m}}\mathbf{S}^{-1}_{\mathbf{sn_m}}(\mathbf{V}_{\mathbf{sn_m}} - \mathbf{B}_{\mathbf{sn_m}}) = \mathbf{T}_{\mathbf{m/st}}\mathbf{G}_{\mathbf{st}} \tag{IV-B.2}$$

Using Equations (III-B.5)-(III-B.6), note the left-hand side of Equation (IV-B.1) can be renamed as $\mathbf{G}_{\mathbf{st}}$, while the left-hand side of Equation (IV-B.2) can be replaced with $\mathbf{G}_{\mathbf{m}}$. In scalar form, Equations (IV-B.1)-(IV-B.2) become

$$G_{x_{st}} = -S_{\Theta}C_{\Psi}G \tag{IV-B.3}$$

$$G_{y_{st}} = S_{\Theta}S_{\Psi}G \tag{IV-B.4}$$

$$G_{z_{st}} = C_{\Theta} G \tag{IV-B.5}$$

$$G_{x_m} = G_{x_{st}} \tag{IV-B.6}$$

$$G_{y_m} = C_{\Phi} G_{y_{st}} + S_{\Phi} G_{z_{st}} \tag{IV-B.7}$$

$$G_{z_m} = -S_{\Phi} G_{y_{st}} + C_{\Phi} G_{z_{st}} \tag{IV-B.8}$$

From an attitude construction perspective, all gravity terms are known parameters while pitch-yaw-roll angles are unknown variables implying a set of nonlinear algebraic equations must be solved.

Manipulation of Equations (IV-B.3)-(IV-B.5) to isolate Θ and Ψ yields

$$\Theta = \tan^{-1}\left(\frac{\sqrt{G_{x_{st}}^2 + G_{y_{st}}^2}}{G_{z_{st}}}\right) \operatorname{sgn}\left(-\frac{1}{C_{\Psi}} \frac{G_{x_{st}}}{G}\right) \quad , \quad \Psi \neq \pm 90 \text{ deg} \tag{IV-B.9}$$

$$\Psi = \tan^{-1}\left(-\frac{G_{y_{st}}}{G_{x_{st}}}\right) \tag{IV-B.10}$$

Further manipulation with Equations (IV-B.7)-(IV-B.8) to isolate Φ yields

$$\Phi = \tan^{-1}\left(\frac{G_{y_m} G_{z_{st}} - G_{z_m} G_{y_{st}}}{G_{y_m} G_{y_{st}} + G_{z_m} G_{z_{st}}}\right) \tag{IV-B.11}$$

The sign function in Equation (IV-B.9) is appended to the solution to recover directional pitch information. Given the gravity components, Equations (IV-B.9)-(IV-B.11) offer analytic closed-form solutions for attitude construction. It is important to note that gravity components are computed from the sensor output voltages and calibration parameters appearing on the left-hand sides of Equations (IV-B.1)-(IV-B.2). The analytic closed-form solution strategy is highly attractive in applications requiring real-time monitoring of wind tunnel testing.

Now consider the iterative numeric attitude construction strategy. The Gauss-Newton regression method will once again be applied here as outlined in Reference 5. Recall the governing sting fixed accelerometer sensor relationships in Equations (III-B.27)-(III-B.29). From

an attitude construction perspective, voltages, calibration terms, and gravity are known parameters while pitch-yaw angles are unknown variables implying a set of nonlinear algebraic equations must be solved. Mathematical pitch-yaw coupling structure implies all three relationships must be considered simultaneously in the solution strategy since each scalar equation involves the same unknown pair (pitch angle, yaw angle). Represent any one of the three sting fixed accelerometer sensor relationships as

$$V_i = F_i(\Theta, \Psi, B_i, S_i, A_i, C_i, G) \tag{IV-B.12}$$

where function F_i denotes the nonlinear functional dependency of voltage V_i on pitch-yaw angles Θ-Ψ, bias B_i, sensitivity S_i, azimuth rotation A_i, coning rotation C_i, and gravity G where i = $x_{sn_{st}}$, $y_{sn_{st}}$, $z_{sn_{st}}$. The right-hand side of this equality can also be expanded in a Taylor series about a reference solution.

$$V_i = V_{i_r} + \frac{\partial F_i(X,P_i)}{\partial X}_r (X - X_r) + \ldots \tag{IV-B.13}$$

$$X = \left[\Theta \; \Psi\right]^T \qquad \frac{\partial F_i(X,P_i)}{\partial X} = \left[\frac{\partial F_i}{\partial \Theta} \; \frac{\partial F_i}{\partial \Psi}\right] \qquad P_i = \left[B_i \; S_i \; A_i \; C_i \; G\right]^T \tag{IV-B.14}$$

In Equation (IV-B.13), X denotes a vector containing the unknown variables, P_i denotes a vector of known parameters, and subscript "r" denotes evaluation at the known reference condition.

Suppose initial estimates for the pitch-yaw variables are known and interpreted to be the reference solution X_r in Equation (IV-B.13). Further suppose that a data set of n triples for each voltage is available. A single triple from this set can be interpreted as V_i appearing in Equation (IV-B.13) for i = $x_{sn_{st}}$, $y_{sn_{st}}$, $z_{sn_{st}}$. Further, P_i is known from calibration processing and the environment. Using the reference solution and parameter data, voltages and their partial derivatives can also be computed from Equation (IV-B.12) and interpreted as V_{i_r} and $\partial F_i(X,P_i)/\partial X_r$. Construct a vector equivalent to Equation (IV-B.13) using the n×3(1+4+1) data set to yield

$$\mathbf{V} = \mathbf{V_r} + \frac{\partial \mathbf{F(X,P)}}{\partial \mathbf{X}}_{\mathbf{r}} (X - X_r) + \ldots \tag{IV-B.15}$$

$$\mathbf{V} = \begin{bmatrix} V_{i_1} \\ V_{i_2} \\ V_{i_n} \end{bmatrix} \qquad \mathbf{V_r} = \begin{bmatrix} V_{i_{1_r}} \\ V_{i_{2_r}} \\ V_{i_{n_r}} \end{bmatrix} \qquad \frac{\partial \mathbf{F(X,P)}}{\partial \mathbf{X}}_{\mathbf{r}} = \begin{bmatrix} \frac{\partial F_i}{\partial \Theta}_{1_r} & \frac{\partial F_i}{\partial \Psi}_{1_r} \\ \frac{\partial F_i}{\partial \Theta}_{2_r} & \frac{\partial F_i}{\partial \Psi}_{2_r} \\ \frac{\partial F_i}{\partial \Theta}_{n_r} & \frac{\partial F_i}{\partial \Psi}_{n_r} \end{bmatrix} \qquad \mathbf{P} = \begin{bmatrix} P_i \end{bmatrix} \tag{IV-B.16}$$

Multiply this expression by $\partial \mathbf{F(X,P)}/\partial \mathbf{X_r}^T$ on the left, perform matrix inversion, neglect higher order terms, and rearrange to yield

$$X = X_r + \left(\frac{\partial \mathbf{F(X,P)}}{\partial \mathbf{X}}_{\mathbf{r}}^T \frac{\partial \mathbf{F(X,P)}}{\partial \mathbf{X}}_{\mathbf{r}}\right)^{-1} \frac{\partial \mathbf{F(X,P)}}{\partial \mathbf{X}}_{\mathbf{r}}^T (\mathbf{V} - \mathbf{V_r}) \tag{IV-B.17}$$

Equation (IV-B.17) represents the iterative Gauss-Newton regression algorithm. X is computed from Equation (IV-B.17) and reinterpreted as the reference solution for the next computational cycle. This process is repeated until a solution tolerance is met.

For completeness, partial derivatives of Equations (III-B.27)-(III-B.29) are given below. For the sting $x_{sn_{st}}$ axis accelerometer sensor, partial derivatives are

$$\frac{\partial V_{x_{sn_{st}}}}{\partial \Theta} = S_{x_{sn_{st}}} \{ - C_{C_{x_{st}}} C_\Theta C_\Psi + S_{A_{x_{st}}} S_{C_{x_{st}}} C_\Theta S_\Psi + C_{A_{x_{st}}} S_{C_{x_{st}}} S_\Theta \} G \tag{IV-B.18}$$

$$\frac{\partial V_{x_{sn_{st}}}}{\partial \Psi} = S_{x_{sn_{st}}} \{ C_{C_{x_{st}}} S_\Theta S_\Psi + S_{A_{x_{st}}} S_{C_{x_{st}}} S_\Theta C_\Psi \} G \tag{IV-B.19}$$

For the sting $y_{sn_{st}}$ axis accelerometer sensor, partial derivatives are

$$\frac{\partial V_{y_{sn_{st}}}}{\partial \Theta} = S_{y_{sn_{st}}}\{C_{A_{y_{st}}} S_{C_{y_{st}}} C_\Theta C_\Psi + C_{C_{y_{st}}} C_\Theta S_\Psi - S_{A_{y_{st}}} S_{C_{y_{st}}} S_\Theta\}G \qquad \text{(IV-B.20)}$$

$$\frac{\partial V_{y_{sn_{st}}}}{\partial \Psi} = S_{y_{sn_{st}}}\{-C_{A_{y_{st}}} S_{C_{y_{st}}} S_\Theta S_\Psi + C_{C_{y_{st}}} S_\Theta C_\Psi\}G \qquad \text{(IV-B.21)}$$

For the sting $z_{sn_{st}}$ axis accelerometer sensor, partial derivatives are

$$\frac{\partial V_{z_{sn_{st}}}}{\partial \Theta} = S_{z_{sn_{st}}}\{-S_{A_{z_{st}}} S_{C_{z_{st}}} C_\Theta C_\Psi - C_{A_{z_{st}}} S_{C_{z_{st}}} C_\Theta S_\Psi - C_{C_{z_{st}}} S_\Theta\}G \qquad \text{(IV-B.22)}$$

$$\frac{\partial V_{z_{sn_{st}}}}{\partial \Psi} = S_{z_{sn_{st}}}\{S_{A_{z_{st}}} S_{C_{z_{st}}} S_\Theta S_\Psi - C_{A_{z_{st}}} S_{C_{z_{st}}} S_\Theta C_\Psi\}G \qquad \text{(IV-B.23)}$$

Now focus attention on attitude construction using the model fixed accelerometer sensors and their corresponding relationships in Equations (III-B.30)-(III-B.32). Development is highly similar to Equations (IV-B.12)-(IV-B.23) and is only briefly discussed here. Voltages, calibration terms, and now sting fixed gravity components are the known parameters while roll angle is the unknown variable leading to a set of nonlinear algebraic equations. Note the sting fixed gravity components can be computed from Equation (III-B.6). The iterative Gauss-Newton regression algorithm represented by Equations (IV-B.12)-(IV-B.17) is again applicable with the only changes affecting the unknown variable and known parameter definitions, and the functional dependence on these quantities. For the model fixed sensor package, expressions for V_i, X and P_i become

$$V_i = F_i(\Phi, B_i, S_i, A_i, C_i, G_{x_{st}}, G_{y_{st}}, G_{z_{st}}) \qquad \text{(IV-B.24)}$$

$$X = [\Phi]^T \qquad \frac{\partial F_i(X,P_i)}{\partial X} = \left[\frac{\partial F_i}{\partial \Phi}\right] \qquad P_i = \left[B_i\, S_i\, A_i\, C_i\, G_{x_{st}}\, G_{y_{st}}\, G_{z_{st}}\right]^T \qquad \text{(IV-B.25)}$$

For completeness, partial derivatives of Equations (III-B.30)-(III-B.32) are given below. For the model x_{sn_m} axis accelerometer sensor, partial derivatives are

$$\frac{\partial V_{x_{sn_m}}}{\partial \Phi} = S_{x_{sn_m}}\{(-S_{A_{x_m}} S_{C_{x_m}} S_\Phi + C_{A_{x_m}} S_{C_{x_m}} C_\Phi) G_{y_{st}} + (S_{A_{x_m}} S_{C_{x_m}} C_\Phi + C_{A_{x_m}} S_{C_{x_m}} S_\Phi) G_{z_{st}}\} \quad \text{(IV-B.26)}$$

For the model y_{sn_m} axis accelerometer sensor, partial derivatives are

$$\frac{\partial V_{y_{sn_m}}}{\partial \Phi} = S_{y_{sn_m}}\{(-C_{C_{y_m}} S_\Phi - S_{A_{y_m}} S_{C_{y_m}} C_\Phi) G_{y_{st}} + (C_{C_{y_m}} C_\Phi - S_{A_{y_m}} S_{C_{y_m}} S_\Phi) G_{z_{st}}\} \quad \text{(IV-B.27)}$$

For the model z_{sn_m} axis accelerometer sensor, partial derivatives are

$$\frac{\partial V_{z_{sn_m}}}{\partial \Phi} = S_{z_{sn_m}}\{(C_{A_{z_m}} S_{C_{z_m}} S_\Phi - C_{C_{z_m}} C_\Phi) G_{y_{st}} + (-C_{A_{z_m}} S_{C_{z_m}} C_\Phi - C_{C_{z_m}} S_\Phi) G_{z_{st}}\} \quad \text{(IV-B.28)}$$

The analytic closed-form and iterative numeric algorithms for accelerometer attitude construction are validated here within a simulated laboratory environment with synthetically generated data using MATLAB. It is important to note the general construction algorithms presented here are not tested in the laboratory with real data within the data acquisition control software environment using LabVIEW. An angular motion profile was generated and the corresponding sensor voltages were computed for specified bias, sensitivity, azimuth angle, and coning angle parameters. This data is intended to represent actual data that would be collected from hardware using the angular calibration table in the laboratory. The motion profile consisted of a linear progression from 0 deg to 10 deg for Θ-Ψ-Φ over 10 s with a time step of 0.01 s which yields n = 1,001. Specified calibration parameter values from Section IV-A are used. Figure 6 shows overlay traces of the exact and computed angular states (both analytic closed-form and iterative numeric strategies). Figures 7-8 show difference traces between exact and computed angular states. The computed values are all in excellent agreement with the exact values validating the accelerometer sensor calibration methodology. Figures 7-8 suggest the

analytic closed-form solution is slightly more accurate than the iterative numeric solution. With noise and resolution effects considered, the iterative numeric solution would be expected slightly more accurate. Appendix C lists the MATLAB software pertaining to accelerometer attitude construction.

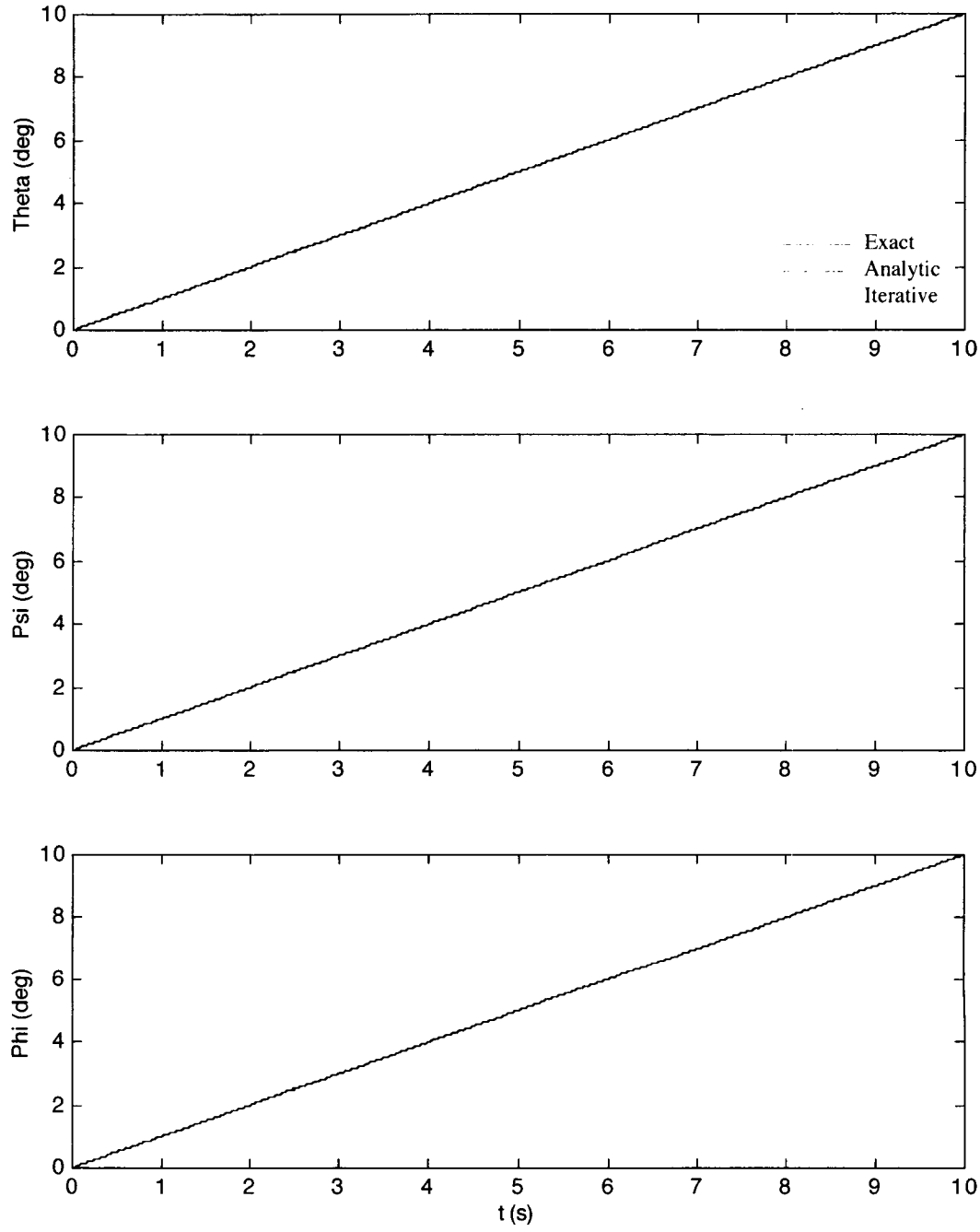

Figure 6 Accelerometer Construction Test Results – Absolute

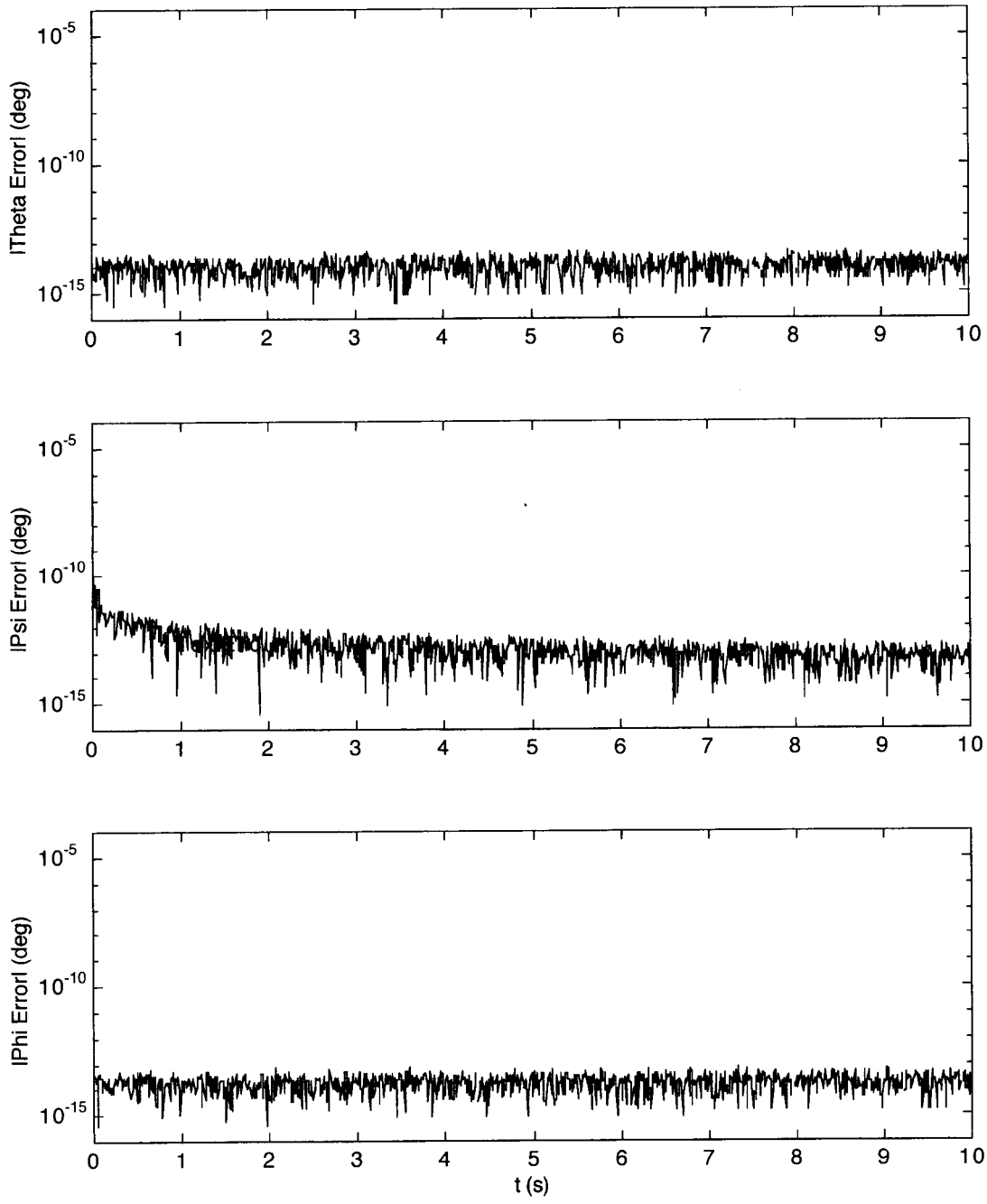

Figure 7 Accelerometer Construction Test Results – Relative (Analytic)

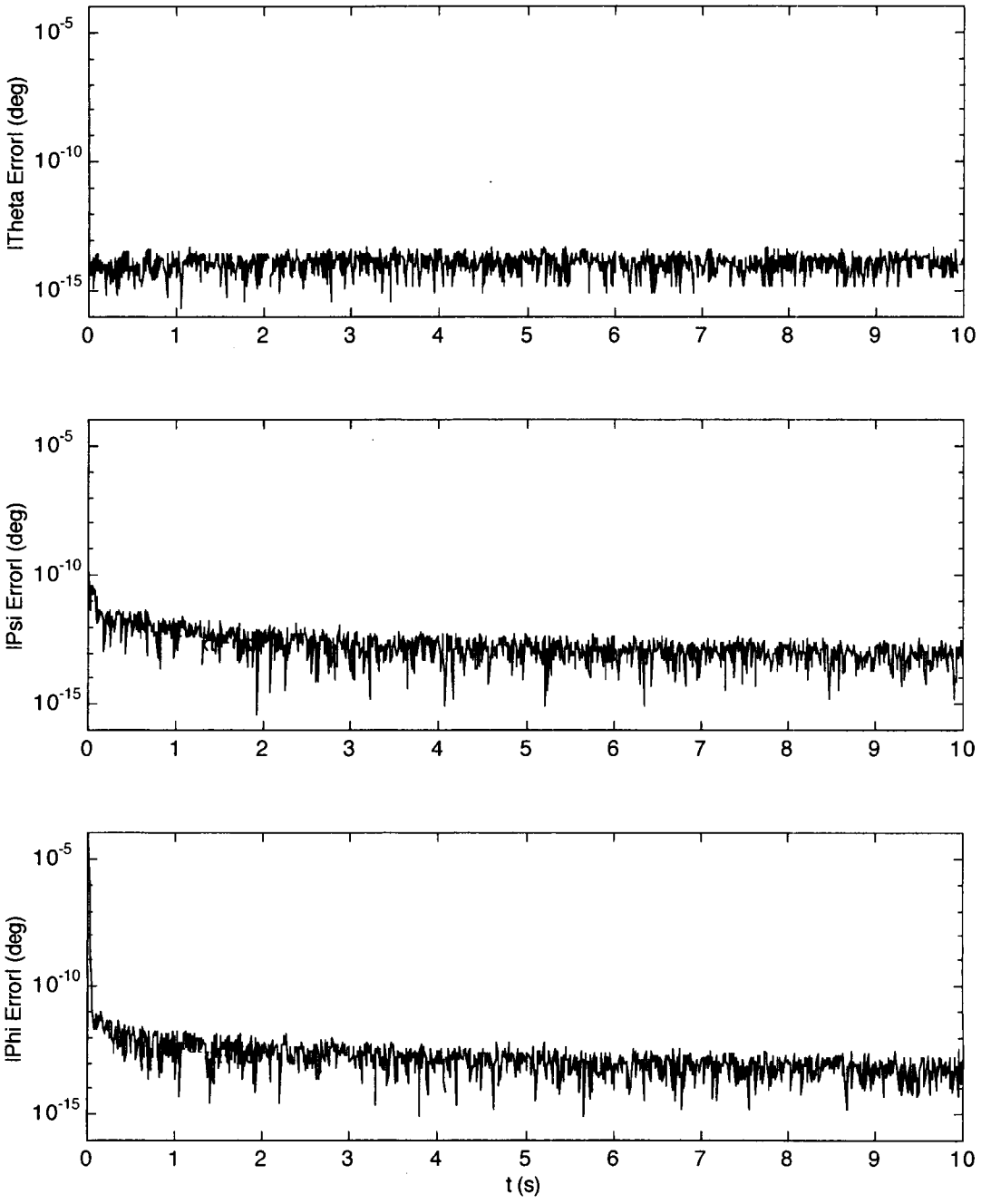

Figure 8 Accelerometer Construction Test Results – Relative (Iterative)

C. Gyro Sensor Calibration

Before the AMS prototype can be used in the attitude construction mode, the gyro sensor package must be calibrated. A consistent set of sensor output voltages and pitch-yaw-roll excitation angles and angle rates, obtained from a controlled high-precision laboratory environment, can be used to determine unknown calibration parameters for each of the three gyros in the model fixed package. Synthetically generated data simulating the laboratory environment, however, will be used for calibration procedure development. Calibration parameters to be addressed include bias ($B_{x_{sn_m}}$, $B_{y_{sn_m}}$, $B_{z_{sn_m}}$), sensitivity ($S_{x_{sn_m}}$, $S_{y_{sn_m}}$, $S_{z_{sn_m}}$), azimuth angle (A_{x_m}, A_{y_m}, A_{z_m}), and coning angle (C_{x_m}, C_{y_m}, C_{z_m}). The calibration parameters for each gyro are determined independently. If deemed to be important, other sensor imperfections could be incorporated into the calibration procedure. For example, temperature corrections, although judged to be an important factor for the 31-Inch Hypersonic Tunnel application, were not considered in the prototype development stage. However, calibration for thermal effects can be appended to the algorithm presented in this section at a more advanced AMS development stage.

A Gauss-Newton iterative nonlinear regression method will be used as a basis for gyro calibration. Further details of the Gauss-Newton algorithm can be found in Reference 17. Recall the governing model fixed gyro sensor relationships in Equations (III-C.16)-(III-C.18). From a sensor calibration perspective, voltages, angular orientation states, and angular orientation state derivatives are known parameters while bias, sensitivity, azimuth angle, and coning angle are unknown variables implying a set of nonlinear algebraic equations must be solved. Implications from sensor model assumptions are that each scalar equation involves only a single unknown quadruple (bias, sensitivity, azimuth angle, coning angle), allowing an independent solution strategy. Represent any one of the three model fixed gyro sensor relationships as

$$V = F(B, S, A, C, \Psi, \Phi, \dot{\Theta}, \dot{\Psi}, \dot{\Phi}) \qquad \text{(IV-C.1)}$$

where function F denotes the nonlinear functional dependency of voltage V on bias B, sensitivity S, azimuth rotation A, coning rotation C, yaw-roll angles Ψ-Φ, and pitch-yaw-roll angle rates $\dot{\Theta}$–$\dot{\Psi}$–$\dot{\Phi}$. The right-hand side of this equality can be expanded in a Taylor series about a reference solution.

$$V = V_r + \frac{\partial F(X,P)}{\partial X}_r (X - X_r) + \ldots \qquad \text{(IV-C.2)}$$

$$X = \begin{bmatrix} B & S & A & C \end{bmatrix}^T \qquad \frac{\partial F(X,P)}{\partial X} = \begin{bmatrix} \frac{\partial F}{\partial B} & \frac{\partial F}{\partial S} & \frac{\partial F}{\partial A} & \frac{\partial F}{\partial C} \end{bmatrix} \qquad P = \begin{bmatrix} \Psi & \Phi & \dot{\Theta} & \dot{\Psi} & \dot{\Phi} \end{bmatrix}^T \qquad \text{(IV-C.3)}$$

In Equation (IV-C.2), X denotes a vector containing the unknown variables, P denotes a vector of known parameters, and subscript "r" denotes evaluation at the known reference condition.

Suppose initial estimates for the bias, sensitivity, azimuth, and coning variables are known and interpreted to be the reference solution X_r in Equation (IV-C.2). Further suppose that a consistent data set of n sextuples for voltage, yaw, roll, pitch rate, yaw rate, and roll rate is available. A single sextuple from this set can be interpreted as V and P appearing in Equation (IV-C.2). Using the reference solution and parameter data, voltage and it's partial derivatives can also be computed from Equation (IV-C.1) and interpreted as V_r and $\partial F(X,P)/\partial X_r$. Construct a vector equivalent to Equation (IV-C.2) using the n×(1+2+3) data set to yield

$$\mathbf{V} = \mathbf{V_r} + \frac{\partial \mathbf{F(X,P)}}{\partial \mathbf{X}}_{\mathbf{r}} (X - X_r) + \ldots \qquad \text{(IV-C.4)}$$

$$\mathbf{V} = \begin{bmatrix} V_1 \\ V_2 \\ \\ V_n \end{bmatrix} \qquad \mathbf{V_r} = \begin{bmatrix} V_{1_r} \\ V_{2_r} \\ \\ V_{n_r} \end{bmatrix} \qquad \frac{\partial \mathbf{F(X,P)}}{\partial \mathbf{X}}_{\mathbf{r}} = \begin{bmatrix} \frac{\partial F}{\partial B}_{1_r} & \frac{\partial F}{\partial S}_{1_r} & \frac{\partial F}{\partial A}_{1_r} & \frac{\partial F}{\partial C}_{1_r} \\ \frac{\partial F}{\partial B}_{2_r} & \frac{\partial F}{\partial S}_{2_r} & \frac{\partial F}{\partial A}_{2_r} & \frac{\partial F}{\partial C}_{2_r} \\ & & & \\ \frac{\partial F}{\partial B}_{n_r} & \frac{\partial F}{\partial S}_{n_r} & \frac{\partial F}{\partial A}_{n_r} & \frac{\partial F}{\partial C}_{n_r} \end{bmatrix} \qquad \text{(IV-C.5)}$$

Multiply this expression by $\partial \mathbf{F(X,P)}/\partial \mathbf{X_r}^T$ on the left, perform matrix inversion, neglect higher order terms, and rearrange to yield

$$\mathbf{X} = \mathbf{X_r} + \left(\frac{\partial \mathbf{F(X,P)}}{\partial \mathbf{X}}_{\mathbf{r}}^{T} \frac{\partial \mathbf{F(X,P)}}{\partial \mathbf{X}}_{\mathbf{r}}\right)^{-1} \frac{\partial \mathbf{F(X,P)}}{\partial \mathbf{X}}_{\mathbf{r}}^{T} (\mathbf{V} - \mathbf{V_r}) \qquad \text{(IV-C.6)}$$

Equation (IV-C.6) represents the iterative Gauss-Newton regression algorithm. X is computed from Equation (IV-C.6) and reinterpreted as the reference solution for the next computational cycle. This process is repeated until a solution tolerance is met.

For completeness, partial derivatives of Equations (III-C.16)-(III-C.18) are given below. For the model x_{sn_m} axis gyro sensor, partial derivatives are

$$\frac{\partial V_{x_{sn_m}}}{\partial B_{x_{sn_m}}} = 1 \qquad \text{(IV-C.7)}$$

$$\begin{aligned}\frac{\partial V_{x_{sn_m}}}{\partial S_{x_{sn_m}}} &= (C_{C_{x_m}} S_\Psi + S_{A_{x_m}} S_{C_{x_m}} C_\Psi C_\Phi + C_{A_{x_m}} S_{C_{x_m}} C_\Psi S_\Phi)\dot{\Theta} \\ &\quad + (S_{A_{x_m}} S_{C_{x_m}} S_\Phi - C_{A_{x_m}} S_{C_{x_m}} C_\Phi)\dot{\Psi} + (C_{C_{x_m}})\dot{\Phi}\end{aligned} \qquad \text{(IV-C.8)}$$

$$\begin{aligned}\frac{\partial V_{x_{sn_m}}}{\partial A_{x_m}} &= S_{x_{sn_m}}\{(C_{A_{x_m}} S_{C_{x_m}} C_\Psi C_\Phi - S_{A_{x_m}} S_{C_{x_m}} C_\Psi S_\Phi)\dot{\Theta} \\ &\quad + (C_{A_{x_m}} S_{C_{x_m}} S_\Phi + S_{A_{x_m}} S_{C_{x_m}} C_\Phi)\dot{\Psi}\}\end{aligned} \qquad \text{(IV-C.9)}$$

$$\begin{aligned}\frac{\partial V_{x_{sn_m}}}{\partial C_{x_m}} &= S_{x_{sn_m}}\{(-S_{C_{x_m}} S_\Psi + S_{A_{x_m}} C_{C_{x_m}} C_\Psi C_\Phi + C_{A_{x_m}} C_{C_{x_m}} C_\Psi S_\Phi)\dot{\Theta} \\ &\quad + (S_{A_{x_m}} C_{C_{x_m}} S_\Phi - C_{A_{x_m}} C_{C_{x_m}} C_\Phi)\dot{\Psi} + (-S_{C_{x_m}})\dot{\Phi}\}\end{aligned} \qquad \text{(IV-C.10)}$$

For the model y_{sn_m} axis gyro sensor, partial derivatives are

$$\frac{\partial V_{y_{sn_m}}}{\partial B_{y_{sn_m}}} = 1 \qquad \text{(IV-C.11)}$$

$$\frac{\partial V_{y_{sn_m}}}{\partial S_{y_{sn_m}}} = (-C_{A_{y_m}} S_{C_{y_m}} S_\Psi + C_{C_{y_m}} C_\Psi C_\Phi - S_{A_{y_m}} S_{C_{y_m}} C_\Psi S_\Phi)\dot{\Theta} + (C_{C_{y_m}} S_\Phi + S_{A_{y_m}} S_{C_{y_m}} C_\Phi)\dot{\Psi} + (-C_{A_{y_m}} S_{C_{y_m}})\dot{\Phi} \quad \text{(IV-C.12)}$$

$$\frac{\partial V_{y_{sn_m}}}{\partial A_{y_m}} = S_{y_{sn_m}}\{(S_{A_{y_m}} S_{C_{y_m}} S_\Psi - C_{A_{y_m}} S_{C_{y_m}} C_\Psi S_\Phi)\dot{\Theta} + (C_{A_{y_m}} S_{C_{y_m}} C_\Phi)\dot{\Psi} + (S_{A_{y_m}} S_{C_{y_m}})\dot{\Phi}\} \quad \text{(IV-C.13)}$$

$$\frac{\partial V_{y_{sn_m}}}{\partial C_{y_m}} = S_{y_{sn_m}}\{(-C_{A_{y_m}} C_{C_{y_m}} S_\Psi - S_{C_{y_m}} C_\Psi C_\Phi - S_{A_{y_m}} C_{C_{y_m}} C_\Psi S_\Phi)\dot{\Theta} + (-S_{C_{y_m}} S_\Phi + S_{A_{y_m}} C_{C_{y_m}} C_\Phi)\dot{\Psi} + (-C_{A_{y_m}} C_{C_{y_m}})\dot{\Phi}\} \quad \text{(IV-C.14)}$$

For the model z_{sn_m} axis gyro sensor, partial derivatives are

$$\frac{\partial V_{z_{sn_m}}}{\partial B_{z_{sn_m}}} = 1 \quad \text{(IV-C.15)}$$

$$\frac{\partial V_{z_{sn_m}}}{\partial S_{z_{sn_m}}} = (S_{A_{z_m}} S_{C_{z_m}} S_\Psi - C_{A_{z_m}} S_{C_{z_m}} C_\Psi C_\Phi - C_{C_{z_m}} C_\Psi S_\Phi)\dot{\Theta} + (-C_{A_{z_m}} S_{C_{z_m}} S_\Phi + C_{C_{z_m}} C_\Phi)\dot{\Psi} + (S_{A_{z_m}} S_{C_{z_m}})\dot{\Phi} \quad \text{(IV-C.16)}$$

$$\frac{\partial V_{z_{sn_m}}}{\partial A_{z_m}} = S_{z_{sn_m}}\{(C_{A_{z_m}} S_{C_{z_m}} S_\Psi + S_{A_{z_m}} S_{C_{z_m}} C_\Psi C_\Phi)\dot{\Theta} + (S_{A_{z_m}} S_{C_{z_m}} S_\Phi)\dot{\Psi} + (C_{A_{z_m}} S_{C_{z_m}})\dot{\Phi}\} \quad \text{(IV-C.17)}$$

$$\frac{\partial V_{z_{sn_m}}}{\partial C_{z_m}} = S_{z_{sn_m}}\{(S_{A_{z_m}} C_{C_{z_m}} S_\Psi - C_{A_{z_m}} C_{C_{z_m}} C_\Psi C_\Phi + S_{C_{z_m}} C_\Psi S_\Phi)\dot{\Theta} + (-C_{A_{z_m}} C_{C_{z_m}} S_\Phi - S_{C_{z_m}} C_\Phi)\dot{\Psi} + (S_{A_{z_m}} C_{C_{z_m}})\dot{\Phi}\} \quad \text{(IV-C.18)}$$

The Gauss-Newton regression algorithm for gyro sensor calibration is validated here within a simulated laboratory environment with synthetically generated data using MATLAB. It is important to note the general calibration algorithm presented here is not tested in the laboratory

with real data within the data acquisition control software environment using LabVIEW. An angular motion profile was generated and the corresponding sensor voltages were computed for specified bias, sensitivity, azimuth angle, and coning angle parameters. This data is intended to represent actual data that would be collected from hardware using a high bandwidth angular calibration table in the laboratory. The motion profile consisted of harmonic excitation with Θ = 10sin(0.125×2π×t), Ψ = 10sin(0.0625×2π×t), and Φ = 10sin(0.25×2π×t) deg for $0 \leq t \leq 10$ s with a time step of 0.01 s which yields n = 1,001. Table 4 lists the specified and computed calibration parameters for all gyro sensors. The computed values are all in excellent agreement with the specified values validating the gyro sensor calibration methodology. Appendix D lists the MATLAB software pertaining to gyro sensor calibration.

Table 4 Gyro Calibration Test Results

Axis	Parameter			
	Specified	Computed	Specified	Computed
	B (v)		S (v/deg/s)	
x_{sn_m}	0.051	0.05100	1.25	1.2500
y_{sn_m}	0.052	0.05200	1.26	1.2600
z_{sn_m}	0.053	0.05300	1.27	1.2700
	A (deg)		C (deg)	
x_{sn_m}	0.14	0.1400	0.11	0.1100
y_{sn_m}	0.15	0.1500	0.12	0.1200
z_{sn_m}	0.16	0.1600	0.13	0.1300

D. Gyro Attitude Construction

Once the gyro sensor package has been calibrated, the AMS prototype can be used for attitude construction. Given numeric knowledge of the calibration parameters, a set of sensor output voltages can be used to determine unknown pitch-yaw-roll angles associated with the

single gyro package mounted in the model fixed reference frame. To verify accurate attitude construction, utilization of a consistent set of sensor output voltages and pitch-yaw-roll excitation angles and angle rates, obtained from a controlled high-precision laboratory environment, is highly desirable. Synthetically generated data simulating the laboratory environment, however, will be used for construction procedure development. All attitude states (Θ-Ψ-Φ) are constructed in a simultaneous fashion due to the coupled gyroscopic dynamics associated with this class of sensors. Analytic closed-form solutions are not feasible here, thus leaving only iterative numeric strategies for gyro attitude construction.

Recall the governing model fixed gyro sensor relationship in Equation (III-C.15). After performing matrix operations on this relationship, one can find

$$\mathbf{T}^{-1}_{\mathbf{sn_m/m}}\mathbf{S}^{-1}_{\mathbf{sn_m}}(\mathbf{V}_{\mathbf{sn_m}} - \mathbf{B}_{\mathbf{sn_m}}) = \mathbf{T}_{\mathbf{m/i1}}\dot{\boldsymbol{\Theta}}_{\mathbf{i1}} + \mathbf{T}_{\mathbf{m/st}}\dot{\boldsymbol{\Psi}}_{\mathbf{st}} + \mathbf{T}_{\mathbf{m/m}}\dot{\boldsymbol{\Phi}}_{\mathbf{m}} \qquad \text{(IV-D.1)}$$

Using Equations (III-C.3)-(III-C.5), note the right-hand side of Equation (IV-D.1) can be compressed into a product of a single matrix and vector, or

$$\mathbf{T}_{\mathbf{m/i1}}\dot{\boldsymbol{\Theta}}_{\mathbf{i1}} + \mathbf{T}_{\mathbf{m/st}}\dot{\boldsymbol{\Psi}}_{\mathbf{st}} + \mathbf{T}_{\mathbf{m/m}}\dot{\boldsymbol{\Phi}}_{\mathbf{m}} = \mathbf{T}_{\mathbf{m/}a}\dot{\mathcal{A}}_a \qquad \text{(IV-D.2)}$$

$$\dot{\mathcal{A}}_a = \left[\dot{\Theta}\ \dot{\Psi}\ \dot{\Phi}\right]^{\mathrm{T}} \qquad \mathbf{T}_{\mathbf{m/}a} = \left[\mathbf{T}_{\mathbf{m/i1}_2}\ \mathbf{T}_{\mathbf{m/st}_3}\ \mathbf{T}_{\mathbf{m/m}_1}\right] \qquad \text{(IV-D.3)}$$

In Equation (IV-D.3), $\mathbf{T}_{\mathbf{m/i1}_2}$, $\mathbf{T}_{\mathbf{m/st}_3}$, and $\mathbf{T}_{\mathbf{m/m}_1}$ denote the first, second, and third columns of $\mathbf{T}_{\mathbf{m/i1}}$, $\mathbf{T}_{\mathbf{m/st}}$, and $\mathbf{T}_{\mathbf{m/m}}$, respectively. Consequently, $\mathbf{T}_{\mathbf{m/}a}$, is not a true coordinate transformation matrix in the rigorous sense. Notational usage of the letters $\mathcal{A}$ and a denote angle. Combining Equations (IV-D.1)-(IV-D.2) with further matrix manipulation yields

$$\dot{\mathcal{A}}_a = \mathbf{T}^{-1}_{\mathbf{m/}a}\mathbf{T}^{-1}_{\mathbf{sn_m/m}}\mathbf{S}^{-1}_{\mathbf{sn_m}}(\mathbf{V}_{\mathbf{sn_m}} - \mathbf{B}_{\mathbf{sn_m}}) \qquad \text{(IV-D.4)}$$

Examination of Equation (IV-D.4) reveals that the right-hand side is a function of the angular states, sensor output voltages, and sensor calibration parameters, while the left-hand side is a function of the angular state derivatives. From an attitude construction perspective, voltages and

calibration terms are known parameters while pitch-yaw-roll angles and their derivatives are unknown variables implying a set of nonlinear coupled differential equations must be solved. Gyro attitude construction is thus a fundamentally different problem than accelerometer based attitude construction.

A 5th order Runge-Kutta numerical integration method will be used as a basis for gyro construction. Details of the Runge-Kutta algorithm can be found in Reference 17. This algorithm requires differential equations in 1st order form. Note Equation (IV-D.4) satisfies this requirement. Represent any one of the three model fixed gyro sensor relationships within Equation (IV-D.4) as

$$\dot{\mathcal{A}}_i = F_i(\mathcal{A}_j, V_k, B_k, S_k, A_k, C_k) \tag{IV-D.5}$$

where function F_i denotes the nonlinear functional dependency of angular state derivative $\dot{\mathcal{A}}_i$ on angular state $\mathcal{A}_j$, voltage V_k, bias B_k, sensitivity S_k, azimuth rotation A_k, and coning rotation C_k, where i,j = 1, 2, 3, $\mathcal{A}_1 = \Theta$, $\mathcal{A}_2 = \Psi$, $\mathcal{A}_3 = \Phi$, and $k = x_{sn_m}, y_{sn_m}, z_{sn_m}$. Equation (IV-D.5) can be interpreted as a nonlinear dynamic system with $\mathcal{A}_j$ as state variables and V_k as inputs.

Suppose initial conditions for the pitch-yaw-roll angular states are known from the pretest AMS alignment. Further suppose that a data set of n triples for each voltage is available. With the input voltages, angular position starting conditions, and calibration parameters, Equation (IV-D.5) can be used to generate state derivatives needed for temporal propagation of the angular states through numerical integration. In the 5th order Runge-Kutta strategy, denote the current angular state at time t as $\mathcal{A}_j(t)$ and let the time step be denoted by Δt. To advance the state to $\mathcal{A}_j(t+\Delta t)$, Equation (IV-D.5) is evaluated 6 times at sequentially projected preliminary angular state solutions across the time step, or

$$
\begin{aligned}
\dot{\mathcal{A}}_{i_1} &= F_i(\mathcal{A}_j(t), V_k(t), B_k, S_k, A_k, C_k) \\
\dot{\mathcal{A}}_{i_2} &= F_i(\mathcal{A}_j(t) + \tfrac{1}{4}\dot{\mathcal{A}}_{j_1}\Delta t, V_k(t + \tfrac{1}{4}\Delta t), B_k, S_k, A_k, C_k) \\
\dot{\mathcal{A}}_{i_3} &= F_i(\mathcal{A}_j(t) + \tfrac{1}{8}\{\dot{\mathcal{A}}_{j_1} + \dot{\mathcal{A}}_{j_2}\}\Delta t, V_k(t + \tfrac{1}{4}\Delta t), B_k, S_k, A_k, C_k) \\
\dot{\mathcal{A}}_{i_4} &= F_i(\mathcal{A}_j(t) + \tfrac{1}{2}\{-\dot{\mathcal{A}}_{j_2} + 2\dot{\mathcal{A}}_{j_3}\}\Delta t, V_k(t + \tfrac{1}{2}\Delta t), B_k, S_k, A_k, C_k) \\
\dot{\mathcal{A}}_{i_5} &= F_i(\mathcal{A}_j(t) + \tfrac{3}{16}\{\dot{\mathcal{A}}_{j_1} + 3\dot{\mathcal{A}}_{j_4}\}\Delta t, V_k(t + \tfrac{3}{4}\Delta t), B_k, S_k, A_k, C_k) \\
\dot{\mathcal{A}}_{i_6} &= F_i(\mathcal{A}_j(t) + \tfrac{1}{7}\{-3\dot{\mathcal{A}}_{j_1} + 2\dot{\mathcal{A}}_{j_2} + 12\dot{\mathcal{A}}_{j_3} - 12\dot{\mathcal{A}}_{j_4} + 8\dot{\mathcal{A}}_{j_5}\}\Delta t, V_k(t + \Delta t), B_k, S_k, A_k, C_k)
\end{aligned}
\qquad \text{(IV-D.6)}
$$

The final estimate for the angular state is obtained by averaging 5 of the preliminary solutions according to

$$
\mathcal{A}_i(t + \Delta t) = \mathcal{A}_i(t) + \frac{1}{90}\{7\dot{\mathcal{A}}_{i_1} + 32\dot{\mathcal{A}}_{i_3} + 12\dot{\mathcal{A}}_{i_4} + 32\dot{\mathcal{A}}_{i_5} + 7\dot{\mathcal{A}}_{i_6}\}\Delta t \qquad \text{(IV-D.7)}
$$

Equations (IV-D.6)-(IV-D.7) represent the iterative Runge-Kutta integration algorithm. $\mathcal{A}_j(t+\Delta t)$ is computed from Equation (IV-D.7) and reinterpreted as the starting condition for the next computational cycle. This process is repeated until the final time is reached. The angular construction accuracy will be a direct function of both the time step size and the angular state initial condition.

The numerical integration algorithm for gyro attitude construction is validated here within a simulated laboratory environment with synthetically generated data using MATLAB. It is important to note the general construction algorithm presented here is not tested in the laboratory with real data within the data acquisition control software environment using LabVIEW. An angular motion profile was generated and the corresponding sensor voltages were computed for specified bias, sensitivity, azimuth angle, and coning angle parameters. This data is intended to represent actual data that would be collected from hardware using a high bandwidth angular calibration table in the laboratory. The motion profile consisted of harmonic excitation with Θ = 10sin(0.125×2π×t), Ψ = 10sin(0.0625×2π×t), and Φ = 10sin(0.25×2π×t) deg for $0 \le t \le 10$ s with a time step of 0.001 s which yields n = 10,001. Specified calibration parameter values from Section IV-C are used. Figure 9 shows overlay traces of the exact and computed angular states. Figure 10 shows difference traces between exact and computed angular states. The computed

values are all in excellent agreement with the exact values validating the gyro attitude construction methodology. Appendix E lists the MATLAB software pertaining to gyro attitude construction.

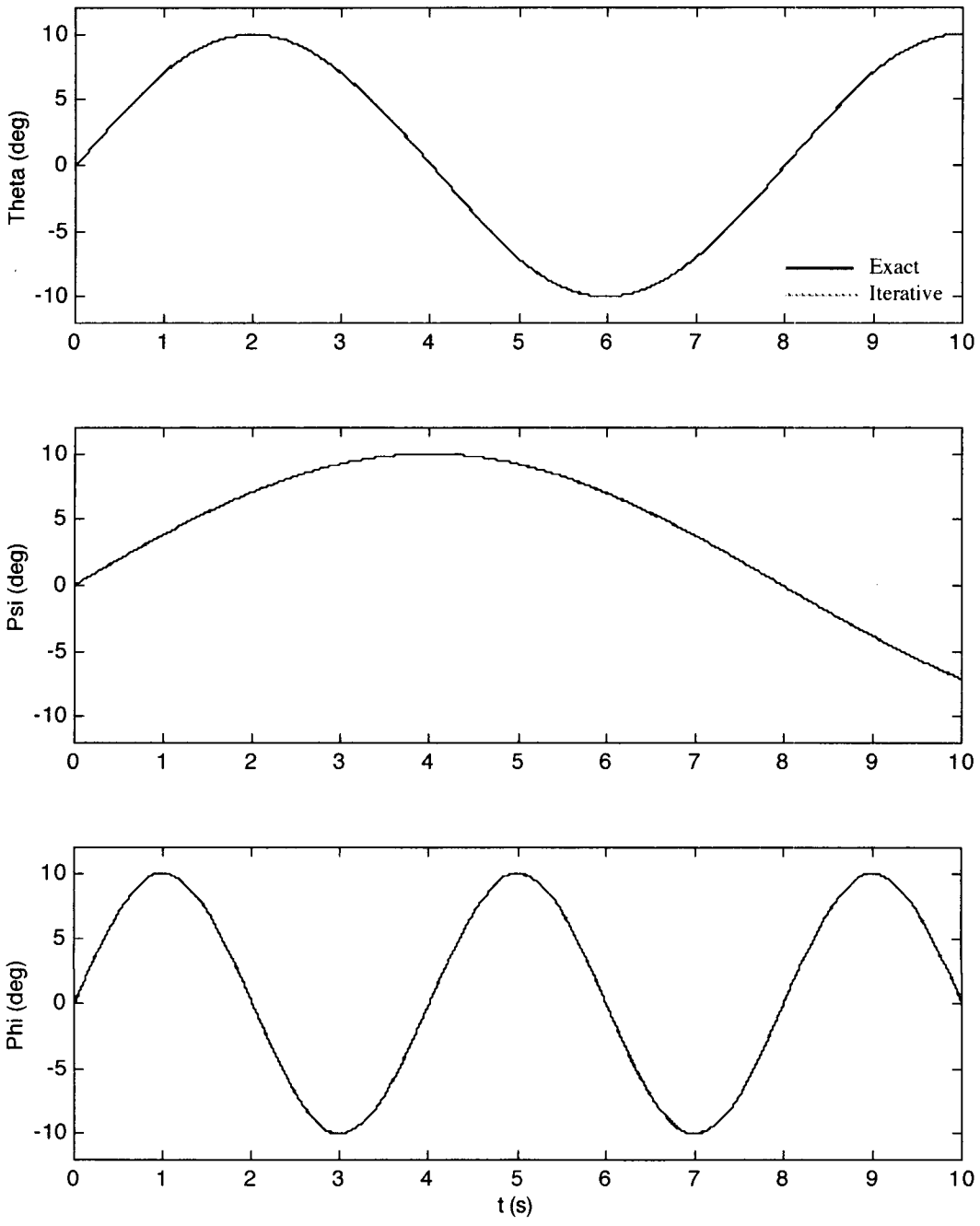

Figure 9 Gyro Construction Test Results – Absolute

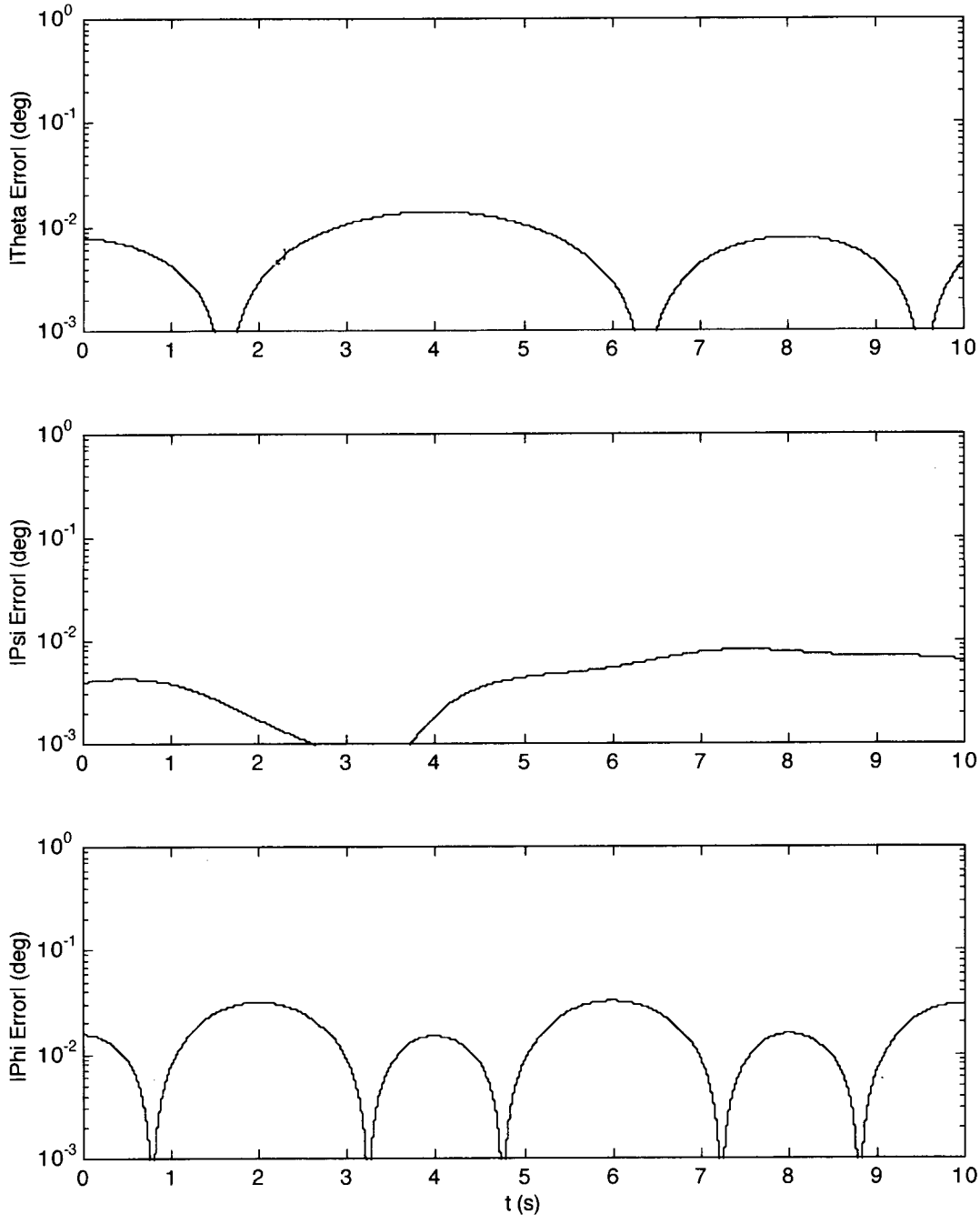

Figure 10 Gyro Construction Test Results – Relative

Section V
Hardware-Software Design and System Integration-Test

A. Hardware Description

For the AMS prototype, very little freedom existed in hardware design or selection. No budgetary resources within the contract, or external to the contract, were available for hardware purchase such as MEMS sensors or data acquisition microprocessor cards. Therefore, utilization of existing NASA LaRC hardware inventories was mandated, and in particular inventories allocated to the Models and Systems Branch. Major hardware components that were made available to the contractors consisted of a Pentium II class personal computer with video monitor, National Instruments 4 channel 200 kHz NI-4452 data acquisition card, Analog Devices ADXL105 MEMS micromachined polysilicon vibrating structure accelerometer, and muRata ENC-03J piezoelectric vibrating gyroscope or rate gyro. Also available were several high fidelity angular calibration tables with motorized drive systems or manual cranks, instrumentation, cables and connectors, and laboratory space to conduct research activities. Critical sensor and data acquisition card components will be briefly discussed.

An Analog Devices ADXL105 accelerometer was used for prototype AMS laboratory development activities based on availability considerations. Figure 11 shows a 3-view drawing of this MEMS accelerometer unit. The ADXL105 MEMS accelerometer uses an open-loop architecture consisting of a micromachined polysilicon vibrating structure outfitted with a central capacitance plate and positioned between two other fixed capacitor plates. The fixed plates are used to nominally vibrate the central plate, as well as to sense unsymmetric motion resulting from accelerations. The sensor outputs a voltage signal proportional to the input acceleration. Table 1 in Section II-C summarized the performance characteristics of this class of sensor, according to vendor published information. Detail sensor specifications can be found in Reference 13.

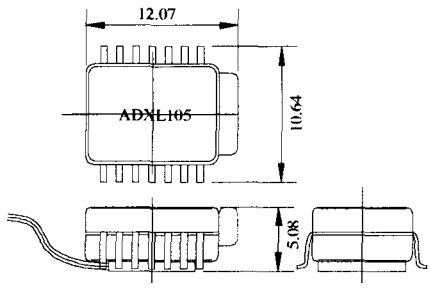

Figure 11 Analog Devices ADXL105 3-View Drawing (mm)

A muRata ENC-03J gyroscope was also used for prototype AMS laboratory development activities based on availability considerations. Figure 12 shows a 3-view drawing of this MEMS gyro unit. The gyroscope is a rate gyro which produces an output voltage signal proportional to input angular rate. The ENC-03J MEMS gyro uses an open-loop architecture consisting of a ceramic bimorph vibrating structure excited electrically. When this oscillating unit experiences an angular rate, an electrical signal is generated proportional to the resulting Coriolis force. Table 2 in Section II-C summarized the performance characteristics of this class of sensor, according to vendor published information. Detail sensor specifications can be found in Reference 15.

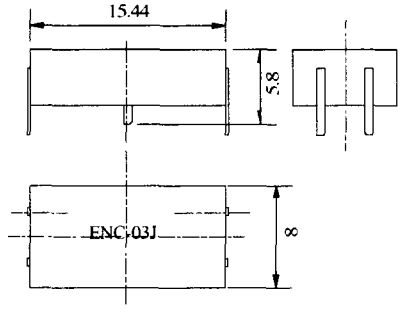

Figure 12 muRata ENC-03J 3-View Drawing (mm)

A National Instruments NI-4452 data acquisition microprocessor card was available for prototype AMS laboratory development activity. Figure 13 shows a top-view photograph of this microprocessor card. The NI-4452 data acquisition card is a 16 bit resolution, 4 analog input channel, high throughput, high dynamic range signal acquisition device. Sampling rate for this

card is 200 kHz with an operational frequency range from DC to 95 kHz. The card incorporates sophisticated real-time anti-aliasing and anti-imaging digital signal processing filters. The NI-4452 also interfaces with lower level NI-DAQ driver software and higher level LabVIEW control software. Detail data acquisition card specifications can be found in Reference 18.

Figure 13 National Instruments NI-4452 Top-View Photograph

B. Software Design

A wide range of design freedom and selection existed with data acquisition controlling software, such as C, Visual Basic, LabVIEW, MATLAB, Data Acquisition Toolbox, etc. National Instruments LabVIEW was selected for this function based on its powerful capabilities, ease of use, compatibility with the NI-4452 data card, and acceptance at NASA LaRC. LabVIEW's graphical user interface was used to design multi-functional control instrumentation software that reads input signals from the data card, processes and filters the input signals, calibrates several key sensor parameters, transforms the acceleration and angular rate data to angular position states, records data to storage devices, and outputs real-time information to a video display in numeric and graphical formats. For the AMS prototype, and with a limited number of data acquisition channels imposed by the hardware, only simplified single-axis pitch calibration-construction software design using a single accelerometer and single gyro was considered in detail. A more capable multi-accelerometer based two angle construction capability was also designed, but to lesser degree of detail. Software design and testing was a

major effort within the overall project. Detail information about LabVIEW capabilities and utilization can be found in References 11-12.

Figures 14-15 show the functional diagram of the AMS prototype control instrumentation software. In the LabVIEW environment, software design consists of graphically interconnecting system supplied and user defined component functions, in an efficient and effective arrangement, to accomplish higher level objectives, such as data acquisition or data processing. The AMS prototype operates in one of two modes (see Figure 3): sensor calibration or attitude construction, and Figures 14-15 reflect this architecture. Figure 14 pertains to sensor calibration while Figure 15 relates to attitude construction. These functional diagrams, and associated component level function diagrams, are the software listing, since LabVIEW auto-codes the low level commands.

In the sensor calibration mode (see Figure 14), 3 analog signals are sampled by the software through the data acquisition card. These signals correspond to accelerometer output voltage, gyro output voltage, and a temperature voltage signal for the accelerometer (recall the ADXL105 unit has a built in temperature sensor). A significant problem was encountered during interfacing the NI-4452 card with core data sampling functions within LabVIEW. Success was ultimately achieved by utilizing and modifying several core data sampling functions from Wyle Laboratories. These component functions from Figure 14 are expanded in Figure 16. Next the 3 element vector signal is split into separate scalar signals and run through low pass Chebyshev filters to reduce high frequency noise. Figure 17 shows the expanded functional diagram for the filters. The signals are then averaged over a sample window (assuming the sensors are at rest) to calibrate the bias parameters. In this preliminary development stage, calibration of sensitivity parameters is not considered. These bias values are then supplied to the attitude construction mode diagram in Figure 15 as the 3 signals entering from the right-hand side.

In the attitude construction mode (see Figure 15), 3 analog signals are again sampled and correspond to accelerometer output voltage, gyro output voltage, and temperature voltage for the

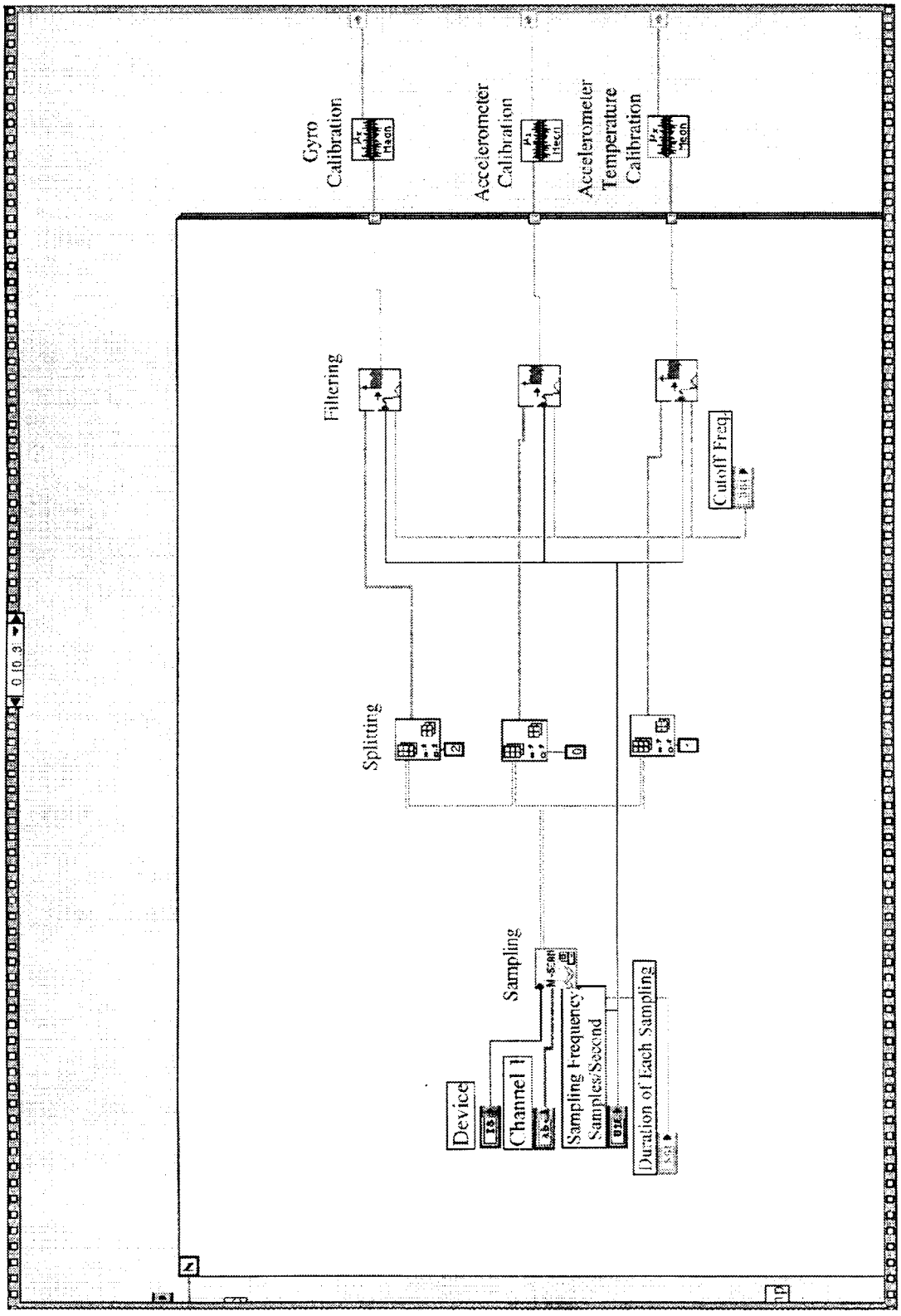

Figure 14 Functional Diagram for Sensor Calibration

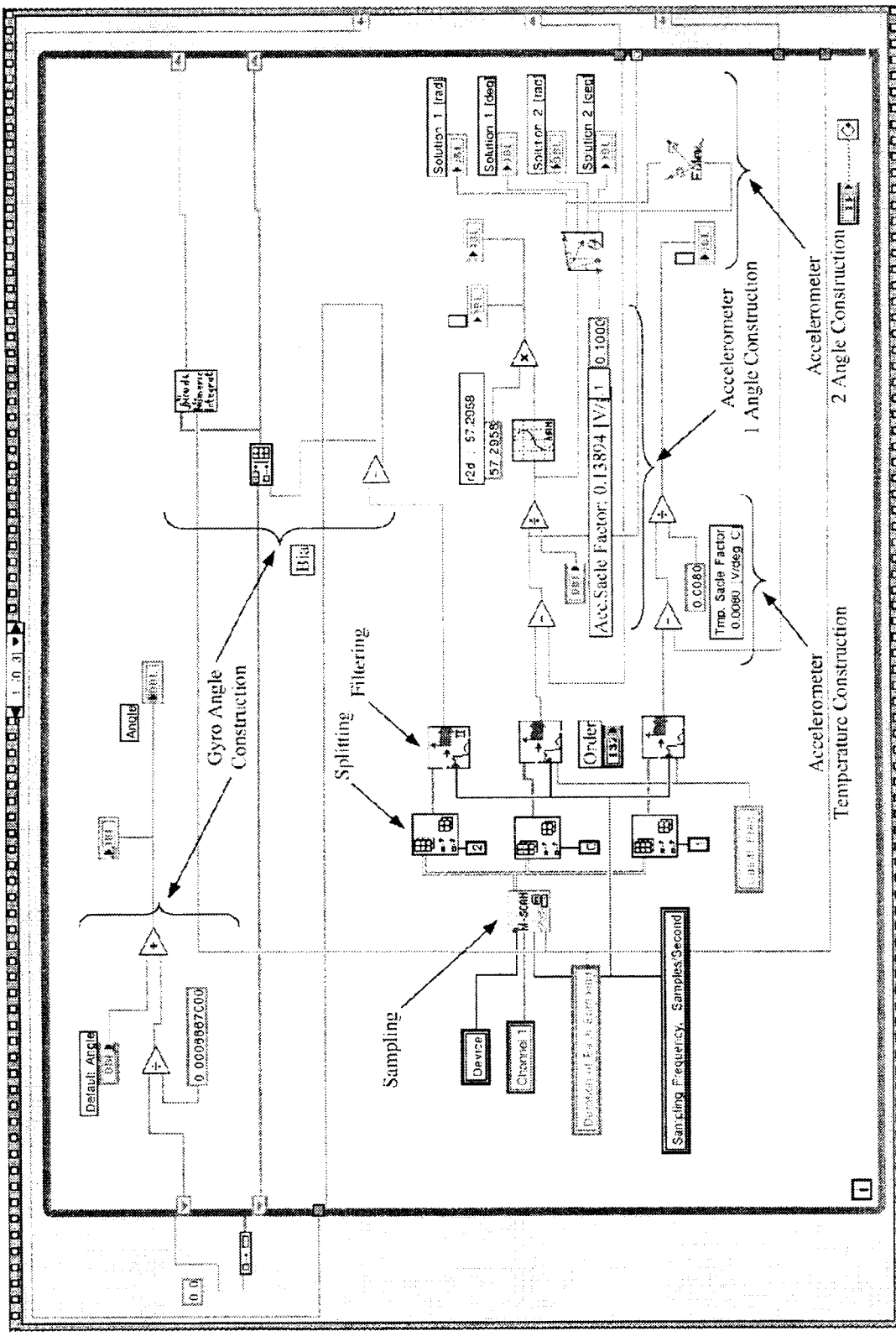

Figure 15 Functional Diagram for Attitude Construction

accelerometer (assuming the sensors are in motion or have been moved from their initial state). The signals are sampled with the modified Wyle Laboratories core functions shown in Figure 16. As shown in Figure 15, the vector signal is again split and filtered in an identical fashion as that noted in Figure 14. For the accelerometer based attitude construction noted in Figure 15, scale factor (or sensitivity) and bias are applied to the accelerometer voltage signal. Note the sensitivity must be manually inputed by the user at this time. The resulting signal (gravity component measurement) is passed to an inverse sine function to generate pitch angle (see Equation (IV-B.3) with $\Psi = 0$ deg), and then units are changed and the result is sent to the user interface panel for display. The gravity component measurement signal can also be passed to a more complex two angle attitude construction algorithm, as indicated in Figure 15. Figure 18 shows the expanded functional diagram representing this algorithm. At this time, the user can manually input two additional gravity component signals and initial angle estimates to reconstruct the associated pitch-roll angles in a framework similar to that presented in Sections III-B and IV-B. Resulting solutions are outputed to the user display panel.

Gyro attitude construction logic noted in Figure 15 is structured differently. After subtracting off the bias value from the filtered gyro voltage signal, the result is temporarily stored in small packets and then numerically integrated as a unit with an initial user supplied value for the integration bin. After this processing, scale factor is taken into account and a default angle value is applied to generate a measured pitch angle, which is also displayed to the user. Temperature voltage signal is also processed with its appropriate calibration values resulting in a temperature measurement which could be used in scheduling accelerometer calibration parameters as the thermal environment changes. At this time, the temperature measurement signal is only displayed as an output. All control instrumentation and measurement functions displayed in Figures 14-15 can be performed in real-time allowing wind tunnel technicians and experimental aerodynamicists to evaluate ongoing test conditions.

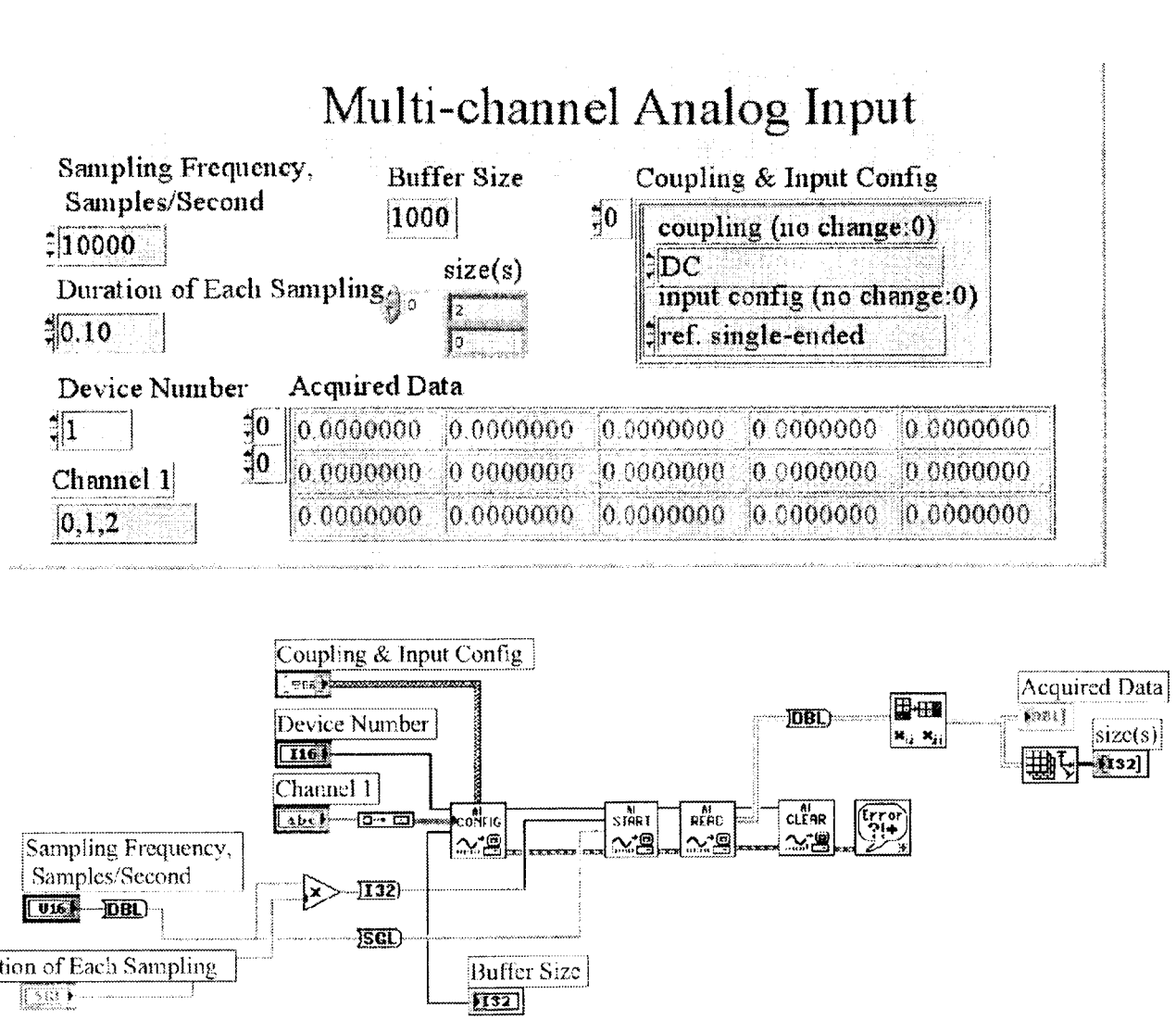

Figure 16 Functional Diagram for Data Sampling

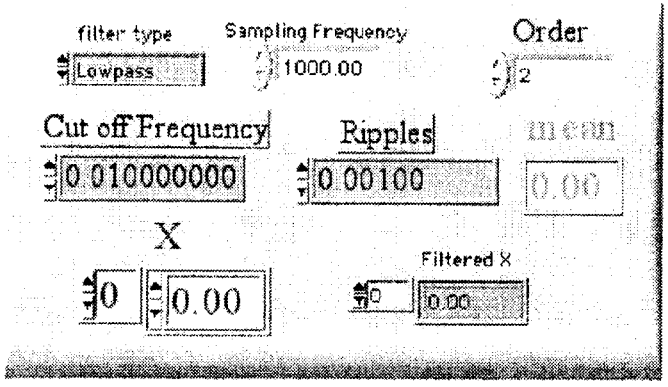

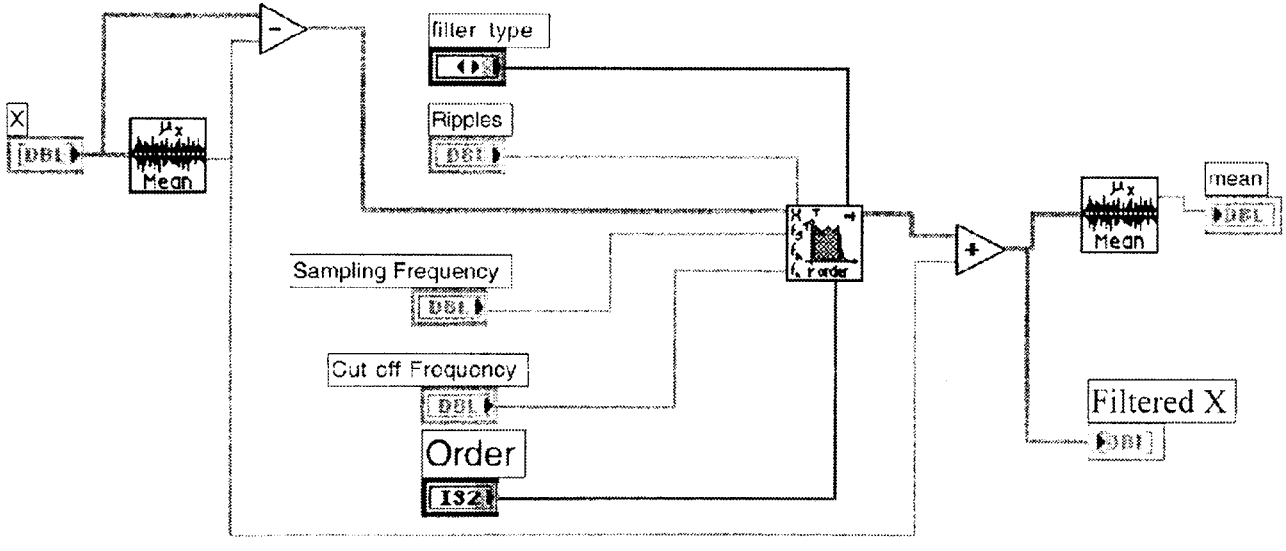

Figure 17 Functional Diagram for Data Filtering

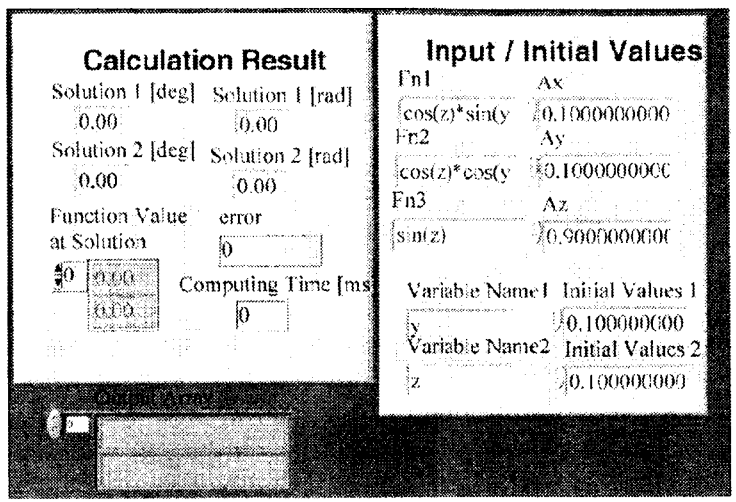

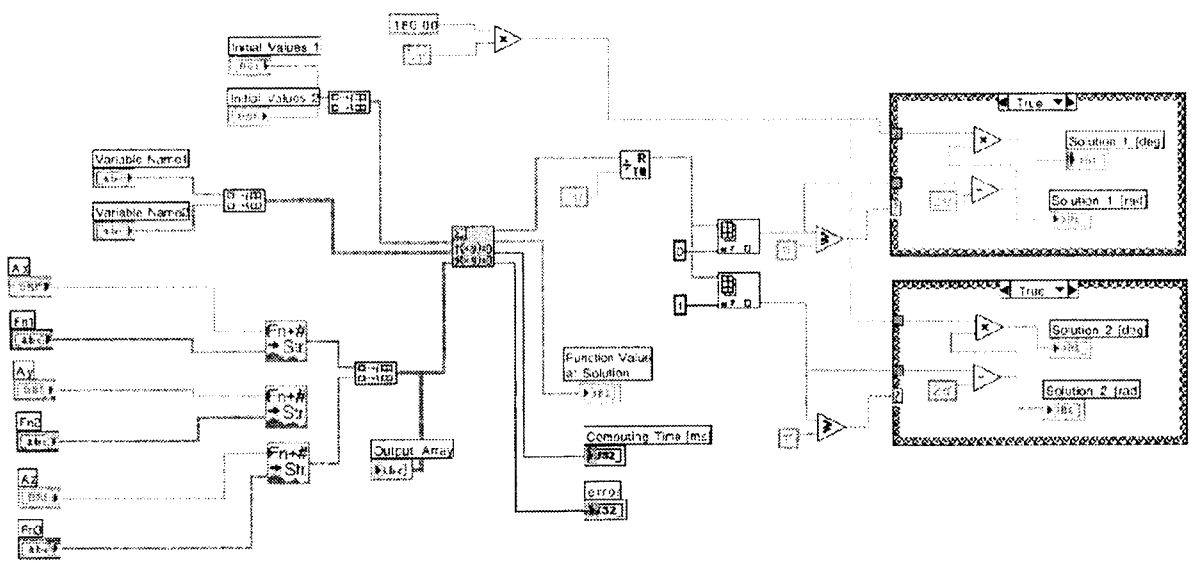

Figure 18 Functional Diagram for Accelerometer Two Angle Construction

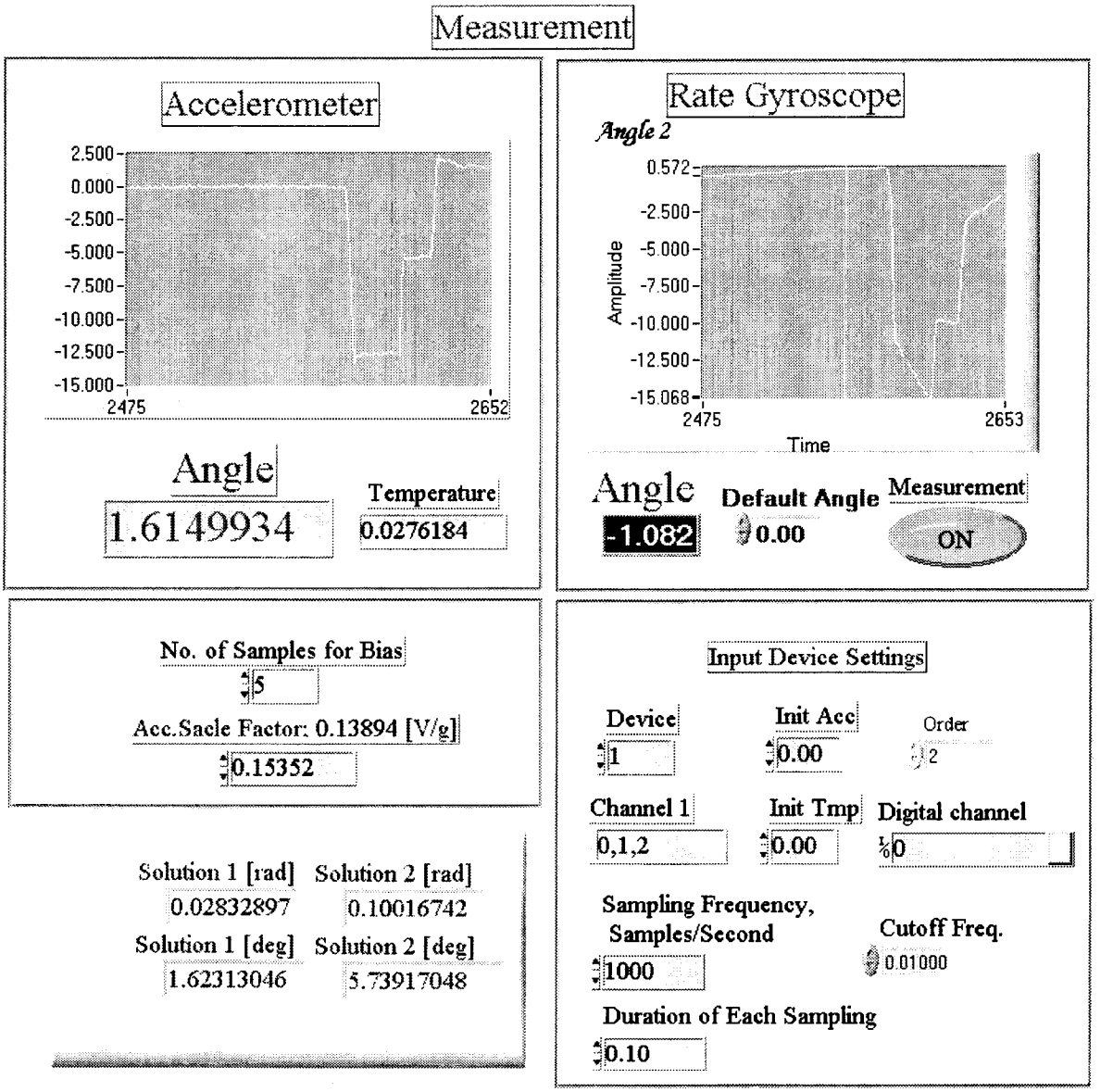

Figure 19 User Interface Panel

The user interface panel is shown in Figure 19. The top-left window in the interface panel displays the pitch angle measured by the accelerometer, and the top-right window displays the pitch angle measured by the gyro. Numeric displays labeled "Angle" in these two upper windows indicate measurement angles presented in real-time. Recent time histories of the pitch measurements are also displayed in graphical format. The bottom-left window also displays the two angle solution results. The mid-left window allows the user to adjust the bias calibration

process, and to manually input the sensitivity values. Finally, the bottom-right window provides a capability to adjust data acquisition parameters and the cut off frequency of the low pass noise filters.

C. Prototype Integration and Test

Significant efforts addressed integration of the hardware and software components into a working end-to-end albeit simplified angular measurement system prototype. At this preliminary development stage, a professionally packaged and fully capable system is not the objective, but rather to explore feasibility of such a system, to benchmark potential performance, and expose any critical problems. Thus, the prototype system is only a temporary arrangement of hardware and software devices. The basic integration task consisted of connecting components to one another such that communication and data transfer functions between components is reliable and accurate. Due to shared laboratory space and equipment, and in particular the angular calibration tables and computer workstation, the prototype components required assembly and disassembly for each laboratory session. This arrangement was a hindrance to rapid progress. Another specific integration problem related to NI-4452 and LabVIEW interfacing. Documentation indicated these products are compatible, but after following published and recommended guidelines, interfacing was not accomplished. A significant amount of time was devoted to resolving this problem. Guidelines were finally abandoned and replaced with the Wyle Laboratories core data sampling software heritage.

After integration tasks were completed, activities focused on prototype testing to demonstrate feasibility, assess potential angular measurement performance, and highlight any deficiencies. With all components properly connected, one ADXL105 accelerometer and one ENC-03J gyro are simultaneously mounted on the angular calibration table. Two methods for assessing angular measurement performance are considered. First, the table is rotated manually by a specified amount to excite and test the AMS prototype. Comparison of the prototype measurement output value with the known table rotation will provide one estimate of the angular

accuracy capability. Second, the table is held at rest and measurements are taken by the AMS system. Comparisons of the prototype measurement signal stability after bias removal with the known zero value for the table will also provide an estimate of the angular measurement capability.

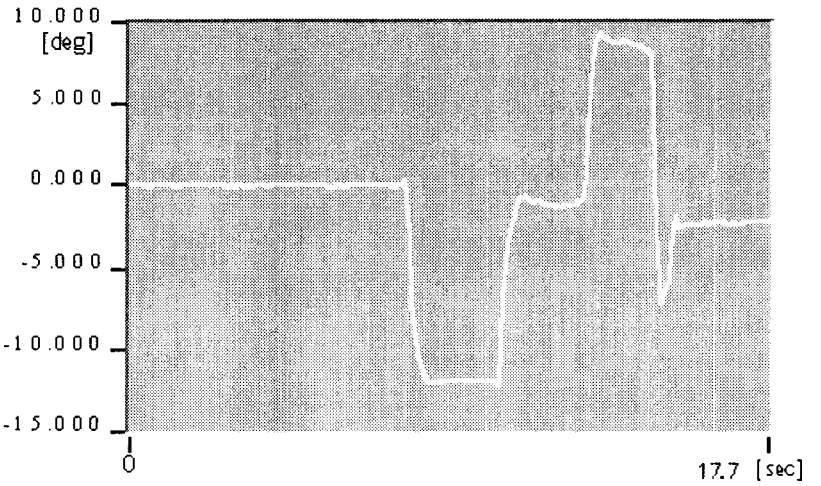

Figure 20 Accelerometer Based AMS Prototype Dynamic Response

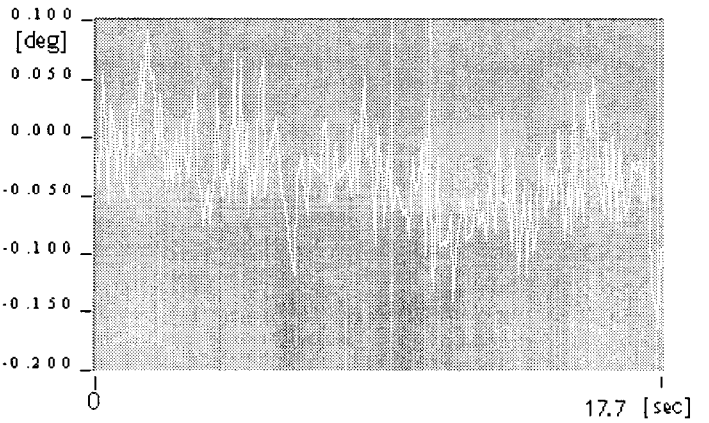

Figure 21 Accelerometer Based AMS Prototype Static Response

Measured angular response of the calibration table using the ADXL105 accelerometer sensor in the AMS prototype is shown in Figures 20-21. In Figure 20, the table was held at rest

initially for approximately 8 s, and then the table was manually rotated to negative, null, positive, and back to null orientations with rapid slew motions followed by short holding periods out to about 17 s. The angular measurement response in Figure 20 accurately tracks this dynamic profile. The negative angular orientation of the table during the rest period was recorded as 12 deg. The measurement responses appears to be within ±0.1 deg of this known value. Angular measurement performance of the AMS prototype using an accelerometer can also be determined by observing Figure 21. Figure 21 shows the measurement reading for a period of approximately 17 s during which the table was held at rest. The response in Figure 21 indicates accelerometer signal drift or bias is small and lies approximately within the ±0.1 deg band. Another important feature to note from Figure 20 is the high bandwidth of the accelerometer sensor. The ADXL105 unit shows a rapid response with little overshoot. The small rise time and overshoot features visible in Figure 20 most likely represent accurate tracking of physiological limitations during manual table excitations. These results solidly confirm the angular measurement accuracy projections made in Section II-C based on manufacture's performance information.

Measured angular response of the calibration table using the ENC-03J gyro sensor in the AMS prototype is shown in Figures 22-23. Recall the ENC-03J gyroscope is mounted on the calibration table simultaneously with the ADXL105 accelerometer. Thus, excitations applied to the ENC-03J gyro are identical to the excitations applied to the ADXL105 accelerometer. Consequently, assuming the accelerometer based measurements are accurate, the angular response of ENC-03J based measurement system displayed in Figures 22-23 can be compared with the ADXL105 system responses shown in Figures 20-21. Note quantitative comparisons are subject to errors in the manually inputed sensitivity values for both sensor units. Figure 22 indicates the angular measurement response tracks the dynamic motion profile in a rough sense, but the gyro output signal drift (indicated by linear growth in angle after integration of the constant rate signal) during rest periods is significant. Even worse is the observation that the drift is not repeatable and shows strong dependency on response history. Note signal drift becomes negative when the gyroscope is turned in the negative direction, and becomes positive when the

accuracy capability. Second, the table is held at rest and measurements are taken by the AMS system. Comparisons of the prototype measurement signal stability after bias removal with the known zero value for the table will also provide an estimate of the angular measurement capability.

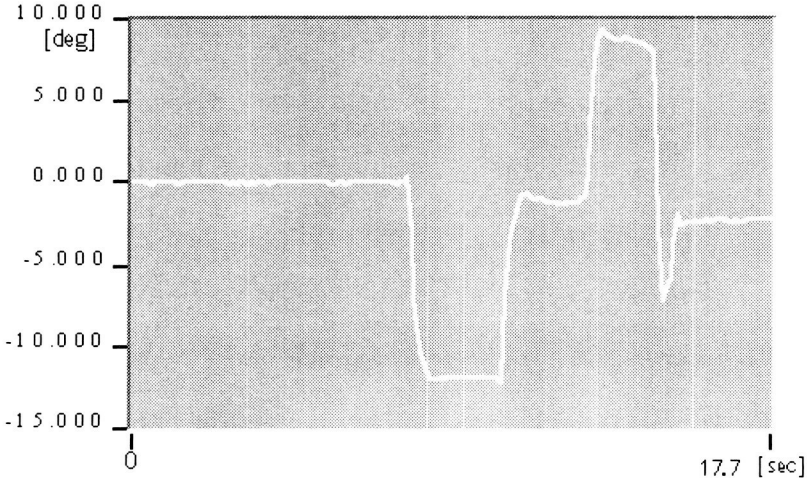

Figure 20 Accelerometer Based AMS Prototype Dynamic Response

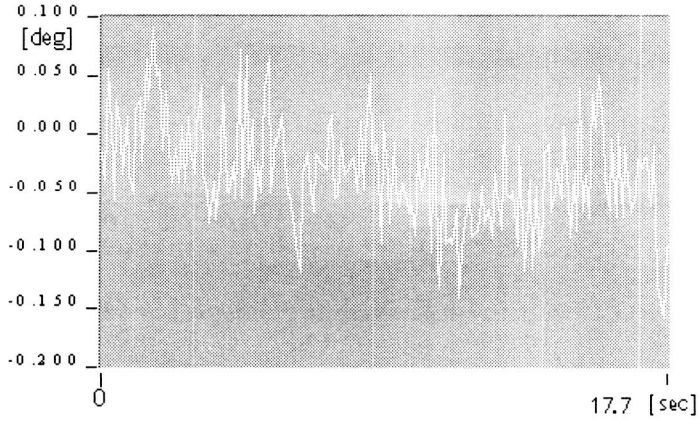

Figure 21 Accelerometer Based AMS Prototype Static Response

Measured angular response of the calibration table using the ADXL105 accelerometer sensor in the AMS prototype is shown in Figures 20-21. In Figure 20, the table was held at rest

All key aspects of the angular measurement system prototype have been investigated. Motion detection, data acquisition, data processing, sensor calibration, and attitude construction functions were all explored and investigated to a level that confirmed concept feasibility. This end-to-end operational capability was tested and demonstrated in the laboratory under real-time conditions with actual hardware and software components. Only simplified single-axis calibration-construction capability was demonstrated, but this was judged to be sufficient for validating feasibility. Angular measurement performance using the accelerometer based prototype was confirmed in meeting the design requirements of ±0.1 deg. Angular measurement requirements for the gyro based prototype unfortunately was not confirmed, under the constraints of gyro sensor availability. The fundamental problem is poor signal drift characteristics of the ENC-03J gyro. Manufacture's performance specifications imply accuracy requirements will be difficult to achieve (see Section II-C) unless 1) drift characteristics are highly repeatable and stable, 2) precise calibration is achieved, and 3) time efficient test procedures are all employed. Methodology for requirement 2 has been offered in Section IV-C and requirement 3 can be addressed in future efforts. However, prototype testing confirmed drift characteristics are highly erratic and unstable (lack of requirement 1). On the otherhand, if given appropriate MEMS performance, the gyro based prototype system should satisfy design objectives. A major conclusion of the work is that better performing gyros are required.

Although the actual prototype system is not professionally packaged, two proposed schematics for an AMS prototype specifically tailored for use in the 31-Inch Hypersonic Tunnel are offered. Recall in this application, only one accelerometer package (3 sensors) is needed since roll angle is always known. Two options are considered. First, an AMS option using only 3 accelerometers is considered in Figure 24. Such an AMS has a capability to measure pitch-yaw angles to ±0.1 deg. ADXL105 accelerometers are used as representative sensors in Figure 24. This AMS arrangement is packaged such that it fits within the tip of typical sting hardware used in the 31-Inch Hypersonic Tunnel. Overall length of the sensor package is about 0.8 in and expected mass of the package with mounting plug is approximately 50 g. The second option uses

3 accelerometers and 3 gyroscopes and provides a capability to measure pitch-yaw-roll angles to ±0.1 deg (assuming high performance gyros are used). This option is shown in Figure 25. The schematic uses ADXL105 accelerometers and ENC-03J gyros as representative sensors (only for dimensional purposes in the gyro case). Expected length of this package is about 1.8 in, and expected mass is 100 g with a mounting plug. Section views show that wires can be placed within voids beside the accelerometers and gyros. Also, cooling pipes which may be needed in the 31-Inch Hypersonic Tunnel application can be placed in these empty spaces. Utilization of motion detection units with multi-axis sensing, such as the MEMSIC units listed in Table 1 or other Samsung gyros not considered in this report, can be very useful for reducing weight and efficient sensor positioning internal to the sting while maximizing empty space for other subsystems.

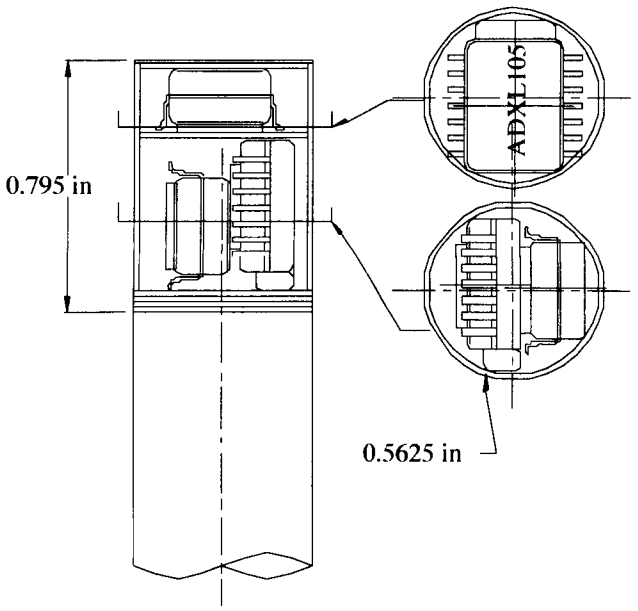

Figure 24 Accelerometer AMS Prototype Schematic

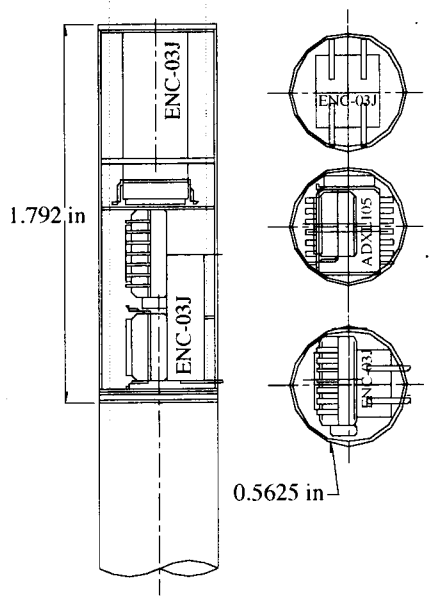

Figure 25 Accelerometer-Gyro AMS Prototype Schematic

Section VI
Conclusions and Recommendations

Investigation and development of a high accuracy angular measurement capability for hypersonic wind tunnel facilities located at NASA LaRC is considered in this effort. Specifically, utilization of micro-electro-mechanical sensors including accelerometers and gyros, coupled with software driven data acquisition hardware, integrated within a prototype measurement system, is addressed. A ±0.1 deg measurement performance in pitch, yaw and roll is formulated from wind tunnel constraints and aerodynamic test objectives. A survey of commercially available MEMS units is used to project potential measurement performance levels that satisfy design requirements. Accelerometer based systems can more easily meet the design requirements than gyro based systems. For the gyro based systems to achieve the required performance, three factors are needed: 1) highly repeatable and stable drift characteristics, 2) highly accurate calibration techniques, and 3) time efficient test procedures.

A very general analytical framework describing mathematical relationships between multi-axis gravitational acceleration and angular rate data to the test article pitch, yaw and roll states is developed. An Eulerian attitude description that is consistent with NASA LaRC tunnel facilities is selected for use. The framework can address advanced wind tunnel facilities incorporating exotic pitch-yaw-roll drive systems, and reduces to simpler applications where roll angle is fixed and known (NASA LaRC application). Two accelerometer sensor packages mounted in the sting fixed and model fixed reference frames, and one gyro sensor package mounted in the model fixed reference frame, are incorporated into the framework. Accelerometer and gyro parameter models include mechanical-electrical hardware aspects; specifically bias, sensitivity, and azimuth-coning misalignments. Sensor calibration procedures for accelerometers and gyros are formulated using nonlinear Gauss-Newton regression logic. These procedures are tested with simulated data and without noise and are found to be highly accurate. Angle construction using

accelerometers are formulated with both analytic closed-form and iterative Gauss-Newton strategies. A two sequence approach using two accelerometer packages facilitates full pitch-yaw-roll construction. In the fixed known roll angle case, only one accelerometer package is required. Angle construction using gyros is formulated using nonlinear Runge-Kutta numerical integration. These procedures are also tested with simulated data without noise and are found to be highly accurate. Sensor calibration and attitude construction results validate feasibility of the measurement system concept.

Design of hardware and software components followed by system integration and test resulted in a prototype measurement system. Modern software tools are used to create multi-functional control instrumentation that reads input signals from a data card, processes and filters input signals, calibrates several key sensor parameters, transforms gravitational acceleration and angular rate data to angular position states, records data to storage devices, and outputs real-time information in numeric and graphical formats. Integration of hardware and software components to a laboratory demonstrated end-to-end simplified angular measurement system prototype is successfully accomplished. Motion detection, data acquisition, data processing, sensor calibration, and attitude construction functions are all explored to a level that confirms concept feasibility. Angular measurement performance using the accelerometer based prototype is confirmed in meeting the ±0.1 deg design requirement. Angular measurement requirements for the gyro based prototype unfortunately is not confirmed. The fundamental problem is poor gyro signal drift characteristics. Prototype testing confirmed drift characteristics are highly erratic and unstable. However, if given appropriate MEMS performance, the gyro based prototype system should satisfy design objectives. A major conclusion of the work is that better performing gyros are required.

The overriding conclusion drawn from this preliminary research effort is that projected feasibility for a MEMS based angular measurement system using high grade accelerometers and gyros, as well as sophisticated calibration and construction logic, that can satisfy current accuracy objectives, is high. However, substantial additional work is necessary to achieve full

success. Effects from noise, initial conditions, and sampling rate on the sensor calibration and attitude construction algorithms should be addressed and minimized with algorithm modification. Rotating earth effects on accelerometer and gyro outputs have been ignored in this study and should be addressed in future work. Measurement and control instrumentation software needs to be greatly enhanced to achieve a useful working system. General multi-axis calibration and construction logic should be incorporated into the software. Alignment procedures should also be considered in any future efforts. A broader range of accelerometer and gyro MEMS should be requisitioned and sampled for potential performance improvements, especially for gyros. Extensive calibration and construction testing including thermal effects should also be conducted to build further confidence in the proposed angular measurement system. Finally, testing in wind tunnel operations and comparisons with existing measurement systems should be pursued.

References

1. Finley, T. D. and Tcheng, P., "Model Attitude Measurements at NASA Langley Research Center," AIAA-92-0763, Proceedings of the 30th AIAA Aerospace Sciences Meeting and Exhibit, Reno, Nevada, January, 1992, pp. n/a.

2. Tripp, J. S., Tcheng, P., Burner, A. W., and Finley, T. D., "Summary Report of the First International Symposium on Strain Gauge Balances and Workshop on AoA/Model Deformation Measurement Techniques," NASA-CP-1999-209101, Langley Research Center, Hampton, Virginia, March, 1999.

3. Biezad, D. J., *Integrated Navigation and Guidance Systems*, American Institute of Aeronautics and Astronautics, Reston, Virginia, 1999.

4. Rogers, R. M., *Applied Mathematics in Integrated Navigation Systems*, American Institute of Aeronautics and Astronautics, Reston, Virginia, 2000.

5. Marshall, R. and Landman, D., "An Improved Method for Determining Pitch and Roll Angles Using Accelerometers," AIAA-2000-2384, Proceedings of the 21st AIAA Aerodynamic Measurement Technology and Ground Testing Conference, Denver, Colorado, June, 2000, pp. n/a.

6. Finely, T. D., "Technique for Calibrating Angular Measurement Devices when Calibration Standards are Unavailable," NASA-TM-104148, Langley Research Center, Hampton, Virginia, August, 1991.

7. Tripp. J. S. and Tcheng, P., "Uncertainty Analysis of Instrument Calibration and Application," NASA-TP-1999-209545, Langley Research Center, Hampton, Virginia, October, 1999.

8. DeLoach, R., "Applications of Modern Experiment Design to Wind Tunnel Testing at NASA Langley Research Center," AIAA-98-0713, Proceedings of the 36th AIAA Aerospace Sciences Meeting and Exhibit, Reno, Nevada, January, 1998, pp. n/a.

9. DeLoach, R., "MDOE Perspectives on Wind Tunnel Testing Objectives," AIAA-2002-2796, Proceedings of the 22nd AIAA Aerodynamic Measurement Technology and Ground Testing Conference, St. Louis, Missouri, June, 2002, pp. n/a.

10. Technical Staff, *Using MATLAB Version 5*, MathWorks, Natick, Massachusetts, January, 1998.

11. Technical Staff, *LabVIEW User Manual*, National Instruments, Austin, Texas, July, 2000.

12. Bishop, R. H., *Learning with LabVIEW6i*, Prentice Hall, Upper Saddle River, New Jersey, 2001.

13. Technical Staff, "High Accuracy ±1 g to ±5 g Single Axis iMEMS Accelerometer with Analog Input, ADXL105," Analog Devices, Norwood, Massachusetts, 1999.

14. Technical Staff, "Low Cost, ±1 g Dual Axis Accelerometer with Analog/Digital Outputs, MX201A, MXA2500A, MXD2020A," MEMSIC, Andover, Massachusetts, April, 2002.

15. Technical Staff, "GYROSTAR Piezoelectric Vibrating Gyroscope ENC/ENV Series," muRata Manufacturing, Kyoto, Japan, March, 1999.

16. Technical Staff, "Micro Gyro Specifications for MG/MGL Series," Samsung Electro-Mechanics, Suwon, Kyongi-do, Korea, January, 2001.

17. Chapra, S. C. and Canale, R. P., *Numerical Methods for Engineers*, McGraw-Hill, New York, New York, 1988.

18. Technical Staff, "The Measurement and Automation Catalog," National Instruments, Austin, Texas, January, 2002.

Appendix A
Statement of Work for PO-L-14635

Development of a High Accuracy Angular Measurement
System for LaRC's Hypersonic Wind Tunnel Facilities

STATEMENT OF WORK

1.0 Introduction

Current angular measurement capability in LaRC's hypersonic wind tunnel facilities is lacking. These current systems are based on primitive mechanical measurement of the model sting pitch orientation. Pitch measurement accuracy is insufficient. Yaw and roll orientation measurements are not available and must be assumed. Wind tunnel tests are often repeated due to the uncertainty of the location of the model after being injected into the tunnel's test chamber. This project focuses on developing a modern and adaptable sensor package capable of measuring pitch, roll and yaw while also meeting the size and accuracy requirements stipulated by LaRC's hypersonic wind tunnels. It is believed that a package consisting of gyros, or a combination of gyros and accelerometers, will be required. Commercially available MEMS sensor technology is projected to have performance levels which can meet both size and accuracy requirements.

1.1 Scope

Angular orientation in pitch, roll and yaw can be directly measured by a gyro based sensor package. Additionally, pitch and roll orientation can be indirectly measured by an accelerometer package with comparison to the gravity vector. Mechanization of angular measurements will be based on these methodologies. The contractors shall provide services of a research and development nature that follow the specifications below

2.0 Information provided

The information related to the angular measurement system will be provided on an as needed basis.

2.1 Materials provided

LaRC shall provide the following materials

MEMS sensors
Laboratory calibration and test equipment

- Dual axis high precision angle indexing table. The table is built by A.G Davis Inc. and is capable of setting 1-degree increment combinations of pitch and roll from 0 to 360 degrees. The table is composed of two separate indexing heads in an orthogonal configuration, each accurate to 1 arc second over the full 360-

degree angle range. The angular position of each table is computer controlled using a serial interface.
- Single axis high precision indexing table. This table is also computer controlled using a serial interface. The table has a range of 360 degrees with a resolution of .0001 degrees.
- Multimeters with scanners for data acquisition such as the HP-3458A

All hardware required to construct a prototype system
- Electrical components such as resistors and capacitors
- Mechanical components such as the housing to hold the sensors

Computer systems and data acquisition components
- Computer with data acquisition cards

Commercial software for developing software for operating the prototype system
- Visual Basic, Labview, Matlab, ect

Environment for testing the prototype system
- Accelerometer laboratory/Wyle Laboratories
- Temperature chamber
- Wind tunnel

Procedures for documenting all work

3.0 Specifications

3.1 Collect and analyze wind tunnel angular measurement requirements.

3.2 Perform a search to find manufacturers of various makes of MEMS gyros and accelerometers. Select the best performing sensors based on the manufacturers specifications and provide LaRC with a report of the results including all relevant information necessary to procure the sensors.

3.3 Derive the governing equations that model the response of various sensor package designs and record the details of each derivation in a document.

3.4 Evaluate the performance of LaRC procured MEMS gyros and accelerometers by conducting tests in LaRC's accelerometer laboratory and at Wyle Laboratories.

3.5 Compare test results with tunnel requirements using LaRC approved statistical procedures and establish a reasonable goal for both package size and performance.

3.6 Develop an overall design and operation method for the system.

3.7 Conduct a preliminary design review and implement suggestions.

3.8 Assemble a pre-prototype sensor package.

3.9 Construct a data acquisition system using LaRC supplied hardware .

3.10 Develop and implement software for calibrating and operating the system.

3.11 Evaluate the sensor package using LaRC equipment and procedures and compare it's performance with the performance goals.

3.12 Determine if enhancements or design changes are necessary in order to meet the performance goals. If changes are necessary implement the changes and go back to 3.11, else continue to 3.13.

3.13 Construct a prototype sensor package.

3.14 Calibrate and test the prototype system in both LaRC's accelerometer laboratory and a wind tunnel.

3.15 Collect, analyze and implement feedback based on test results.

Appendix B
Accelerometer Sensor Calibration Listing

```
%-------------------------------------------------------------------------%
%
%                       3 Axis Accelerometer Package Calibration
%                                   - Sting Package -
%
%-------------------------------------------------------------------------%
% This File Calibrates 3 Accelerometer Oriented in 3 Axis
% File Name 'AccCalib00_Sting'
%
% Research Funded by
% Measurement & Instrumentation Branch of NASA Langley Research Center
% NASA LaRC Hampton VA. 23681
% Instructor in ODU Side: Dr. Newman
% Program Coded in MATLAB by Si-bok Yu
% Aerospace Engr. Dept., Old Dominion Univ.
% Latest Updated in Oct. 2002
%
%-------------------------------------------------------------------------%
%
%                                   Inputs
%
% Need Sensor Voltage Output at N Different Pitch, Yaw and Roll Orientations
% for each of 3 Axis
%
%
%                                   Outputs
%
% b     % Bias [V]
% S     % Sensitivity [V/g]
% Om    % Coning Angle [rad]
% A     % Azimuth Angle [rad]
%
%-------------------------------------------------------------------------%

clear;
r2d         = 180/pi;
d2r         = pi/180;
Tolerance   = 1e-32;
G           = 1;

%-------------------------------------------------------------------------%
% Load Pitch, Yaw, and Roll Motion, and Voltage Output
load SimAccData_Sting

%-------------------------------------------------------------------------%
% Initial Guess Values
b0  = 1.23;         % Bias [V]
S0  = 0.45;         % Sensitivity [V/g]
Om0 = 0.06*d2r;     % Coning Angle [rad]
A0  = 0.07*d2r;     % Azimuth Angle [rad]
```

```
A_vector = [b0 S0 Om0 A0]';

nData=length(Phi_m);

for iSen=1:3,
   for ii=1:100,
      b  = A_vector(1);
      S  = A_vector(2);
      Om = A_vector(3);
      A  = A_vector(4);

      for jj=1:nData-1,

         Th  = Th_m(jj);
         Psi = Psi_m(jj);

         vx  = Vxst(jj);
         vy  = Vyst(jj);
         vz  = Vzst(jj);

         if iSen == 1
Z(jj,1)=1;
Z(jj,2)=  ( -cos(Om)*cos(Psi)*sin(Th)         + sin(Om)*sin(A)*sin(Psi)*sin(Th)
           -sin(Om)*cos(A)*cos(Th)                                              )*g;
Z(jj,3)=S*(  sin(Om)*cos(Psi)*sin(Th)         + cos(Om)*sin(A)*sin(Psi)*sin(Th)
           -cos(Om)*cos(A)*cos(Th)                                              )*g;
Z(jj,4)=S*(  sin(Om)*cos(A)*sin(Psi)*sin(Th) + sin(Om)*sin(A)*cos(Th)           )*g;
D(jj,1)=vx-b
      -S*( -cos(Om)*cos(Psi)*sin(Th)         + sin(Om)*sin(A)*sin(Psi)*sin(Th)
           -sin(Om)*cos(A)*cos(Th)                                              )*g;
        elseif iSen == 2
Z(jj,1)=1;
Z(jj,2)=  (  sin(Om)*cos(A)*cos(Psi)*sin(Th) + cos(Om)*sin(Psi)*sin(Th)
           +sin(Om)*sin(A)*cos(Th)                                              )*g;
Z(jj,3)=S*(  cos(Om)*cos(A)*cos(Psi)*sin(Th) - sin(Om)*sin(Psi)*sin(Th)
           +cos(Om)*sin(A)*cos(Th)                                              )*g;
Z(jj,4)=S*( -sin(Om)*sin(A)*cos(Psi)*sin(Th) + sin(Om)*cos(A)*cos(Th)           )*g;
D(jj,1)=vy-b
      -S*(  sin(Om)*cos(A)*cos(Psi)*sin(Th) + cos(Om)*sin(Psi)*sin(Th)
           +sin(Om)*sin(A)*cos(Th)                                              )*g;
        elseif iSen == 3
Z(jj,1)=1;
Z(jj,2)=  ( -sin(Om)*sin(A)*cos(Psi)*sin(Th) - sin(Om)*cos(A)*sin(Psi)*sin(Th)
           +cos(Om)*cos(Th)                                                     )*g;
Z(jj,3)=S*( -cos(Om)*sin(A)*cos(Psi)*sin(Th) - cos(Om)*cos(A)*sin(Psi)*sin(Th)
           -sin(Om)*cos(Th)                                                     )*g;
Z(jj,4)=S*( -sin(Om)*cos(A)*cos(Psi)*sin(Th) + sin(Om)*sin(A)*sin(Psi)*sin(Th) )*g;
D(jj,1)=vz-b
      -S*( -sin(Om)*sin(A)*cos(Psi)*sin(Th) - sin(Om)*cos(A)*sin(Psi)*sin(Th)
           +cos(Om)*cos(Th)                                                     )*g;
        end;

      end;
      dA = inv( Z' *Z ) * ( Z' *D );
      A_vector  = A_vector + dA;

      error_D = sum(dA.^2);
```

```
      error_D = sqrt(error_D);
      if error_D < Tolerance
         ii
         break;
      end;

      [iSen ii jj/1000 error_D]

   end;

   if iSen == 1
      b_x  = A_vector(1);
      S_x  = A_vector(2);
      Om_x = A_vector(3);
      A_x  = A_vector(4);
   elseif iSen == 2
      b_y  = A_vector(1);
      S_y  = A_vector(2);
      Om_y = A_vector(3);
      A_y  = A_vector(4);
   elseif iSen == 3
      b_z  = A_vector(1);
      S_z  = A_vector(2);
      Om_z = A_vector(3);
      A_z  = A_vector(4);
   end;

end;

[b_x S_x Om_x*r2d A_x*r2d]
[b_y S_y Om_y*r2d A_y*r2d]
[b_z S_z Om_z*r2d A_z*r2d]

save AccCalData b_x b_y b_z S_x S_y S_z Om_x Om_y Om_z A_x A_y A_z
```

```
%-------------------------------------------------------------------------%
%
%                 3 Axis Accelerometer Package Calibration
%                             - Model Package -
%
%-------------------------------------------------------------------------%
% This File Calibrates 3 Accelerometer Oriented in 3 Axis
% File Name 'AccCalib00_Model'
%
% Research Funded by
% Measurement & Instrumentation Branch of NASA Langley Research Center
% NASA LaRC Hampton VA. 23681
% Instructor in ODU Side: Dr. Newman
% Program Coded in MATLAB by Si-bok Yu
% Aerospace Engr. Dept., Old Dominion Univ.
% Latest Updated in Oct. 2002
%
%-------------------------------------------------------------------------%
%
%                                    Inputs
%
% Need Sensor Voltage Output at N Different Pitch, Yaw and Roll Orientations
% for each of 3 Axis
%
%
%                                    Outputs
%
% b    % Bias [V]
% S    % Sensitivity [V/g]
% Om   % Coning Angle [rad]
% A    % Azimuth Angle [rad]
%
%-------------------------------------------------------------------------%

clear;
r2d         = 180/pi;
d2r         = pi/180;
Tolerance   = 1e-32;
g           = 1;

%-------------------------------------------------------------------------%
% Load Pitch, Yaw, and Roll Motion, and Voltage Output
load SimAccData_Model

%-------------------------------------------------------------------------%
% Initial Guess Values
b0  = 1.23;             % Bias [V]
S0  = 0.45;             % Sensitivity [V/g]
Om0 = 0.06*d2r;         % Coning Angle [rad]
A0  = 0.07*d2r;         % Azimuth Angle [rad]
A_vector = [b0 S0 Om0 A0]';

nData=length(Phi_m);

for iSen=1:3,
   for ii=1:100,
      b  = A_vector(1);
```

```
        S  = A_vector(2);
        Om = A_vector(3);
        A  = A_vector(4);

        for jj=1:nData-1,

           Phi = Phi_m(jj);        Th  = Th_m(jj);        Psi = Psi_m(jj);

           vx  = Vxm(jj);          vy  = Vym(jj);         vz  = Vzm(jj);

           if iSen == 1
Z(jj,1)=1;
Z(jj,2)=  ( -cos(Om)*cos(Psi)*sin(Th)
            +(sin(Om)*sin(A)*cos(Phi)+sin(Om)*cos(A)*sin(Phi))*sin(Psi)*sin(Th)
            +(sin(Om)*sin(A)*sin(Phi)-sin(Om)*cos(A)*cos(Phi))*cos(Th)          )*g;
Z(jj,3)=S*(  sin(Om)*cos(Psi)*sin(Th)
            +(cos(Om)*sin(A)*cos(Phi)+cos(Om)*cos(A)*sin(Phi))*sin(Psi)*sin(Th)
            +(cos(Om)*sin(A)*sin(Phi)-cos(Om)*cos(A)*cos(Phi))*cos(Th)          )*g;
Z(jj,4)=S*(  sin(Om)*cos(A)*cos(Phi)-sin(Om)*sin(A)*sin(Phi))*sin(Psi)*sin(Th)
            +(sin(Om)*sin(A)*cos(Phi)+sin(Om)*cos(A)*sin(Phi))*cos(Th)          )*g;
D(jj,1)=vx-b
       -S*( -cos(Om)*cos(Psi)*sin(Th)
            +(sin(Om)*sin(A)*cos(Phi)+sin(Om)*cos(A)*sin(Phi))*sin(Psi)*sin(Th)
            +(sin(Om)*sin(A)*sin(Phi)-sin(Om)*cos(A)*cos(Phi))*cos(Th)          )*g;
         elseif iSen == 2
Z(jj,1)=1;
Z(jj,2)=  (  sin(Om)*cos(A)*cos(Psi)*sin(Th)
            +(cos(Om)*cos(Phi)sin(Om)*sin(A)*sin(Phi))*sin(Psi)*sin(Th)
            +(cos(Om)*sin(Phi)+sin(Om)*sin(A)*cos(Phi))*cos(Th)                 )*g;
Z(jj,3)=S*(  cos(Om)*cos(A)*cos(Psi)*sin(Th)
            +(-sin(Om)*cos(Phi)-cos(Om)*sin(A)*sin(Phi))*sin(Psi)*sin(Th)
            +(-sin(Om)*sin(Phi)+cos(Om)*sin(A)*cos(Phi))*cos(Th)                )*g;
Z(jj,4)=S*( -sin(Om)*sin(A)*cos(Psi)*sin(Th)
            -sin(Om)*cos(A)*sin(Phi)*sin(Psi)*sin(Th)
            +sin(Om)*cos(A)*cos(Phi)*cos(Th)                                    )*g;
D(jj,1)=vy-b
       -S*(  sin(Om)*cos(A)*cos(Psi)*sin(Th)
            +(cos(Om)*cos(Phi)-sin(Om)*sin(A)*sin(Phi))*sin(Psi)*sin(Th)
            +(cos(Om)*sin(Phi)+sin(Om)*sin(A)*cos(Phi))*cos(Th)                 )*g;
         elseif iSen == 3
Z(jj,1)=1;
Z(jj,2)=  ( -sin(Om)*sin(A)*cos(Psi)*sin(Th)
            +(-sin(Om)*cos(A)*cos(Phi)-cos(Om)*sin(Phi))*sin(Psi)*sin(Th)
            +(-sin(Om)*cos(A)*sin(Phi)+cos(Om)*cos(Phi))*cos(Th)                )*g;
Z(jj,3)=S*( -cos(Om)*sin(A)*cos(Psi)*sin(Th)
            +(-cos(Om)*cos(A)*cos(Phi)+sin(Om)*sin(Phi))*sin(Psi)*sin(Th)
            +(-cos(Om)*cos(A)*sin(Phi)-sin(Om)*cos(Phi))*cos(Th)                )*g;
Z(jj,4)=S*( -sin(Om)*cos(A)*cos(Psi)*sin(Th)
            +sin(Om)*sin(A)*cos(Phi)*sin(Psi)*sin(Th)
            +sin(Om)*sin(A)*sin(Phi)*cos(Th)                                    )*g;
D(jj,1)=vz-b
       -S*( -sin(Om)*sin(A)*cos(Psi)*sin(Th)
            +(-sin(Om)*cos(A)*cos(Phi)-cos(Om)*sin(Phi))*sin(Psi)*sin(Th)
            +(-sin(Om)*cos(A)*sin(Phi)+cos(Om)*cos(Phi))*cos(Th)                )*g;
         end;

      end;
```

```
        dA = inv( Z' *Z ) * ( Z' *D );
        A_vector  = A_vector + dA;

        error_D = sum(dA.^2);
        error_D = sqrt(error_D);
        if error_D < Tolerance
           ii
           break;
        end;

        [iSen ii jj/1000 error_D]

    end;

    if iSen == 1
        b_x2  = A_vector(1);
        S_x2  = A_vector(2);
        Om_x2 = A_vector(3);
        A_x2  = A_vector(4);
    elseif iSen == 2
        b_y2  = A_vector(1);
        S_y2  = A_vector(2);
        Om_y2 = A_vector(3);
        A_y2  = A_vector(4);
    elseif iSen == 3
        b_z2  = A_vector(1);
        S_z2  = A_vector(2);
        Om_z2 = A_vector(3);
        A_z2  = A_vector(4);
    end;

end;

[b_x2 S_x2 Om_x2*r2d A_x2*r2d]
[b_y2 S_y2 Om_y2*r2d A_y2*r2d]
[b_z2 S_z2 Om_z2*r2d A_z2*r2d]

save AccCalData2 b_x2 b_y2 b_z2 S_x2 S_y2 S_z2 Om_x2 Om_y2 Om_z2 A_x2 A_y2
A_z2
```

Appendix C
Accelerometer Attitude Construction Listing

```
%-------------------------------------------------------------------------%
%
%     Pitch, Yaw, and Roll Angle Calculation from Accelerometer Package
%                        - Sting & Model Packages -
%
%-------------------------------------------------------------------------%
% This File Calibrates Pitch, Yaw, and Roll Angle from Acc. Oriented in 3 Axis
% File Name 'Acc_Angle'
%
% Research Funded by
% Measurement & Instrumentation Branch of NASA Langley Research Center
% NASA LaRC Hampton VA. 23681
% Instructor in ODU Side: Dr. Newman
% Program Coded in MATLAB by Si-bok Yu
% Aerospace Engr. Dept., Old Dominion Univ.
% Oct. 2002
%
%-------------------------------------------------------------------------%
%
% This File Takes Accelerometer Package Calibration Information from
%'AccCalib00_Sting' & 'AccCalib00_Model'
% The Information Includes
% b   % Bias [V]
% S   % Sensitivity [V/g]
% Om  % Coning Angle [rad]
% A   % Azimuth Angle [rad]
%
%                                    Outputs
%
% This File Gives Output
% Pitch Angle [rad]
% Yaw Angle   [rad]
% These Outputs are used as Inputs to Calculate the Additional Output
% Roll Angle  [rad]
%
%-------------------------------------------------------------------------%

clear;
r2d         = 180/pi;
d2r         = pi/180;
Tolerance   = 1e-10;
g           = 1;

%-------------------------------------------------------------------------%
% Load Calibration Information for Sting Package
% Load Bias, Sensitivity, Coning Angle, and Azimuth Angle Data
load AccCalData
% Load Calibration Information for Model Package
load AccCalData2
```

```
% Load Voltage Output from the Sting Package
% at Corresponding Pitch, Yaw, and Roll Motion
load SimAccData2_Sting
% Load Voltage Output from the Model Package
load SimAccData2_Model

% Initial Value for Computing Orientation of the Model
Phi0  = 0.1;
Th0   = 0.1;
Psi0  = 0.1;

nData = length(Vxst);

%-------------------------------------------------------------------------%
%
% Find Angles Using Iterative Method (Gauss Newton)
%
%-------------------------------------------------------------------------%
for jj=1:nData,

      Vx = Vxst(jj);
      Vy = Vyst(jj);
      Vz = Vzst(jj);

      A_vector = [Th0 Psi0]';

      for ii=1:10,
            Th  = A_vector(1);
            Psi = A_vector(2);

Z(1,1)=S_x*( -cos(Om_x)*cos(Psi)*cos(Th)
             +sin(Om_x)*sin(A_x)*sin(Psi)*cos(Th)
             +sin(Om_x)*cos(A_x)*sin(Th)                  )*g;
Z(1,2)=S_x*( +cos(Om_x)*sin(Psi)*sin(Th)
             +sin(Om_x)*sin(A_x)*cos(Psi)*sin(Th)         )*g;
Z(2,1)=S_y*( +sin(Om_y)*cos(A_y)*cos(Psi)*cos(Th)
             +cos(Om_y)*sin(Psi)*cos(Th)
             -sin(Om_y)*sin(A_y)*sin(Th)                  )*g;
Z(2,2)=S_y*( -sin(Om_y)*cos(A_y)*sin(Psi)*sin(Th)
             +cos(Om_y)*cos(Psi)*sin(Th)                  )*g;
Z(3,1)=S_z*( -sin(Om_z)*sin(A_z)*cos(Psi)*cos(Th)
             -sin(Om_z)*cos(A_z)*sin(Psi)*cos(Th)
             -cos(Om_z)*sin(Th)                           )*g;
Z(3,2)=S_z*( +sin(Om_z)*sin(A_z)*sin(Psi)*sin(Th)
             -sin(Om_z)*cos(A_z)*cos(Psi)*sin(Th)         )*g;

D(1)=Vx-b_x -S_x*( -cos(Om_x)*cos(Psi)*sin(Th)
                   +sin(Om_x)*sin(A_x)*sin(Psi)*sin(Th)
                   -sin(Om_x)*cos(A_x)*cos(Th)            )*g;
D(2)=Vy-b_y -S_y*(  sin(Om_y)*cos(A_y)*cos(Psi)*sin(Th)
                   +cos(Om_y)*sin(Psi)*sin(Th)
                   +sin(Om_y)*sin(A_y)*cos(Th)            )*g;
D(3)=Vz-b_z -S_z*( -sin(Om_z)*sin(A_z)*cos(Psi)*sin(Th)
                   -sin(Om_z)*cos(A_z)*sin(Psi)*sin(Th)
                   +cos(Om_z)*cos(Th)                     )*g;
```

```
            dA = inv( Z' *Z ) * ( Z' *D' );
            A_vector  = A_vector + dA;

            error_D = sum(dA.^2);
            error_D = sqrt(error_D);
            if error_D < Tolerance
                  [jj ii error_D]
            break;
            end;

      end;    % ii Loop

      Vx2 = Vxm(jj);
      Vy2 = Vym(jj);
      Vz2 = Vzm(jj);

      Th  = A_vector(1);
      Psi = A_vector(2);

      A_vector2 = [Phi0]';

      for ii=1:10,
            Phi = A_vector2(1);

Z(1,1)=S_x2*(
      +(-sin(Om_x2)*sin(A_x2)*sin(Phi)+sin(Om_x2)*cos(A_x2)*cos(Phi))*sin(Psi)*sin(T
      +(sin(Om_x2)*sin(A_x2)*cos(Phi)+sin(Om_x2)*cos(A_x2)*sin(Phi))*cos(Th)  )*g;
Z(2,1)=S_y2*(
      +(-cos(Om_y2)*sin(Phi)-sin(Om_y2)*sin(A_y2)*cos(Phi))*sin(Psi)*sin(Th)
      +(cos(Om_y2)*cos(Phi)-sin(Om_y2)*sin(A_y2)*sin(Phi))*cos(Th)            )*g;
Z(3,1)=S_z2*(
      +(sin(Om_z2)*cos(A_z2)*sin(Phi)-cos(Om_z2)*cos(Phi))*sin(Psi)*sin(Th)
      +(-sin(Om_z2)*cos(A_z2)*cos(Phi)-cos(Om_z2)*sin(Phi))*cos(Th)           )*g;

D(1)=Vx2-b_x2 -S_x2*(  -cos(Om_x2)*cos(Psi)*sin(Th)
    +(sin(Om_x2)*sin(A_x2)*cos(Phi)+sin(Om_x2)*cos(A_x2)*sin(Phi))*sin(Psi)*sin(Th)
    +(sin(Om_x2)*sin(A_x2)*sin(Phi)-sin(Om_x2)*cos(A_x2)*cos(Phi))*cos(Th)    )*g;
D(2)=Vy2-b_y2 -S_y2*(   sin(Om_y2)*cos(A_y2)*cos(Psi)*sin(Th)
    +(cos(Om_y2)*cos(Phi)-sin(Om_y2)*sin(A_y2)*sin(Phi))*sin(Psi)*sin(Th)
    +(cos(Om_y2)*sin(Phi)+sin(Om_y2)*sin(A_y2)*cos(Phi))*cos(Th)            )*g;
D(3)=Vz2-b_z2 -S_z2*(  -sin(Om_z2)*sin(A_z2)*cos(Psi)*sin(Th)
    +(-sin(Om_z2)*cos(A_z2)*cos(Phi)-cos(Om_z2)*sin(Phi))*sin(Psi)*sin(Th)
    +(-sin(Om_z2)*cos(A_z2)*sin(Phi)+cos(Om_z2)*cos(Phi))*cos(Th)           )*g;

            dA2 = inv( Z' *Z ) * ( Z' *D' );
            A_vector2  = A_vector2 + dA2;

            error_D = sum(dA2.^2);
            error_D = sqrt(error_D);
            if error_D < Tolerance
                  [jj ii error_D]
            break;
            end;

      end;    % ii Loop

   Phi = A_vector2(1);
```

```
   Phi_n(jj) = Phi;
   Th_n(jj)  = Th;
   Psi_n(jj) = Psi;

end;   % jj loop


save AccAngle


%-------------------------------------------------------------------------%
%
%                          Closed-Form Solution
%
%-------------------------------------------------------------------------%

% Bias and Sensitivity Matrices for Sting Package
B_sn_st = [b_x b_y b_z].';
S_sn_st = [S_x 0   0
           0   S_y 0
           0   0   S_z];

% Bias and Sensitivity Matrices for Model Package
B_sn_m = [b_x2 b_y2 b_z2].';
S_sn_m = [S_x2 0    0
          0    S_y2 0
          0    0    S_z2];


for qq = 1:nData

      Vx_st = Vxst(qq);
      Vy_st = Vyst(qq);
      Vz_st = Vzst(qq);

      Vx_m = Vxm(qq);
      Vy_m = Vym(qq);
      Vz_m = Vzm(qq);

      V_sn_st = [Vx_st Vy_st Vz_st].';

      V_sn_m  = [Vx_m  Vy_m  Vz_m ].';

      T_sn_x_st_st1 = [ cos(Om_x)           sin(Om_x)*sin(A_x) -sin(Om_x)*cos(A_x)];
      T_sn_y_st_st2 = [-sin(Om_y)*cos(A_y)  cos(Om_y)           sin(Om_y)*sin(A_y)];
      T_sn_z_st_st3 = [ sin(Om_z)*sin(A_z) -sin(Om_z)*cos(A_z)  cos(Om_z)];

      T_sn_st_st = [T_sn_x_st_st1
                    T_sn_y_st_st2
                    T_sn_z_st_st3];

      T_sn_x_m_m1 = [ cos(Om_x2)           sin(Om_x2)*sin(A_x2) -sin(Om_x2)*cos(A_x2)
      T_sn_y_m_m2 = [-sin(Om_y2)*cos(A_y2)  cos(Om_y2)           sin(Om_y2)*sin(A_y2)
      T_sn_z_m_m3 = [ sin(Om_z2)*sin(A_z2) -sin(Om_z2)*cos(A_z2)  cos(Om_z2)];
```

```
        T_sn_m_m = [T_sn_x_m_m1
                    T_sn_y_m_m2
                    T_sn_z_m_m3];

        G_st = inv(T_sn_st_st)*inv(S_sn_st)*(V_sn_st - B_sn_st);

        G_m  = inv(T_sn_m_m)*inv(S_sn_m)*(V_sn_m - B_sn_m);

        G_x_st = G_st(1);
        G_y_st = G_st(2);
        G_z_st = G_st(3);

        G_x_m = G_m(1);
        G_y_m = G_m(2);
        G_z_m = G_m(3);

        psi(qq)  = atan2(G_y_st,-G_x_st);
        thta(qq) = atan(sqrt(G_x_st^2+G_y_st^2)/G_z_st)*sign(G_x_st/1/cos(psi(qq)));
        phi(qq)  = atan2(G_y_m*G_z_st-G_z_m*G_y_st,G_y_m*G_y_st+G_z_m*G_z_st);

end                 % End of pp Loop
```

Appendix D
Gyro Sensor Calibration Listing

```
%-------------------------------------------------------------------------%
%
%                      3 Axis Gyroscope Package Calibration
%
%-------------------------------------------------------------------------%
% This File Calibrates 3 Gyroscope Oriented in 3 Axis
% File Name 'GyroCalib00'
%
% Research Funded by
% Measurement & Instrumentation Branch of NASA Langley Research Center
% NASA LaRC Hampton VA. 23681
% Instructor in ODU Side: Dr. Newman
% Program Coded in MATLAB by Si-bok Yu
% Aerospace Engr. Dept., Old Dominion Univ.
% Oct. 2002
%
%-------------------------------------------------------------------------%
%
%                                  Inputs
%
% Need Sensor Voltage Output at N Different Yaw/Roll Orientations
% and Pitch/Yaw/Roll Rates for each of 3 Axis
%
%
%                                  Outputs
%
% b     % Bias [V]
% S     % Sensitivity [V/g]
% Om    % Coning Angle [rad]
% A     % Azimuth Angle [rad]
%
%-------------------------------------------------------------------------%

clear;
r2d=180/pi;
d2r=pi/180;
Tolerance=1e-10;

%-------------------------------------------------------------------------%
% Load Pitch, Yaw, and Roll Motion, and Voltage Output
% at the Corresponding Pitch, Yaw, and Roll Motion
load SimData

%-------------------------------------------------------------------------%
% Initial Guess Values
b0  = 0.05;     % Bias [V]
S0  = 1.25;     % Sensitivity [V/g]
Om0 = 0.1*d2r; % Coning Angle [rad]
A0  = 0.1*d2r; % Azimuth Angle [rad]
A_vector = [b0 S0 Om0 A0]';
```

```
nData=length(Phi_m);

for iSen=1:3,
   for ii=1:20,
      b  = A_vector(1);
      S  = A_vector(2);
      Om = A_vector(3);
      A  = A_vector(4);

      for jj=1:nData-1,

         Phi = Phi_m(jj);
         Th  = Th_m(jj);
         Psi = Psi_m(jj);

         dPhi = dPhi_m(jj);
         dTh  = dTh_m(jj);
         dPsi = dPsi_m(jj);

         vx=Vx_m(jj);
         vy=Vy_m(jj);
         vz=Vz_m(jj);

         if iSen == 1
Z(jj,1)=1;
Z(jj,2)=     cos(Om)*(sin(Psi)*dTh+dPhi)
            +sin(Om)*sin(A)*(cos(Phi)*cos(Psi)*dTh+sin(Phi)*dPsi)
            -sin(Om)*cos(A)*(-sin(Phi)*cos(Psi)*dTh+cos(Phi)*dPsi);
Z(jj,3)=S*( -sin(Om)*(sin(Psi)*dTh+dPhi)
            +cos(Om)*sin(A)*(cos(Phi)*cos(Psi)*dTh+sin(Phi)*dPsi)
            -cos(Om)*cos(A)*(-sin(Phi)*cos(Psi)*dTh+cos(Phi)*dPsi)    );
Z(jj,4)=S*(  sin(Om)*cos(A)*(cos(Phi)*cos(Psi)*dTh+sin(Phi)*dPsi)
            +sin(Om)*sin(A)*(-sin(Phi)*cos(Psi)*dTh+cos(Phi)*dPsi)    );
D(jj,1)=vx-b
       -S*(  cos(Om)*(sin(Psi)*dTh+dPhi)
            +sin(Om)*sin(A)*(cos(Phi)*cos(Psi)*dTh+sin(Phi)*dPsi)
            -sin(Om)*cos(A)*(-sin(Phi)*cos(Psi)*dTh+cos(Phi)*dPsi)    );
         elseif iSen == 2
Z(jj,1)=1;
Z(jj,2)=    -sin(Om)*cos(A)*(sin(Psi)*dTh+dPhi)
            +cos(Om)*(cos(Phi)*cos(Psi)*dTh+sin(Phi)*dPsi)
            +sin(Om)*sin(A)*(-sin(Phi)*cos(Psi)*dTh+cos(Phi)*dPsi);
Z(jj,3)=S*( -cos(Om)*cos(A)*(sin(Psi)*dTh+dPhi)
            -sin(Om)*(cos(Phi)*cos(Psi)*dTh+sin(Phi)*dPsi)
            +cos(Om)*sin(A)*(-sin(Phi)*cos(Psi)*dTh+cos(Phi)*dPsi)    );
Z(jj,4)=S*(  sin(Om)*sin(A)*(sin(Psi)*dTh+dPhi)
            +sin(Om)*cos(A)*(-sin(Phi)*cos(Psi)*dTh+cos(Phi)*dPsi)    );
D(jj,1)=vy-b
       -S*( -sin(Om)*cos(A)*(sin(Psi)*dTh+dPhi)
            +cos(Om)*(cos(Phi)*cos(Psi)*dTh+sin(Phi)*dPsi)
            +sin(Om)*sin(A)*(-sin(Phi)*cos(Psi)*dTh+cos(Phi)*dPsi)    );
         elseif iSen == 3
Z(jj,1)=1;
Z(jj,2)=     sin(Om)*sin(A)*(sin(Psi)*dTh+dPhi)
            -sin(Om)*cos(A)*(cos(Phi)*cos(Psi)*dTh+sin(Phi)*dPsi)
            +cos(Om)*(-sin(Phi)*cos(Psi)*dTh+cos(Phi)*dPsi);
```

```
Z(jj,3)=S*(  cos(Om)*sin(A)*(sin(Psi)*dTh+dPhi)
            -cos(Om)*cos(A)*(cos(Phi)*cos(Psi)*dTh+sin(Phi)*dPsi)
            -sin(Om)*(-sin(Phi)*cos(Psi)*dTh+cos(Phi)*dPsi)          );
Z(jj,4)=S*(  sin(Om)*cos(A)*(sin(Psi)*dTh+dPhi)
            +sin(Om)*sin(A)*(cos(Phi)*cos(Psi)*dTh+sin(Phi)*dPsi)    );
D(jj,1)=vz-b
       -S*(  sin(Om)*sin(A)*(sin(Psi)*dTh+dPhi)
            -sin(Om)*cos(A)*(cos(Phi)*cos(Psi)*dTh+sin(Phi)*dPsi)
            +cos(Om)*(-sin(Phi)*cos(Psi)*dTh+cos(Phi)*dPsi)          );
         end;

      end;
           dA = inv( Z' *Z ) * ( Z' *D );
         A_vector  = A_vector + dA;
         %if A_vector(4) > 2*pi
         %   A_vector(4) = A_vector(4) - 2*pi;
         %end;

         error_D = sum(dA.^2);
         error_D = sqrt(error_D);
         if error_D < Tolerance
            [iSen ii]
            break;
         end;

   end;

   if iSen == 1
      b_x  = A_vector(1);
      S_x  = A_vector(2);
      Om_x = A_vector(3);
      A_x  = A_vector(4);
   elseif iSen == 2
      b_y  = A_vector(1);
      S_y  = A_vector(2);
      Om_y = A_vector(3);
      A_y  = A_vector(4);
   elseif iSen == 3
      b_z  = A_vector(1);
      S_z  = A_vector(2);
      Om_z = A_vector(3);
      A_z  = A_vector(4);
   end;

end;

[b_x S_x Om_x*r2d A_x*r2d]
[b_y S_y Om_y*r2d A_y*r2d]
[b_z S_z Om_z*r2d A_z*r2d]

save GyroCalData b_x b_y b_z S_x S_y S_z Om_x Om_y Om_z A_x A_y A_z
```

Appendix E
Gyro Attitude Construction Listing

```
%-------------------------------------------------------------------------%
%
%       Pitch, Yaw, and Roll Angle Calculation from Gyroscope Package
%
%-------------------------------------------------------------------------%
% This File Calibrates Pitch, Yaw, and Roll Angle from Gyroscopes Oriented in 3 Axis
% File Name 'Gyro_Angle'
%
% Research Funded by
% Measurement & Instrumentation Branch of NASA Langley Research Center
% NASA LaRC Hampton VA. 23681
% Instructor in ODU Side: Dr. Newman
% Program Coded in MATLAB by Si-bok Yu
% Aerospace Engr. Dept., Old Dominion Univ.
% Feb. 2002
%
%-------------------------------------------------------------------------%
%
% This File Takes Gyroscope Package Calibration Information from
%'GyroCalib00'
% The Information Includes
% b     % Bias [V]
% S     % Sensitivity [V/g]
% Om    % Coning Angle [rad]
% A     % Azimuth Angle [rad]
%
%                                   Outputs
%
% This File Gives Output
% Pitch Rate [rad/s]
% Yaw   Rate [rad/s]
% Roll  Rate [rad/s]
% which are Integrated To Yield
% Pitch Angle [rad]
% Yaw   Angle [rad]
% Roll  Angle [rad]
%
%-------------------------------------------------------------------------%

clear;
r2d=180/pi;
d2r=pi/180;
Tolerance=1e-10;

%-------------------------------------------------------------------------%
% Load Calibration Information
% Load Bias, Sensitivity, Coning Angle, and Azimuth Angle Data
load GyroCalData

%-------------------------------------------------------------------------%
```

```
% Load Voltage Output from the Gyroscope Package
% at the Corresponding Pitch, Yaw, and Roll Motion
load SimData2


%-------------------------------------------------------------------------%
% Initial Orientation of the Model
Phi0=0;
Th0 =0;
Psi0=0;
%-------------------------------------------------------------------------%
% Initial Guess Values
P0=(Vx_m(1) - b_x) /S_x;  Q0=(Vy_m(1) - b_y) /S_y;  R0=(Vz_m(1) - b_z) /S_z;

Tmt =[1   sin(Psi0)             0;
      0   cos(Phi0)*cos(Psi0)   sin(Phi0);
      0  -sin(Phi0)*cos(Psi0)   cos(Phi0)];

dEuler0 = inv(Tmt) * [P0 Q0 R0]';

dPhi0=dEuler0(1);  dTh0 =dEuler0(2);  dPsi0=dEuler0(3);

nData=length(Vx_m);

X=[0 0 0]';
%-------------------------------------------------------------------------%
% Find Angles with Iteration Method
for jj=1:nData,

      V_x=Vx_m(jj);
      V_y=Vy_m(jj);
      V_z=Vz_m(jj);

      save GyroEOM_Inputs V_x V_y V_z

%-------------------------------------------------------------------------%
% Use Runge-Kutta 5th Order Method from 'Numerical Method for Engineering,'
% Chapra & Canale, McGraw Hill, P. 604, 1990
   k1=GyroEOM_rk5( X(:,jj)                                          ,t(jj));
   k2=GyroEOM_rk5( X(:,jj) +1/4*dt*k1'                              ,t(jj)+1/4*dt);
   k3=GyroEOM_rk5( X(:,jj) +1/8*dt*k1' +1/8*dt*k2'                  ,t(jj)+1/4*dt);
   k4=GyroEOM_rk5( X(:,jj) -1/2*dt*k2' +dt*k3'                      ,t(jj)+1/2*dt);
   k5=GyroEOM_rk5( X(:,jj)+3/16*dt*k1' +9/16*dt*k4'                 ,t(jj)+3/4*dt);
   k6=GyroEOM_rk5( X(:,jj) -3/7*dt*k1' +2/7*dt*k2' +12/7*dt*k3' -12/7*dt*k4'
                           +8/7*dt*k5'                              ,t(jj)+dt);

   X(:,jj+1)=X(:,jj) + (1/90 * (7*k1+32*k3+12*k4+32*k5+7*k6))'*dt;
   clear k1 k2 k3 k4 k5 k6;

   [jj X(1,jj)*r2d X(2,jj)*r2d X(3,jj)*r2d]

      Phi_n(jj) = X(1,jj);     Th_n(jj)  = X(2,jj);     Psi_n(jj) = X(3,jj);

end;   % jj loop

save GyroAngle
```

```
function f=GyroEOM_rk5(X,t)
%-------------------------------------------------------------------------%
%
%              Equation of Motion of the Gyroscope Sensor Package
%
%-------------------------------------------------------------------------%
% This is in the Form of Non-Linear State-Space Equation
% This File is being Called by the Main File 'Gyro_Angle'
%
% Research Funded by
% Measurement & Instrumentation Branch of NASA Langley Research Center
% NASA LaRC Hampton VA. 23681
% Instructor in ODU Side: Dr. Newman
% Program Coded in MATLAB by Si-bok Yu
% Aerospace Engr. Dept., Old Dominion Univ.
% Mar. 2002
%
%-------------------------------------------------------------------------%
%
% This File Takes Accelerometer Package Calibration Information from
%'GyroCalib00'
% The Information Includes
% b     % Bias [V]
% S     % Sensitivity [V/g]
% Om    % Coning Angle [rad]
% A     % Azimuth Angle [rad]
%
%                              Inputs
%                  ( Gyroscope Package Voltage Output )
%                            Vx, Vy, Vz
%
%-------------------------------------------------------------------------%

%-------------------------------------------------------------------------%
% Load Calibration Information from 'GyroCalib00'
% Load Bias, Sensitivity, Coning Angle, and Azimuth Angle Data
load GyroCalData

%-------------------------------------------------------------------------%
% Load Voltage Calibration Information from 'GyroCalib00'
load GyroEOM_Inputs

   Phi  =X(1);
   Th   =X(2);
   Psi  =X(3);


f(1) = ((cos(Om_y)*cos(Om_z)+sin(Om_y)*sin(A_y)*sin(Om_z)*cos(A_z))        ...
   /(cos(Om_x)*cos(Om_y)*cos(Om_z)+cos(Om_x)*sin(Om_y)*sin(A_y)            ...
   *sin(Om_z)*cos(A_z)+sin(Om_y)*cos(A_y)*sin(Om_x)*sin(A_x)*cos(Om_z)     ...
   -sin(Om_y)*cos(A_y)*sin(Om_x)*cos(A_x)*sin(Om_z)*cos(A_z)+sin(Om_z)     ...
   *sin(A_z)*sin(Om_x)*sin(A_x)*sin(Om_y)*sin(A_y)+sin(Om_z)*sin(A_z)      ...
   *sin(Om_x)*cos(A_x)*cos(Om_y))-sin(Psi)*cos(Phi)/cos(Psi)/(cos(Phi)^2   ...
   +sin(Phi)^2)*sin(Om_y)*(cos(A_y)*cos(Om_z)+sin(A_y)*sin(Om_z)           ...
   *sin(A_z))/(cos(Om_x)*cos(Om_y)*cos(Om_z)+cos(Om_x)*sin(Om_y)           ...
   *sin(A_y)*sin(Om_z)*cos(A_z)+sin(Om_y)*cos(A_y)*sin(Om_x)*sin(A_x)      ...
   *cos(Om_z)-sin(Om_y)*cos(A_y)*sin(Om_x)*cos(A_x)*sin(Om_z)*cos(A_z)     ...
```

```
    +sin(Om_z)*sin(A_z)*sin(Om_x)*sin(A_x)*sin(Om_y)*sin(A_y)+sin(Om_z)     ...
    *sin(A_z)*sin(Om_x)*cos(A_x)*cos(Om_y))-sin(Psi)*sin(Phi)/cos(Psi)      ...
    /(cos(Phi)^2+sin(Phi)^2)*sin(Om_z)*(-sin(Om_y)*cos(A_y)*cos(A_z)        ...
    +cos(Om_y)*sin(A_z))/(cos(Om_x)*cos(Om_y)*cos(Om_z)+cos(Om_x)           ...
    *sin(Om_y)*sin(A_y)*sin(Om_z)*cos(A_z)+sin(Om_y)*cos(A_y)*sin(Om_x)     ...
    *sin(A_x)*cos(Om_z)-sin(Om_y)*cos(A_y)*sin(Om_x)*cos(A_x)*sin(Om_z)     ...
    *cos(A_z)+sin(Om_z)*sin(A_z)*sin(Om_x)*sin(A_x)*sin(Om_y)*sin(A_y)      ...
    +sin(Om_z)*sin(A_z)*sin(Om_x)*cos(A_x)*cos(Om_y)))/S_x*(V_x-b_x)        ...
    +(-sin(Om_x)*(sin(A_x)*cos(Om_z)-cos(A_x)*sin(Om_z)*cos(A_z))           ...
    /(cos(Om_x)*cos(Om_y)*cos(Om_z)+cos(Om_x)*sin(Om_y)*sin(A_y)            ...
    *sin(Om_z)*cos(A_z)+sin(Om_y)*cos(A_y)*sin(Om_x)*sin(A_x)*cos(Om_z)     ...
    -sin(Om_y)*cos(A_y)*sin(Om_x)*cos(A_x)*sin(Om_z)*cos(A_z)+sin(Om_z)     ...
    *sin(A_z)*sin(Om_x)*sin(A_x)*sin(Om_y)*sin(A_y)+sin(Om_z)*sin(A_z)      ...
    *sin(Om_x)*cos(A_x)*cos(Om_y))-sin(Psi)*cos(Phi)/cos(Psi)/(cos(Phi)^2   ...
    +sin(Phi)^2)*(cos(Om_x)*cos(Om_z)+sin(Om_x)*cos(A_x)*sin(Om_z)          ...
    *sin(A_z))/(cos(Om_x)*cos(Om_y)*cos(Om_z)+cos(Om_x)*sin(Om_y)           ...
    *sin(A_y)*sin(Om_z)*cos(A_z)+sin(Om_y)*cos(A_y)*sin(Om_x)*sin(A_x)      ...
    *cos(Om_z)-sin(Om_y)*cos(A_y)*sin(Om_x)*cos(A_x)*sin(Om_z)*cos(A_z)     ...
    +sin(Om_z)*sin(A_z)*sin(Om_x)*sin(A_x)*sin(Om_y)*sin(A_y)+sin(Om_z)     ...
    *sin(A_z)*sin(Om_x)*cos(A_x)*cos(Om_y))+sin(Psi)*sin(Phi)/cos(Psi)      ...
    /(cos(Phi)^2+sin(Phi)^2)*sin(Om_z)*(cos(Om_x)*cos(A_z)+sin(Om_x)        ...
    *sin(A_x)*sin(A_z))/(cos(Om_x)*cos(Om_y)*cos(Om_z)+cos(Om_x)            ...
    *sin(Om_y)*sin(A_y)*sin(Om_z)*cos(A_z)+sin(Om_y)*cos(A_y)*sin(Om_x)     ...
    *sin(A_x)*cos(Om_z)-sin(Om_y)*cos(A_y)*sin(Om_x)*cos(A_x)*sin(Om_z)     ...
    *cos(A_z)+sin(Om_z)*sin(A_z)*sin(Om_x)*sin(A_x)*sin(Om_y)*sin(A_y)      ...
    +sin(Om_z)*sin(A_z)*sin(Om_x)*cos(A_x)*cos(Om_y)))/S_y*(V_y-b_y)        ...
    +(sin(Om_x)*(sin(A_x)*sin(Om_y)*sin(A_y)+cos(A_x)*cos(Om_y))            ...
    /(cos(Om_x)*cos(Om_y)*cos(Om_z)+cos(Om_x)*sin(Om_y)*sin(A_y)            ...
    *sin(Om_z)*cos(A_z)+sin(Om_y)*cos(A_y)*sin(Om_x)*sin(A_x)*cos(Om_z)     ...
    -sin(Om_y)*cos(A_y)*sin(Om_x)*cos(A_x)*sin(Om_z)*cos(A_z)+sin(Om_z)     ...
    *sin(A_z)*sin(Om_x)*sin(A_x)*sin(Om_y)*sin(A_y)+sin(Om_z)*sin(A_z)      ...
    *sin(Om_x)*cos(A_x)*cos(Om_y))+sin(Psi)*cos(Phi)/cos(Psi)/(cos(Phi)^2   ...
    +sin(Phi)^2)*sin(Om_y)*(cos(Om_x)*sin(A_y)-sin(Om_x)*cos(A_x)           ...
    *cos(A_y))/(cos(Om_x)*cos(Om_y)*cos(Om_z)+cos(Om_x)*sin(Om_y)           ...
    *sin(A_y)*sin(Om_z)*cos(A_z)+sin(Om_y)*cos(A_y)*sin(Om_x)*sin(A_x)      ...
    *cos(Om_z)-sin(Om_y)*cos(A_y)*sin(Om_x)*cos(A_x)*sin(Om_z)*cos(A_z)     ...
    +sin(Om_z)*sin(A_z)*sin(Om_x)*sin(A_x)*sin(Om_y)*sin(A_y)+sin(Om_z)     ...
    *sin(A_z)*sin(Om_x)*cos(A_x)*cos(Om_y))+sin(Psi)*sin(Phi)/cos(Psi)      ...
    /(cos(Phi)^2+sin(Phi)^2)*(cos(Om_x)*cos(Om_y)+sin(Om_x)*sin(A_x)        ...
    *sin(Om_y)*cos(A_y))/(cos(Om_x)*cos(Om_y)*cos(Om_z)+cos(Om_x)           ...
    *sin(Om_y)*sin(A_y)*sin(Om_z)*cos(A_z)+sin(Om_y)*cos(A_y)*sin(Om_x)     ...
    *sin(A_x)*cos(Om_z)-sin(Om_y)*cos(A_y)*sin(Om_x)*cos(A_x)*sin(Om_z)     ...
    *cos(A_z)+sin(Om_z)*sin(A_z)*sin(Om_x)*sin(A_x)*sin(Om_y)*sin(A_y)      ...
    +sin(Om_z)*sin(A_z)*sin(Om_x)*cos(A_x)*cos(Om_y)))/S_z*(V_z-b_z);


f(2)= (cos(Phi)/cos(Psi)/(cos(Phi)^2+sin(Phi)^2)*sin(Om_y)*(cos(A_y)        ...
    *cos(Om_z)+sin(A_y)*sin(Om_z)*sin(A_z))/(cos(Om_x)*cos(Om_y)*cos(Om_z) ...
    +cos(Om_x)*sin(Om_y)*sin(A_y)*sin(Om_z)*cos(A_z)+sin(Om_y)*cos(A_y)     ...
    *sin(Om_x)*sin(A_x)*cos(Om_z)-sin(Om_y)*cos(A_y)*sin(Om_x)*cos(A_x)     ...
    *sin(Om_z)*cos(A_z)+sin(Om_z)*sin(A_z)*sin(Om_x)*sin(A_x)*sin(Om_y)     ...
    *sin(A_y)+sin(Om_z)*sin(A_z)*sin(Om_x)*cos(A_x)*cos(Om_y))+sin(Phi)     ...
    /cos(Psi)/(cos(Phi)^2+sin(Phi)^2)*sin(Om_z)*(-sin(Om_y)*cos(A_y)        ...
    *cos(A_z)+cos(Om_y)*sin(A_z))/(cos(Om_x)*cos(Om_y)*cos(Om_z)            ...
    +cos(Om_x)*sin(Om_y)*sin(A_y)*sin(Om_z)*cos(A_z)+sin(Om_y)*cos(A_y)     ...
    *sin(Om_x)*sin(A_x)*cos(Om_z)-sin(Om_y)*cos(A_y)*sin(Om_x)*cos(A_x)     ...
    *sin(Om_z)*cos(A_z)+sin(Om_z)*sin(A_z)*sin(Om_x)*sin(A_x)*sin(Om_y)     ...
```

```
*sin(A_y)+sin(Om_z)*sin(A_z)*sin(Om_x)*cos(A_x)*cos(Om_y)))/S_x          ...
*(V_x-b_x)+(cos(Phi)/cos(Psi)/(cos(Phi)^2+sin(Phi)^2)*(cos(Om_x)         ...
*cos(Om_z)+sin(Om_x)*cos(A_x)*sin(Om_z)*sin(A_z))/(cos(Om_x)            ...
*cos(Om_y)*cos(Om_z)+cos(Om_x)*sin(Om_y)*sin(A_y)*sin(Om_z)*cos(A_z)    ...
+sin(Om_y)*cos(A_y)*sin(Om_x)*sin(A_x)*cos(Om_z)-sin(Om_y)*cos(A_y)     ...
*sin(Om_x)*cos(A_x)*sin(Om_z)*cos(A_z)+sin(Om_z)*sin(A_z)*sin(Om_x)     ...
*sin(A_x)*sin(Om_y)*sin(A_y)+sin(Om_z)*sin(A_z)*sin(Om_x)*cos(A_x)      ...
*cos(Om_y))-sin(Phi)/cos(Psi)/(cos(Phi)^2+sin(Phi)^2)*sin(Om_z)         ...
*(cos(Om_x)*cos(A_z)+sin(Om_x)*sin(A_x)*sin(A_z))/(cos(Om_x)            ...
*cos(Om_y)*cos(Om_z)+cos(Om_x)*sin(Om_y)*sin(A_y)*sin(Om_z)*cos(A_z)    ...
+sin(Om_y)*cos(A_y)*sin(Om_x)*sin(A_x)*cos(Om_z)-sin(Om_y)*cos(A_y)     ...
*sin(Om_x)*cos(A_x)*sin(Om_z)*cos(A_z)+sin(Om_z)*sin(A_z)*sin(Om_x)     ...
*sin(A_x)*sin(Om_y)*sin(A_y)+sin(Om_z)*sin(A_z)*sin(Om_x)*cos(A_x)      ...
*cos(Om_y)))/S_y*(V_y-b_y)+(-cos(Phi)/cos(Psi)/(cos(Phi)^2              ...
+sin(Phi)^2)*sin(Om_y)*(cos(Om_x)*sin(A_y)-sin(Om_x)*cos(A_x)           ...
*cos(A_y))/(cos(Om_x)*cos(Om_y)*cos(Om_z)+cos(Om_x)*sin(Om_y)           ...
*sin(A_y)*sin(Om_z)*cos(A_z)+sin(Om_y)*cos(A_y)*sin(Om_x)*sin(A_x)      ...
*cos(Om_z)-sin(Om_y)*cos(A_y)*sin(Om_x)*cos(A_x)*sin(Om_z)*cos(A_z)     ...
+sin(Om_z)*sin(A_z)*sin(Om_x)*sin(A_x)*sin(Om_y)*sin(A_y)+sin(Om_z)     ...
*sin(A_z)*sin(Om_x)*cos(A_x)*cos(Om_y))-sin(Phi)/cos(Psi)/(cos(Phi)^2   ...
+sin(Phi)^2)*(cos(Om_x)*cos(Om_y)+sin(Om_x)*sin(A_x)*sin(Om_y)          ...
*cos(A_y))/(cos(Om_x)*cos(Om_y)*cos(Om_z)+cos(Om_x)*sin(Om_y)           ...
*sin(A_y)*sin(Om_z)*cos(A_z)+sin(Om_y)*cos(A_y)*sin(Om_x)*sin(A_x)      ...
*cos(Om_z)-sin(Om_y)*cos(A_y)*sin(Om_x)*cos(A_x)*sin(Om_z)*cos(A_z)     ...
+sin(Om_z)*sin(A_z)*sin(Om_x)*sin(A_x)*sin(Om_y)*sin(A_y)+sin(Om_z)     ...
*sin(A_z)*sin(Om_x)*cos(A_x)*cos(Om_y)))/S_z*(V_z-b_z);


f(3)=(sin(Phi)/(cos(Phi)^2+sin(Phi)^2)*sin(Om_y)*(cos(A_y)*cos(Om_z)     ...
   +sin(A_y)*sin(Om_z)*sin(A_z))/(cos(Om_x)*cos(Om_y)*cos(Om_z)          ...
   +cos(Om_x)*sin(Om_y)*sin(A_y)*sin(Om_z)*cos(A_z)+sin(Om_y)*cos(A_y)   ...
   *sin(Om_x)*sin(A_x)*cos(Om_z)-sin(Om_y)*cos(A_y)*sin(Om_x)*cos(A_x)   ...
   *sin(Om_z)*cos(A_z)+sin(Om_z)*sin(A_z)*sin(Om_x)*sin(A_x)*sin(Om_y)   ...
   *sin(A_y)+sin(Om_z)*sin(A_z)*sin(Om_x)*cos(A_x)*cos(Om_y))-cos(Phi)   ...
   /(cos(Phi)^2+sin(Phi)^2)*sin(Om_z)*(-sin(Om_y)*cos(A_y)*cos(A_z)      ...
   +cos(Om_y)*sin(A_z))/(cos(Om_x)*cos(Om_y)*cos(Om_z)+cos(Om_x)         ...
   *sin(Om_y)*sin(A_y)*sin(Om_z)*cos(A_z)+sin(Om_y)*cos(A_y)*sin(Om_x)   ...
   *sin(A_x)*cos(Om_z)-sin(Om_y)*cos(A_y)*sin(Om_x)*cos(A_x)*sin(Om_z)   ...
   *cos(A_z)+sin(Om_z)*sin(A_z)*sin(Om_x)*sin(A_x)*sin(Om_y)*sin(A_y)    ...
   +sin(Om_z)*sin(A_z)*sin(Om_x)*cos(A_x)*cos(Om_y)))/S_x*(V_x-b_x)      ...
   +(sin(Phi)/(cos(Phi)^2+sin(Phi)^2)*(cos(Om_x)*cos(Om_z)+sin(Om_x)     ...
   *cos(A_x)*sin(Om_z)*sin(A_z))/(cos(Om_x)*cos(Om_y)*cos(Om_z)          ...
   +cos(Om_x)*sin(Om_y)*sin(A_y)*sin(Om_z)*cos(A_z)+sin(Om_y)*cos(A_y)   ...
   *sin(Om_x)*sin(A_x)*cos(Om_z)-sin(Om_y)*cos(A_y)*sin(Om_x)*cos(A_x)   ...
   *sin(Om_z)*cos(A_z)+sin(Om_z)*sin(A_z)*sin(Om_x)*sin(A_x)*sin(Om_y)   ...
   *sin(A_y)+sin(Om_z)*sin(A_z)*sin(Om_x)*cos(A_x)*cos(Om_y))+cos(Phi)   ...
   /(cos(Phi)^2+sin(Phi)^2)*sin(Om_z)*(cos(Om_x)*cos(A_z)+sin(Om_x)      ...
   *sin(A_x)*sin(A_z))/(cos(Om_x)*cos(Om_y)*cos(Om_z)+cos(Om_x)          ...
   *sin(Om_y)*sin(A_y)*sin(Om_z)*cos(A_z)+sin(Om_y)*cos(A_y)*sin(Om_x)   ...
   *sin(A_x)*cos(Om_z)-sin(Om_y)*cos(A_y)*sin(Om_x)*cos(A_x)*sin(Om_z)   ...
   *cos(A_z)+sin(Om_z)*sin(A_z)*sin(Om_x)*sin(A_x)*sin(Om_y)*sin(A_y)    ...
   +sin(Om_z)*sin(A_z)*sin(Om_x)*cos(A_x)*cos(Om_y)))/S_y*(V_y-b_y)      ...
   +(-sin(Phi)/(cos(Phi)^2+sin(Phi)^2)*sin(Om_y)*(cos(Om_x)*sin(A_y)     ...
   -sin(Om_x)*cos(A_x)*cos(A_y))/(cos(Om_x)*cos(Om_y)*cos(Om_z)          ...
   +cos(Om_x)*sin(Om_y)*sin(A_y)*sin(Om_z)*cos(A_z)+sin(Om_y)*cos(A_y)   ...
   *sin(Om_x)*sin(A_x)*cos(Om_z)-sin(Om_y)*cos(A_y)*sin(Om_x)*cos(A_x)   ...
   *sin(Om_z)*cos(A_z)+sin(Om_z)*sin(A_z)*sin(Om_x)*sin(A_x)*sin(Om_y)   ...
```

```
    *sin(A_y)+sin(Om_z)*sin(A_z)*sin(Om_x)*cos(A_x)*cos(Om_y))                ...
    +cos(Phi)/(cos(Phi)^2+sin(Phi)^2)*(cos(Om_x)*cos(Om_y)+sin(Om_x)          ...
    *sin(A_x)*sin(Om_y)*cos(A_y))/(cos(Om_x)*cos(Om_y)*cos(Om_z)              ...
    +cos(Om_x)*sin(Om_y)*sin(A_y)*sin(Om_z)*cos(A_z)+sin(Om_y)*cos(A_y)       ...
    *sin(Om_x)*sin(A_x)*cos(Om_z)-sin(Om_y)*cos(A_y)*sin(Om_x)*cos(A_x)       ...
    *sin(Om_z)*cos(A_z)+sin(Om_z)*sin(A_z)*sin(Om_x)*sin(A_x)*sin(Om_y)       ...
    *sin(A_y)+sin(Om_z)*sin(A_z)*sin(Om_x)*cos(A_x)*cos(Om_y)))/S_z           ...
    *(V_z-b_z);

return;
```

REPORT DOCUMENTATION PAGE

Form Approved
OMB No. 0704-0188

1. REPORT DATE *(DD-MM-YYYY)*	2. REPORT TYPE	3. DATES COVERED *(From - To)*
01- 08 - 2003	Contractor Report	

4. TITLE AND SUBTITLE

Development of a High Accuracy Angular Measurement System for Langley Research Center Hypersonic Wind Tunnel Facilities

5a. CONTRACT NUMBER

5b. GRANT NUMBER

5c. PROGRAM ELEMENT NUMBER

6. AUTHOR(S)

Brett Newman and Si-bok Yu

5d. PROJECT NUMBER

L-14635

5e. TASK NUMBER

5f. WORK UNIT NUMBER

718-20-01-01

7. PERFORMING ORGANIZATION NAME(S) AND ADDRESS(ES)

NASA Langley Research Center
Hampton, VA 23681-2199

Old Dominion University
Norfolk, VA 23508

8. PERFORMING ORGANIZATION REPORT NUMBER

9. SPONSORING/MONITORING AGENCY NAME(S) AND ADDRESS(ES)

National Aeronautics and Space Administration
Washington, DC 20546-0001

10. SPONSOR/MONITOR'S ACRONYM(S)

NASA

11. SPONSOR/MONITOR'S REPORT NUMBER(S)

NASA/CR-2003-212401

12. DISTRIBUTION/AVAILABILITY STATEMENT

Unclassified - Unlimited
Subject Category 35
Availability: NASA CASI (301) 621-0390 Distribution: Nonstandard

13. SUPPLEMENTARY NOTES

Langley Technical Monitor: Ray D. Rhew
An electronic version can be found at http://techreports.larc.nasa.gov/ltrs/ or http://ntrs.nasa.gov

14. ABSTRACT

Modern experimental and test activities demand innovative and adaptable procedures to maximize data content and quality while working within severely constrained budgetary and facility resource environments. This report describes development of a high accuracy angular measurement capability for NASA Langley Research Center hypersonic wind tunnel facilities to overcome these deficiencies. Specifically, utilization of micro-electro-mechanical sensors including accelerometers and gyros, coupled with software driven data acquisition hardware, integrated within a prototype measurement system, is considered. Development methodology addresses basic design requirements formulated from wind tunnel facility constraints and current operating procedures, as well as engineering and scientific test objectives. Description of the analytical framework governing relationships between time dependent multi-axis acceleration and angular rate sensor data and the desired three dimensional Eulerian angular state of the test model is given. Calibration procedures for identifying and estimating critical parameters in the sensor hardware is also addressed.

15. SUBJECT TERMS

Accelerometers; Hypersonic; Wind-Tunnel; Accuracy

16. SECURITY CLASSIFICATION OF:			17. LIMITATION OF ABSTRACT	18. NUMBER OF PAGES	19a. NAME OF RESPONSIBLE PERSON
a. REPORT	b. ABSTRACT	c. THIS PAGE			STI Help Desk (email: help@sti.nasa.gov)
					19b. TELEPHONE NUMBER *(Include area code)*
U	U	U	UU	114	(301) 621-0390